Christian L. HUBER

Development of a low cost enzymatic electrochemical microfluidic glucose biosensor for continuous measurement incorporating electrode fouling and interference prevention

Diploma thesis

Institute for Genomics and Bioinformatics
University of Technology Graz
Petersgasse 14, A – 8010 Graz
Head: Univ.-Prof. Dipl.-Ing. Dr.techn. Rudolf Stollberger

Mentor: Dr. Jeffrey D. Newman

Reviewer: Univ.-Ass. Dr. Marcel Scheideler

Graz, December, 2010

Acknowledgements

I would like to express my gratitude to my supervisor Dr. Jeff Newman and to Prof. David Cullen, who both were always available with good advice. Thanks also to my Austrian supervisor Univ.-Ass. Dr. Marcel Scheideler, for his support at my home university. Furthermore, Nikolaos Asproulis and Matyas Benke provided valuable theoretical and practical input to the project. Thanks to Heather Simpkins for proofreading my thesis.

I want to thank also my team members Maxime Labbé and Minh-Anh Tu for their friendship, humour and motivation. They were working on different aspects of this project and always willing to discuss encountered difficulties and problems.

Thanks to Adhesives Research Inc. for providing the used polymer layers as free samples.

Special thanks go to my parents and my sister, who always supported me in all my decisions. I also owe my girlfriend Okka Gerdes a debt of gratitude for her love, support and patience.

Last but not least, I want to say thank you to my best friends Thomas Kern, Gerald Bachler and Werner Mittmannsgruber, they kept my life as a student interesting and made it an unforgettable time.

Abstract (deutsch)

Weltweit leiden mehr als 220 Millionen Menschen an Diabetes Mellitus, einer lebenslangen, unheilbaren Stoffwechselkrankheit, die die Blutzuckerregulation des Körpers beeinträchtigt. Die konventionelle Therapie stützt sich heute weitgehend auf die Eigeninitiative der Patienten und besteht aus der Messung einer, durch Stich in die Fingerbeere gewonnenen, Probe und anschließender Insulininjektion. Bei dieser Art der Blutzuckermessung handelt es sich um eine Punktmessung, die keine Rückschlüsse über eine steigende oder fallende Tendenz zulässt. Darüber hinaus ist sie fehleranfällig und aufgrund der häufigen Lanzettenstiche unangenehm für den Patienten. Um eine weniger störanfällige und patientenfreundlichere Messmethode zu ermöglichen, wurde in dieser Arbeit das Konzept eines kostengünstigen, enzymatischen, elektrochemischen, mikrofluidischen Biosensors für eine kontinuierliche Messung entwickelt. Ziel dieses Projektes war die Herstellung eines experimentellen Prototyps um die Probleme und das Potenzial dieses Konzeptes zu identifizieren, sowie Schwerpunkte für die zukünftige Forschung aufzudecken. Der Sensor nutzt eine flüssige Membran, die sich selbst ständig erneuert, um Störeinflüsse auszuschließen. Der mikrofluidische Chip des Sensors wurde durch Laminierung mehrerer, zuvor mittels CO_2-Laser geschnittener, Polymer-Membran Schichten aufgebaut. Sowohl das biologische Element des Biosensors (Glucose Oxidase) als auch ein, in einem eigens entwickelten Siebdruck-verfahren aufgebrachtes, Dreielektrodensystem wurden in die obere bzw. in die untere Polymer-Membran integriert. Versuche an unterschiedlichen Sensordesigns mittels gefärbter Lösungen und verschiedener Viskositäten zeigten Schwierigkeiten im Strömungsverhalten. Im Problemlösungsprozess konnten Verbesserungen erzielt werden, es sind jedoch weitere Optimierungen notwendig. Die Elektroden zeigten sowohl bei Messung mit Standardlösungen als auch mit Enzymlösungen hohe Reproduzierbarkeit und Linearität, bei einer unteren Nachweisgrenze von 0,05mM.

Schlüsselwörter: H-filter, diabetes mellitus, glucose oxidase, laser-cutting, lamination

Abstract (english)

Globally more than 220 million people are suffering from diabetes mellitus, a lifelong, incurable metabolic disorder affecting the body's blood glucose regulation. Currently, therapy is mainly by self management by finger prick testing and subsequent insulin application. As this type of measurement lacks the important trend information and is prone to interferences, not to mention the discomfort of finger pricking, there is a need for less error prone and more convenient continuous glucose sensing. Therefore, the concept of a low cost, enzymatic, electrochemical, microfluidic glucose biosensor for continuous measurement, integrating a continuously renewable liquid membrane to prevent electrode fouling and interferences, was developed. The design intended the lamination of prior laser-cut polymer layers incorporating immobilised glucose oxidase as biological recognition element and a screen-printed three electrode system for amperometric detection. The optimal laser-cutting settings were determined empirically and different designs cut. The laminated microfluidic chips were tested with stained solutions of different viscosities, which revealed some difficulties with the fluid conduct. In the troubleshooting process, improvements were achieved, but further research is necessary. For electrochemical detection, a manual screen-printing procedure was developed taking care to keep the surface as regular as possible. It showed good repeatability, reproducibility and linearity, revealing a limit of detection of 0.05mM. Due to the problems encountered with the microfluidic chip and also the time constraints, experiments with the enzyme in solution, instead of the immobilised glucose oxidase, were carried out, showing good response at the electrodes. As the approach was meant to serve as an experimental prototype, it successfully identified problems which need further investigation, the opportunities of the proposed concept and future work to overcome the encountered difficulties.

Keywords: H-filter, diabetes mellitus, glucose oxidase, laser-cutting, lamination

Table of contents

Eidesstattliche Erklärung

Ich erkläre an Eides statt, dass ich die vorliegende Arbeit selbstständig verfasst, andere als die angegebenen Quellen/Hilfsmittel nicht benutzt und die den benutzten Quellen wörtlich und inhaltlich entnommenen Stellen als solche kenntlich gemacht habe.

Statutory Declaration

I declare that I have authored this thesis independently, that I have not used other than the declared sources / resources and that I have explicitly marked all material which has been quoted either literally or by content from the used sources.

…… ……

date (signature)

List of tables

List of figures

Notation

$C_6H_6O_6$	Dehydroascorbic acid
$C_6H_8O_6$	Ascorbic acid
CE	Counter electrode
CMC	Carboxymethyl cellulose sodium salt
DNA	Deoxyribonucleic acid
e^-	Electron
FAD	Flavine adenine dinucleotide
$Fe(CN)_6^{3-}$	Ferricyanide
$Fe(CN)_6^{4-}$	Ferrocyanide
GDH	Glucose dehydrogenase
GOx	Glucose oxidase
H^+	Proton
H_2O	Water
H_2O_2	Hydrogen peroxide
H_2SO_4	Sulphuric acid
I_3^-	Triiodide
ISE	Ion-selective electrode
ISF	Interstitial fluid
ISFET	Ion-selective field-effect transistor
IVF	*In vitro* fertilisation
$K_4Fe(CN)_6$	Potassium ferrocyanide
KCl	Potassium chloride
KI	Potassium iodide
KIO_3	Potassium iodate
$KMnO_4$	Potassium permanganate
LOC	Lab-on-chip
Na_2HPO_4	Disodium hydrogen phosphate
NAD	Nicotine adenine dinucleotide
NaH_2PO_4	Sodium dihydrogen phosphate
O_2	Molecular oxygen
PET	Polyethylene terephthalate
PQQ	Pyrroloquinoline quinone
R^2	Coefficient of determination
RE	Reference electrode
Rpm	Rounds per minute
S/N	Signal to noise ratio
UV	Ultra violet
WE	Working electrode
µTAS	Micrototal analysis system

CHAPTER I: INTRODUCTION AND LITERATURE REVIEW

1 Description of the project

This section discusses the background of the problem and shows the market for the proposed technology. Furthermore the aims and objectives of the project are stated and an outline of this work is given.

1.1 Background to the challenge

Interferences are a major issue in present enzymatic electrochemical glucose biosensors. These are caused due to the non-specificity of the biological recognition element or the non-selectivity of the electrodes. Other compounds in the sample other than the analyte may be catalysed by the enzyme, leading to erroneous measurements. Furthermore, every species in the sample that is oxidizable at the working potential is detected at the electrodes, not only the one produced by the enzymatic reaction. The most widely used principle to reduce these interferences in contemporary biosensors is to protect the electrodes through physical barriers such as polymer membranes (Turner, 1992). These interference problems and possible improvements are further discussed for glucose biosensors in Section 4.3.

Another challenge is, that continuous biosensors often suffer from fouling, particularly from high molecular weight species such as proteins. The adsorption of these non electro-active molecules to the electrode surface leads to a decreasing sensor response over time (Turner, 1992). Also an issue in blood measuring biosensors is fouling from components of the immune system resulting in a loss of sensitivity during the measurements (Piechotta *et al.*, 2005). These fouling problems and possible improvements for glucose biosensors are described in more detail in Section 4.4.

The ideal biosensor needs no sample preparation, is only specific to the analyte and never suffers from fouling. The attempted project should progress one step further into the direction of this ideal biosensor device.

1.2 Market

As yet, there is no known cure for diabetes. Into consideration as a possible cure comes pancreas transplantation, but there is a lack of donor organs and furthermore, the recipients will be exposed to increased infection risk due to the subsequent immunosuppressive therapy. Another possible option for the far future may offer engineered cell lines, stem cell therapy or xenotransplantation. The recent trend in research for diabetes treatment is towards a closed loop system, also called artificial pancreas which aims at the automation of insulin dosing and administration following the glucose measurement. These miniaturised systems combine a glucose sensor and an insulin pump into one device in order to reach near normal glucose profiles. In a word, to replace the natural functions of the patient's dysfunctional pancreas. The devices consist of three key elements, a continuous glucose biosensor, an algorithm for the prediction of the insulin delivery rate and a pump for insulin administration. Much effort has been spent during recent decades on the development of miniaturised continuous glucose biosensors, mainly on alternative sensing sites in the form of subcutaneous interstitial fluid (ISF) sensors, due to the mentioned problems for the measurement in whole blood. In the literature, there is no clear consensus about the correlation in terms of delay and response of ISF compared to blood plasma glucose levels. Generally ISF and blood contain similar glucose concentrations; the problems are rapidly rising or falling blood glucose levels, which may lead to a lag in ISF glucose concentrations (Wang, 2001; Piechotta *et al.*, 2005; Steil and Rebrin, 2005; Newman and Turner, 2005; Wang, 2008). The proposed concept for a continuous glucose biosensor for measurement in blood could bypass the circuitous way of measurement in ISF.

1.3 Aims

The aim of the project is to investigate the use of laminated microfluidic structures for biosensor fabrication. This should be demonstrated by the production of a microfluidic, enzymatic glucose biosensor with a continuously renewable liquid membrane, by making use of unique physical effects occurring only on a micro-scale. This should have a highly reproducible structure and will never foul, since all proteins will be continuously washed away.

1.4 Objectives

The objectives of this project are to design a biosensor system which meets all the required aims by the fabrication of a microfluidic device using low cost technologies such as screen-printing, laser-cutting and lamination. Therefore selection of the geometry and dimensions of the sensor based on diffusion times is carried out. The approach comprises also the integration of an electrochemical detection system and immobilised glucose oxidase (GOx) enzymes into the microfluidic system in order to form a liquid membrane which is capable of screening out interferences and will never foul due to the absence of a physical membrane. Practical testing and optimization is carried out by the use of an automated electrochemical analyser. The attempted approach is meant to serve as an experimental prototype device to identify problems, opportunities and future work of the proposed concept.

Furthermore, this project is carried out as part of a bigger programme in order to investigate the feasibility and opportunities for future work with microfluidics in Cranfield Health. This involves teamwork with two other MSc students during some stages of the project. Tu (2010) is working on design issues for the microfluidic chip in relation to laminar flow behaviour, and Labbé (2010) is working on the influence of the fluid viscosity on the flow conduct in the microfluidic channels. My part is the implementation of a biosensor prototype for continuous glucose measurement using low cost microfluidic techniques.

1.5 Outline

The following introduction and literature review will start with a general description of the disease diabetes mellitus. It will explain why the maintenance, hence the measurement of blood glucose levels, is so important for diabetics. Therefore a short overview of the field of biosensors in general will be given, then glucose sensors will be explained in more detail. The underlying theory of the methods and elements used in the design and implementation of the attempted microfluidic device will be addressed. This will cover the use of enzymes as biological recognition elements especially GOx. A short overview of microfluidics will be given, followed by electrochemical detection principles.

Following the introduction and literature review chapter, the specific methodology of the experimental setup and the fabrication techniques will be mentioned. The next chapter will contain the results of the experiments carried out. Under the heading Discussion, the results of the previous chapter will be interpreted and compared to published literature, followed by the conclusions, which will state the main findings, and suggest future work and recommendations. On the last pages the references and the appendix will be found.

2 Diabetes Mellitus

This section gives an overview of the background and classification of diabetes. Then the signs and symptoms including long-term complications and diabetic emergencies are stated. Some epidemiological data are given and the current therapy is described.

2.1 Background

Diabetes currently is a life-long, incurable metabolic disorder characterised by elevated blood glucose concentrations (hyperglycaemia) due to defects in insulin secretion or action (Ricci *et al*., 2005). Insulin is a vital hormone, used by the body to absorb glucose from the bloodstream into the cells, where it acts as an energy source (Newman and Turner, 2005). Furthermore, it turns hepatic glucose production off during and after meals (carbohydrate intake) (Reach and Wilson, 1992). Diabetes mellitus is a major cause for reduced life expectancy, morbidity and reduced quality of life due to long-term complications or hyper and hypoglycaemic emergencies (WHO, 2006; Holt and Kumar, 2010).

2.2 Classification of diabetes mellitus

Due to the different mechanisms of cause and clinical presentations of diabetes, it has been classified by the WHO into three categories, which are further explained in the following sections. It is important for the treatment, to know the type of diabetes. For better personalised diabetes therapy, there are thoughts of classifying the main categories into further sub-types (Holt and Kumar, 2010).

2.2.1 Type 1 diabetes

About 10% of diabetes patients are suffering from type 1 diabetes, previously known as insulin-dependent, or childhood onset diabetes mellitus. This autoimmune idiopathic disease causes an absolute insulin deficiency due to the destruction of β-cells in the islet cells of Langerhans in the pancreas. It is caused by genetic susceptibility in combination with environmental triggers which are not well understood yet (Turner and Wass, 2002; WHO, 2009; Holt and Kumar, 2010).

2.2.2 Type 2 diabetes

About 90% of diabetes patients are suffering from type 2 diabetes (formerly referred to as non-insulin dependent, or adult onset diabetes mellitus) due to insulin resistance of body cells. There are many different sub-types such as latent slowly progressing type 1 diabetes in children, which may progress to type 1 diabetes, or latent autoimmune diabetes in adults. Obesity has proven to be a major trigger for type 2 diabetes (Turner and Wass, 2002; WHO, 2009; Holt and Kumar, 2010).

2.2.3 Others

Every deregulation of blood glucose levels which does not fit into type 1 or type 2 diabetes is classified into this category. Some examples are gestational diabetes, genetic defects and endocrinopathies (Turner and Wass, 2002).

2.3 Signs and symptoms

There are some acute symptoms affecting a person's well-being if blood sugar levels are too high or to low. These are reversible, whereas the long-term complications resulting from poor glycaemic control are mainly irreversible. Diabetes diagnosis is often missed due to the various and insidious symptoms which are often misinterpreted by clinicians (Holt and Kumar, 2010).

2.3.1 Hyperglycaemia

Hyperglycaemic symptoms are similar in both types of diabetes, but the onset is typically more rapid in type 1 diabetes. Hyperglycaemia causes polyuria resulting in dehydration and increased thirst. Other symptoms comprise

constant hunger, tiredness, exhaustion, weight loss, pruritus vulvae or balanitis, lethargy and vision changes such as blurred vision. If untreated, hyperglycaemia can lead to an emergency called diabetic ketoacidosis (see Section 2.3.4). WHO defines hyperglycaemia as fasting venous plasma glucose levels higher than 7mM or venous glucose levels higher than 11mM two hours after ingestion of 75g oral glucose load (Watkins, 1998; Holt and Kumar, 2010; WHO, 2006).

2.3.2 Hypoglycaemia

Hypoglycaemic symptoms are caused for various reasons. A lack of glucose in the brain can lead to headache, confusion, drowsiness, loss of balance and coordination, visual disturbances like double vision and changes in behaviour and personality. Effects on the autonomous nervous system can result in sweating, tremor and anxiety. Also the gastrointestinal tract is affected, which can lead to hunger, nausea and belching. Palpitations are common. The symptom profiles depend on age and vary for each patient. There is no clear consensus about the definition of hypoglycaemia in diabetes patients. In most publications it is stated either as 3.0 or 3.9mM (Watkins, 1998; Holt and Kumar, 2010; Amiel *et al.*, 2008).

2.3.3 Complications

One of the long-term complications in diabetes patients is cardiovascular disease. This is highly preventable by maintaining a healthy lifestyle (not smoking, taking physical exercise), diet (fruit and vegetables, fish, low fat, less alcohol) and taking prescribed medication (blood pressure, blood glucose, anti-obesity drugs). The major reason for premature mortality in diabetics is due to macrovascular disease like heart attack, stroke and peripheral vascular disease. Microvascular disease is a major cause for disability in diabetes patients, as it can lead to blindness, kidney failure, nerve damage and amputation of lower limbs (Ricci *et al*., 2005; WHO, 2006; Holt and Kumar, 2010).

2.3.4 Emergencies

Severe hyperglycaemic patients often feel quite well and their potentially life threatening condition remains unrecognised thus undiagnosed. Hyperglycaemic emergencies, namely diabetic ketoacidosis and hyperosmolar hyperglycaemic syndrome require immediate hospital treatment with insulin and fluid replacement. Therapy of recovered patients needs to be reviewed and maybe adapted to prevent future recurrence (Holt and Kumar, 2010).

On the other hand, hypoglycaemia unawareness can result in severe hypoglycaemia due to a lack of warning symptoms like headache, confusion, hunger, sweat, nausea and anxiety, appearing in about 25% of long-standing diabetes patients, particularly in those with poor glycaemic control. This may lead to sudden changes in personality, intellectual functions or consciousness level up to brain damage and sudden coma (Ricci *et al*., 2005; Holt and Kumar, 2010).

2.4 Epidemiology

Diabetes is a global public health problem and one of the major causes of disability and death. Worldwide more than 220 million people suffer from diabetes mellitus, which caused about 1.1 million deaths in 2005 (WHO, 2009). Figure 1 shows the global distribution of diabetes prevalence in 2000 and the estimated prevalence in 2030. The WHO also assessed that diabetes related deaths will double by 2030, mainly in developing countries. Today, about 50% of deaths occur in patients under the age of seventy years (Wang, 2001; WHO, 2009).

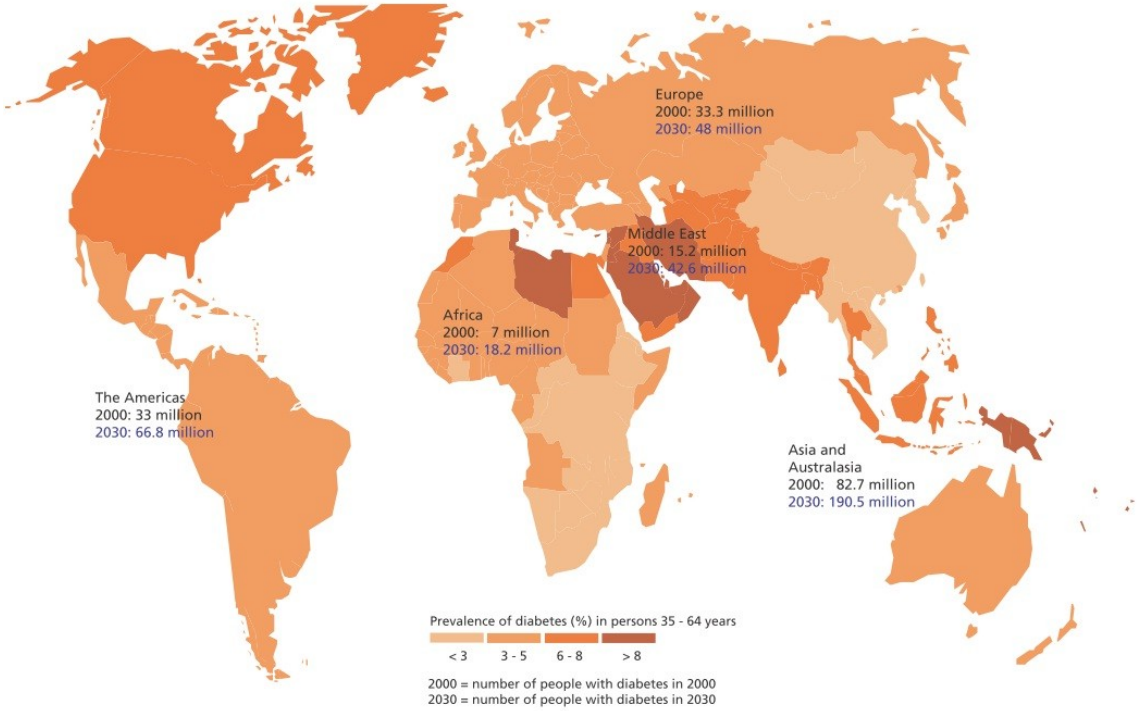

Figure 1: Worldwide distribution of diabetes prevalence in 2005 and estimated numbers for 2030 (adapted from WHO, 2004)

2.5 Therapy

Diabetes therapy is mainly by the self-management of the diabetic patient after advice by specialist clinicians on lifestyle, nutrition and medication. This includes frequent self monitoring of glucose levels by finger prick testing and subsequent action either by oral drugs or insulin injection (Holt and Kumar, 2010; Watkins, 1998).

In type 2 diabetes, the first step is lifestyle modification and dietary advice including physical activity, no smoking, reducing alcohol intake and weight reduction. If this does not lead to adequate results, oral drug therapy is indicated. If blood glucose levels cannot be controlled by oral hypoglycaemic agents, insulin therapy should be started. In type 1 diabetes, insulin treatment is vital, along with the diet and lifestyle changes mentioned for type 2 diabetes (Holt and Kumar, 2010). Additional important aims in diabetes care are control of weight and avoidance of hazards to the feet (Watkins, 1998).

For insulin therapy, there are currently two treatment approaches available, conventional therapy (bolus insulin injections) or an open loop insulin pump system (continuous insulin infusion) after dose estimation by finger prick

glucose measurement. The biggest disadvantage of the currently used finger prick tests is the fact that it is a point measurement and gives no information about the trend and the fluctuations between measurements. This problem could be solved by the application of continuous glucose biosensors. Furthermore, in conjunction with an insulin pump and an algorithm to determine the flow rate, a so-called artificial pancreas or closed loop system could be realised. These systems adapt automatically to exercise and diet changes leading to near normal glucose profiles (Turner *et al.*, 1987). Figure 2 shows the differences between conventional therapy, open loop and closed loop systems.

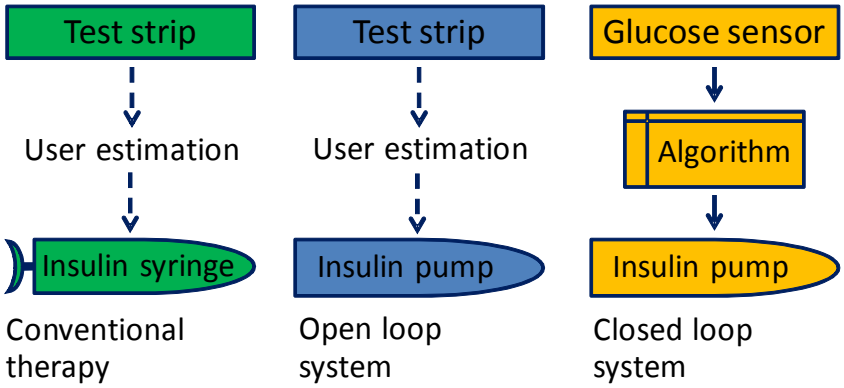

Figure 2: Scheme of possible approaches for insulin therapy (adapted from Turner et al., 1987)

As already mentioned in Section 2.3.4, hypoglycaemic unawareness is a big issue in diabetic persons. With the help of a continuous glucose biosensor, a warning system for the diabetes patient could be realised, to avoid blood glucose levels outside a normal range, particularly hypoglycaemic episodes (Reach and Wilson, 1992).

3 Biosensors in general

A biosensor is not, as many people believe, a sensor which measures biological signals. Biological signal monitors exist, but they are significantly different from biosensors. This section contains the definition of a biosensor and describes the classification of the same. As a last point the broad range of biosensor applications is stated.

3.1 Definition of a biosensor

A biosensor is a device that exploits the specificity of a biological recognition component in combination with a transducer to translate a not directly detectable biological or chemical parameter into a measurable electrical signal. Figure 3 shows the elements of a classic biosensor. The biological recognition component specifically interacts with the target molecule producing a signal proportional to the analyte concentration. This signal is converted by the transducer into an electrical signal which can be measured (Wang, 2002; Malhotra and Turner, 2003).

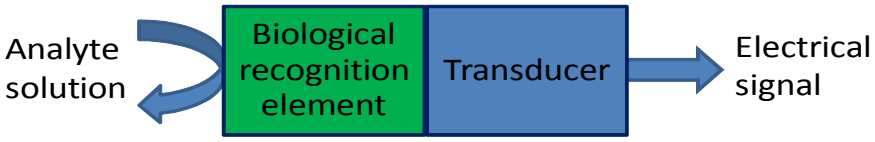

Figure 3: Schematic illustration of the components of a biosensor

3.2 Classification of biosensors

Biosensors can be classified either by the type of transduction or by the biological recognition element.

3.2.1 Classification by detection method

The classification by detection method can be distinguished by three different electrochemical methods: amperometric, potentiometric and conductometric amongst others such as optical, acoustic and calorimetric detection techniques (Malhotra and Turner, 2003). The electrochemical methods are further described in Section 7.1.

3.2.2 Classification by biological recognition element

Classification by the biological component is done by categorisation either into biocatalytic or bioaffinity recognition mechanisms. In the kind of biocatalytic recognition element sensors, either an enzyme, a whole cell (or cell organelles) or tissue is immobilised on the transducer as the biological compound. This type of biosensor is the most widely studied in literature and is also the most widespread that is practically applied. Bioaffinity, also called biocomplexing, recognition elements, are comprised of DNA and RNA methods, immunological reactions (antibody-antigen) and receptor/antagonist/agonist based biosensors.

The latter ones use ion-channels, membrane receptors or binding proteins as biological recognition components. Due to some drawbacks such as the narrow linear operating range and fewer possibilities for continuous measurement, development of bioaffinity based biosensors is not yet as far as the biocatalyst based ones (Thévenot *et al*., 1999; Malhotra and Turner, 2003).

3.3 Applications of biosensors

Biosensors are applied in a very broad range of human health care and medical and clinical diagnostics including intensive, bed side, and point of care. In the chemical and pharmaceutical industry they are used for process control and substance testing as well as for drug discovery, analysis and detection. There are also applications in veterinary medicine, for example in *in vitro* fertilisation (IVF), and in the defence and security industry for the detection of biological warfare agents. In environmental analysis, biosensors are used for waste-water monitoring and water pollution surveillance. In food quality control, purity and freshness as well as contaminants can be quantified (Malhotra and Turner, 2003).

4 Glucose biosensors

Glucose biosensors are used in a broad spectrum of applications in chemical, pharmaceutical, food and beverage, biotechnological and other industries (Bankar *et al.*, 2009). This section gives an overview of the history and describes the three generations of glucose biosensors. Then the interference and fouling problems are discussed in further detail, followed by the last point, which is state of the art.

4.1 Brief history of glucose sensing

Glucose sensing started with non biosensors. The first glucose patient test kits detected abnormal glucose concentrations in urine due to chemical reactions resulting in a colour-change, which was compared by eye to standards (series of printed colours). This measurement indicated that during the last few hours the blood glucose levels were elevated. However, hypoglycaemia was not detectable with this method. Then test strips, also producing a colour-change due to biochemical reactions, but working with a drop of blood instead of urine,

were developed. With these test strips, for the first time, hypoglycaemic conditions were detectable. They were in the first instance evaluated by eye and later on reflectance based glucose meters were used, resulting in objective and more accurate measurement (Reach and Wilson, 1992). The first glucose reflectance meter was commercialised in 1966. Four years earlier, in 1962 the first concept for a glucose biosensor was proposed by Clark and Lyons. They used Clark's oxygen electrode in conjunction with a thin layer of entrapped GOx enzyme on the surface and monitored the oxygen consumption during the reaction. But not until 1973 was the first commercial glucose biosensor for direct measurement of whole blood, based on Clark's idea (it detected hydrogen peroxide production instead of oxygen consumption) produced, due to the rapid development of reflectance based glucose meters at this time. However, this first electrochemical glucose biosensor was withdrawn from the market due to interference problems. In 1975, after overcoming these interference issues by the introduction of a second membrane (see Section 4.3) it was re-launched. These first biosensor devices became standard in many hospital and chemistry laboratories all over the world and remain so to this day. Since then the basic construction and working principle of these types of glucose biosensors has changed very little. In 1984, the use of a mediator to reduce susceptibility to interferents and oxygen dependency was introduced the first time (Cass *et al.*, 1984; Newman and Turner, 2005; Newman and Setford, 2006). In 1987 the first test-strips for self-monitoring were commercialised and modified electrodes to increase the sensor performance were developed. During the 1990s and 2000s, much effort has been spent on the development of minimally-invasive implantable biosensors measuring ISF glucose concentrations and the enhancement of the electron transfer between the enzyme's active site and the electrode surface (Wang, 2001). But the most effort has been spent on commercialisation of the home use finger prick tests. Abbott Laboratories, Bayer Corp., Lifescan and Roche emerged as the four main suppliers of glucose biosensors accounting for about 80% of the total meter market. It was not until 2000 that biosensor technology overtook reflectance devices, which are now redundant (Mendosa, 1999).

4.2 Generations of glucose biosensors

Glucose biosensors can be categorized according to their different working principles. Development and improvements of Clarke's first oxygen electrode biosensor led to the following three generations of glucose sensors.

4.2.1 First generation

In the first generation of glucose biosensors, the enzyme glucose oxidase (GOx) produces hydrogen peroxide (H_2O_2) in the presence of the natural mediator, molecular oxygen (O_2). Either the decrease in O_2 concentration is detected by an oxygen electrode, or the produced H_2O_2 is oxidised at the electrode and related to the glucose concentration. However, especially in *in vivo* applications, the concentration of unbound oxygen can be very low in comparison to the glucose concentration and therefore limit the enzymatic reaction (Malhotra and Turner, 2003; Wang, 2001). Figure 4 shows the working principle of a first generation glucose biosensor.

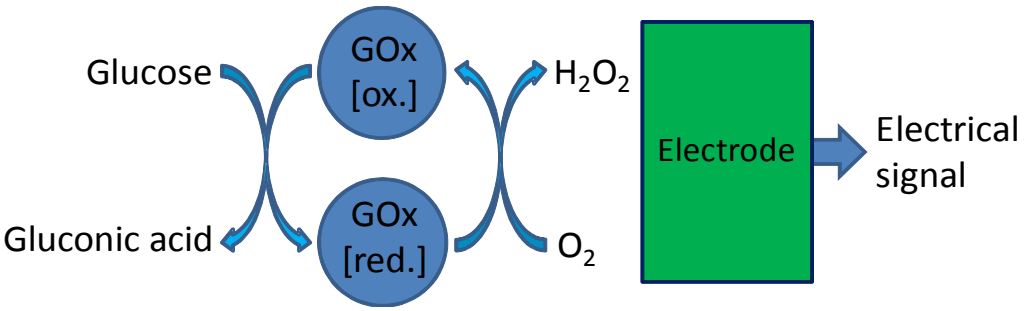

Figure 4: Working principle of a first generation glucose biosensor, [ox.], oxidised form; [red.], reduced form (adapted from Newman and Turner, 2005)

4.2.2 Second generation

The problem of limited oxygen diffusion to the enzyme of first generation glucose biosensors can be overcome by replacing the natural electron sink (oxygen) with an artificial mediator. This electron acceptor accelerates the transfer of e^- between the enzyme's redox centre and the electrode surface and makes it oxygen independent. An additional advantage of this working principle is the lower electrode working potential, which makes it less susceptible to interferences. However, due to the toxicity of the often relatively soluble mediators, they are normally not usable in *in vivo* glucose biosensors. Furthermore, mediated glucose biosensors lack reproducibility and have short

operational lifetimes (Malhotra and Turner, 2003; Wang, 2001; Newman and Turner, 2005). Figure 5 shows the working principle of a second generation glucose biosensor.

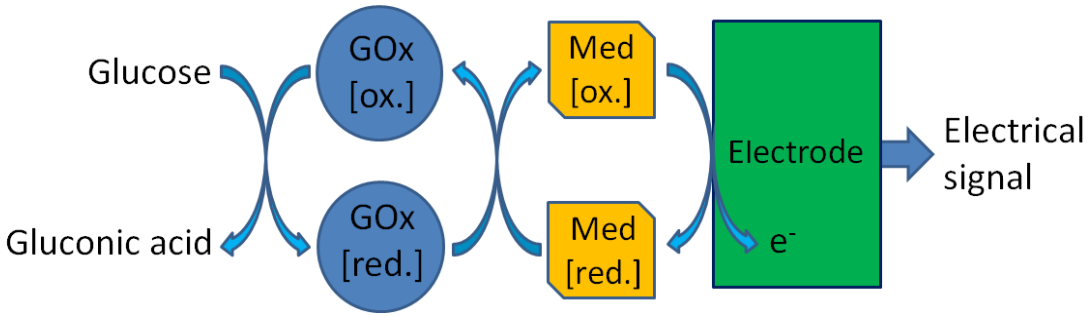

Figure 5: Working principle of a second generation glucose biosensor, [ox.], oxidised form; [red.], reduced form; Med, mediator (adapted from Newman and Turner, 2005; Wang, 2001)

4.2.3 Third generation

The most preferred, but also the most complicated glucose sensors, are the third generation glucose biosensors. These work without a mediator but enhance the electron transfer by a chemical link of the active site of the enzyme to the electrode surface (Malhotra and Turner, 2003).

4.3 Interference problem

As already mentioned, interferences are caused either due to the non-specificity of the enzymatic reaction, or due to the non-selectivity of the electrodes for the enzyme product.

4.3.1 Enzyme interferences

Many of the currently used home glucose testing strips are based on glucose dehydrogenase (GDH) in combination with one of three possible cofactors, pyrroloquinoline quinone (PQQ), flavine adenine dinucleotide (FAD) or nicotine adenine dinucleotide (NAD). Three of the four major manufacturers of home glucose testing strips switched enzymes during the last 6 months to GDH-FAD systems. Two of these previously used GDH-PQQ, which is prone to interferences from cross-reacting sugars, such as disaccharide maltose and monosaccharides xylose and galactose. Certain drugs containing, or metabolised to, the mentioned non-glucose sugars can lead to up to 15 fold

elevated blood glucose measurements which may result in inappropriate insulin administration. It has been revealed recently, that six people have died in healthcare facilities due to these interference problems since 2008. GDH-FAD and GDH-NAD as well as GOx based biosensors have shown to be unaffected by these non-glucose sugar interferences (Schultz, 2009; Hirsch *et al.*, 2010). However, more than 100 deaths associated with blood glucose monitoring were reported from 1992 to 2009 for various reasons (Newman, 2010).

4.3.2 Electrode interferences

All species which can be oxidised at the working potential are detected at the electrodes, therefore, sensors using blood as a sample are particularly susceptible to interference from ascorbic acid (vitamin C), uric acid and acetaminophen (paracetamol) (Piechotta *et al.*, 2005). Some methods have been applied to biosensors to diminish these interferences, but the perfect technique has not yet been found.

A widely applied technique is to coat the electrodes with a protective polymer barrier for size or charge exclusion. The problem is that this membrane suppresses the glucose signal as well and not every interfering compound can be excluded. Furthermore these layers showed limited *in vivo* operational stability (Piechotta *et al.*, 2005; Jia *et al.*, 2010). A pre-oxidising membrane was introduced to convert interferents into non electro-active species before they reach the electrode surface (Jia *et al.*, 2010). Also the introduction of mediators which shuttle electrons between the enzyme and the electrode to lower the working potential, hence leading to less oxidation of interferents, is widely used. This method suffers from low operational stability, particularly at biological pH values (7.35 – 7.45 in blood) (Ricci *et al.*, 2005). Another possibility is to use interstitial fluid instead of blood, resulting in lower interferences due to the lower concentration of interferents. The drawback of this method is a delay in sensor response. Two identical sensors, one with and one without the enzyme, have been used for differential measurement and derivation of the concentration without interferences. But the slightest difference between the two sensors leads to incorrect measurements, therefore costly high precision fabrication

methods are required (Piechotta *et al.*, 2005). Also electrophoretic separation of the neutral hydrogen peroxide and the anionic uric acid and ascorbic acid before detection was applied resulting in a more complicated, hence a more error-prone and a more expensive device (Wang, 2002).

4.4 Fouling problem

In vivo applications encounter many issues due to fouling of the interfaces of biosensors by proteins and cells. Therefore much effort has been spent in the development of new materials which mimic physiological properties in order to increase functional stability (Turner, 1992; Zhang *et al*., 2000).

The most promising way to prevent fouling is by the modification of polymers, but it is still not satisfactory for long-term continuous biosensor applications in biological fluids such as blood. Electro-polymerisation, to create films of conducting polymers on electrode surfaces, minimised electrode fouling. Also polypyrrole films, with a subsequently covalently bonded redox-dye, prevented fouling of the electrodes. Attempts to bond anticoagulants such as heparin onto artificial surfaces were not very successful. This only reduced the rate of fouling, not the end result, furthermore, it leached from the surface into the sample solution (Turner, 1992; Zhang *et al*., 2000).

4.5 State of the art

Glucose biosensors used in diabetes care are, currently, disposable strips for finger prick tests, minimally invasive alternative site continuous biosensors for ISF sensing, either wearable or as bedside monitors, or, but rarely used, invasive continuous glucose biosensors for measurement in whole blood. Also alternative site capillary blood monitoring is available, as it makes testing less painful than the finger prick tests, although there are many controversies about the lag time as well as in ISF testing. The continuous monitoring device use is on the increase, as it provides important glucose trend data and is more convenient for the user. To obtain blood glucose information with non-invasive methods has been tried for decades, but no commercially available product can compete with the other techniques in terms of accuracy and reliability (Jungheim and Koschinsky, 2002; Ferrante do Amaral and Wolf, 2008).

4.5.1 Conventional finger prick testing

Currently the management of diabetes mellitus is based on this method in order to minimise complications. Disposable finger prick test strips are used in conventional diabetes therapy, which means an estimation of the amount of insulin to administer based on glucose measurement and the amount of carbohydrates in the intended meal. The major drawbacks of this method are the lack of continuous control and trend data, infection risk, tissue and nerve damage, and discomfort of finger pricking (Wilkins and Atanasov, 1996; Ferrante do Amaral and Wolf, 2008).

4.5.2 Continuous measurement glucose biosensors

During recent decades, much effort has been spent in the development of minimally invasive glucose biosensors for ISF. Despite the controversies in the correlation of glucose levels in blood and ISF, especially during rapid concentration changes, this is the most promising way towards implantable closed loop systems today. Such a device represents the first example of individualised medical care. To date, the key obstacles of this artificial pancreas system are long term stability, due to biofouling and enzyme degradation, and interferences from electro-active species. Less attention has been given recently to continuous glucose monitoring systems for measurement in whole blood, due to the biocompatibility problems which have not been overcome yet (Wilkins and Atanasov, 1996; Wang, 2008).

4.5.3 Non-invasive glucose measurement

Non-invasive measurement means to obtain information without mechanical intervention, by the remote detection of characteristic properties of the analyte. Many methods have been tried so far, such as reverse iontophoresis, polarimetry, fluorescence, metabolic heat conformation, ultrasound and electromagnetic, as well as different spectroscopy techniques such as near-infra-red absorption, photoacoustic, Raman, thermal emission and bioimpedance. Another approach for non-invasive glucose measurement is the analysis of excreted body fluids such as saliva, urine, sweat or tears. Generally speaking, there is no meaningful correlation between blood glucose levels and

the concentration in physiological fluids. First, there are many non-pathologic factors which can affect these fluids, such as diet and exercise. Second, the lag-time between excreted fluids and blood glucose concentration can be very long. Although many patents have been filed during the past decades, none of the proposed methods has achieved comparable precision, accuracy, sensitivity and reliability to the standard invasive glucose measurement techniques (Wilkins and Atanasov, 1996; Ferrante do Amaral and Wolf, 2008).

5 Enzymes as biological recognition element

The biological component of the biosensor in the case of this work is the enzyme glucose oxidase (GOx). This section explains what enzymes are and what they do in general. The advantages and disadvantages of the different enzyme immobilisation methods are listed. Moreover, the widespread applications of the used enzyme GOx are described and the reaction mechanism is shown.

5.1 Enzymes in general

An enzyme is a large polypeptide macromolecule composed of proteins which mediates the catalysis of biochemical reactions. It speeds up the reaction of a substrate to a product, but does not undergo a chemical change itself. Enzymes are characterised by high acceleration rates of catalysis (turnover rates of 10^2 – 10^5 per second) and high selectivity for the appropriate substrate (Wang, 2002).

5.2 Enzyme immobilisation methods

Immobilisation means the attachment of a soluble biomolecule, such as an enzyme, to a solid phase to make it insoluble and therefore reusable. There are several available approaches for enzyme immobilisation. The following list gives a short overview of the methods used and the advantages and disadvantages of each. Figure 6 shows the basic principle of each immobilisation method described.

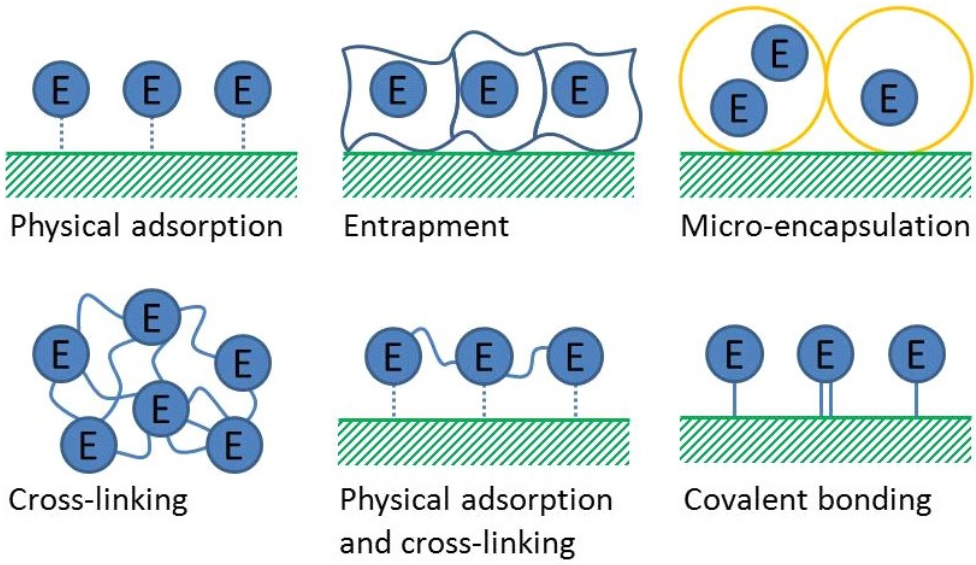

Figure 6: Principles of different enzyme immobilisation methods (adapted from Turner et al., 1987)

5.2.1 Physical adsorption

This is the oldest, and one of the simplest immobilisation methods (Wu *et al*., 2004). It uses only weak binding forces such as Van der Waals' interaction, multiple salt linkages, electron transition complexes and hydrogen bonds. It was one of the most used methods in earlier days, as it works well on cellulose support materials (Trevan, 1980; Turner *et al.*, 1987; Price and Stevenson, 1999; Malhotra and Turner, 2003).

Advantages: Physical adsorption is simple, inexpensive and usually needs no reagents or chemical surface modification (Turner *et al.*, 1987; Gizeli and Lowe, 2002).

Disadvantages: Due to the weak binding forces, the immobilisation is relatively unstable. It gains generally low yields and on hydrophobic surfaces denaturation can lead to partially or totally inactivation. Changes of pH, temperature and solvent or ionic strength can lead to desorption. These conditions can be maintained in many applications but also the addition of the substrate can cause troubles, and no enzyme can work without the substrate (Trevan, 1980; Gizeli and Lowe, 2002; Malhotra and Turner, 2003).

5.2.2 Entrapment

The enzyme to immobilise is trapped within a matrix of a polymer, paste or ink. The pore size has to be big enough for the substrate and the product molecule to pass through and ideally restrict any other species which could cause interference (Turner *et al.*, 1987; Gizeli and Lowe, 2002; Wu *et al*., 2004).

Advantages: Often used today, as it can be produced on a large scale. Furthermore it improves the enzyme stability (Gizeli and Lowe, 2002; Wu *et al*., 2004).

Disadvantages: Free radicals can cause denaturation, the diffusion is limited for big substrates and some pores may be big enough for enzymes to escape. The latter problem can be solved by additional cross-linking (see Section 5.2.4) (Turner *et al.*, 1987; Gizeli and Lowe, 2002).

5.2.3 Micro-encapsulation

In this method the whole enzyme solution is immobilised into an artificial membrane, similar to the cell membrane in natural cells. The small substrate and product species cross this barrier by diffusion, while the big enzyme is enclosed within the synthetic membrane (Malhotra and Turner, 2003).

Although there are some advantages over other immobilisation methods this is not very widely used in biosensor applications (Malhotra and Turner, 2003).

Advantages: It is a simple method for immobilisation of macromolecules. A particular advantage over entrapment is higher surface area per enzyme (Malhotra and Turner, 2003).

Disadvantages: It is difficult to produce on a large scale. Furthermore the response is slower due to the diffusion limitation of the membrane. Small molecules and ions can diffuse across the barrier and cause interferences (Price and Stevenson, 1999; Gizeli and Lowe, 2002).

5.2.4 Cross-linking

Cross linkers are bi-functional chemical agents that lead to polymerisation and can bind enzymes to solid supports. Cross-linking is often used in combination

with other immobilisation methods such as entrapment and micro-encapsulation but most widely with physical adsorption (Turner *et al.*, 1987).

Advantages: The cross-linking agent most widely used is glutaraldehyde, which is cheap and available in industrial quantities (Price and Stevenson, 1999).

Disadvantages: Causes cross-linking of the enzyme to itself, which leads to lower activity, as some enzymes serve only as support. Furthermore diffusion limitations and low mechanical strength are an issue (Malhotra and Turner, 2003).

5.2.5 Covalent bonding

In this immobilisation method, covalent bonds are formed between the enzyme, and either a membrane matrix, or directly the surface of the support material. Therefore functional groups, other than these at the active site of the enzyme are used, to sustain its activity. A technique to protect the enzyme's activity is to immobilise it in the presence of the substrate or a suitable competitive inhibitor (Turner *et al.*, 1987; Malhotra and Turner, 2003; Wu *et al*., 2004).

Advantages: This is the most stable immobilisation method due to the covalent binding forces. Furthermore there are low diffusion limitations resulting in a high enzyme turnover rate (Gizeli and Lowe, 2002).

Disadvantages: It is more expensive and complicated, as it usually requires the modification of the support surface, called activation. This derivatisation introduces the functional groups involved in the immobilisation procedure (Gizeli and Lowe, 2002; Malhotra and Turner, 2003).

5.3 Choice of immobilisation method

As there is too little knowledge available today to predict the exact consequences of the immobilisation procedure on the enzyme structure and activity, the method is usually chosen and optimised empirically. However, there are some considerations which have to be taken into account, such as the type of support material, the reaction conditions and the physical properties of the analyte (size and charge of the molecule). Anyway, the most widely used

techniques are covalent bonding and adsorption (Malhotra and Turner, 2003; Wu *et al*., 2004).

5.4 Applications of glucose oxidase

The enzyme GOx is one of the most important proteins used in industrial procedures today. It is of high commercial interest and used in many applications, such as biosensors, for monitoring glucose concentrations in body fluids for diabetes care, but also for glucose determination in the fermentation industry. In the food and beverage industry it is used as an additive to extend shelf life and as a colour and flavour stabiliser. GOx is used in oral hygiene products as anti-microbial agent and bactericide. It is used for the production of gluconic acid and in the textile industry for bleaching and de-coloration processes. Another application is the production of electrical energy by conversion of biochemical energy using GOx as a biocatalyst in biofuel cells (Bankar *et al.*, 2009).

5.5 Reaction mechanism of glucose oxidase

Glucose is oxidised by GOx in the presence of molecular oxygen, according to Equation 1, to glucono-δ-lactone and hydrogen peroxide.

$$Glucose + O_2 \rightleftharpoons Glucono-\delta-lactone + H_2O_2 \quad (1)$$

The produced glucono-δ-lactone is hydrolysed spontaneously in the presence of water, as shown in Equation 2, to gluconic acid.

$$Glucono-\delta-lactone + H_2O \rightleftharpoons Gluconic\ acid \quad (2)$$

The first glucose biosensors measured the consumption of oxygen during the reaction in Equation 1, to determine the glucose concentration. Today, the electro-active product H_2O_2 (see Equation 1) is used for electrochemical detection (Rose, 1980). Figure 7 shows the principle of the glucose biosensor exploiting this reaction mechanism and Section 7.3 describes the reaction at the electrode in greater detail.

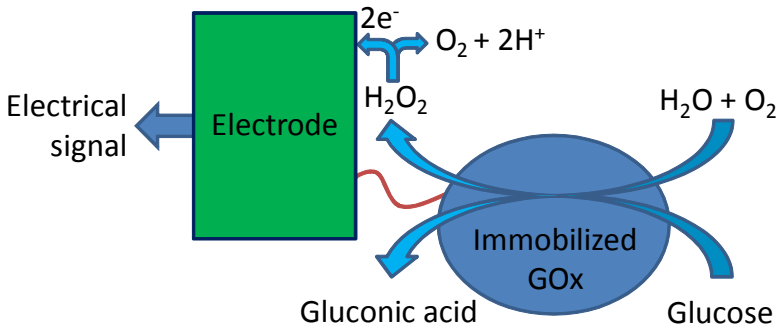

Figure 7: Glucose biosensor operating principle

6 Microfluidics

This section starts with a general description, followed by the history of microfluidics. The advantages are discussed, then some micro-fabrication techniques are elucidated. The underlying theory of the microfluidic phenomena is explained and functions already implemented are listed. Some possible applications are given followed by the last point, which is state of the art.

6.1 General description

Previously the slogan for technical devices has been: the bigger the better. During recent decades this motto has changed in several technological areas to: miniaturisation as far as possible. This trend is illustrated by computerisation, where smaller packing density is the equivalent of higher processing power. The silicon technology used in the semiconductor and microprocessor industries has pioneered many microfluidic device production methods (Fiorini and Chiu, 2005). Microfluidics is the manipulation and measuring of chemical, physical and biological processes through a combination of micro and nano-scaled production technology with the unique physical characteristics of fluids at these small volumes (Jönsson, 2004). Hence, it is not only about downscaling existing devices, but also taking advantage of these unique properties, which are further discussed in Section 6.5.

6.2 Brief history of microfluidics

More than thirty years ago, the first miniaturised device for analytics, a gas chromatographic analyser, was produced using a silicon fabrication technique. Due to the lack of fabrication technology at that time the response of the scientific and research community was virtually non-existent. Not until 1990 did

the principle of analytical miniaturised devices re-emerge by way of the fabrication of an open-tubular liquid chromatograph. As the analytical performance of sensors at this time was rather poor, the initial reason for miniaturisation was to increase the selectivity and lifetime of the devices. The reduction in the size of the device and the decreased reagent consumption were noted simply as a positive side effect. At the same time the micro-total analysis systems (μTAS) principle was proposed for the first time. A μTAS performs one or even several laboratory analysis procedures, starting from sample preparation, through processing to detection, on one single microfluidic chip. From 1994 on, the number of publications on μTAS increased rapidly. New approaches in micro-fabrication, analytical, and detection methods broadened the application of on-chip based analysis. This led to the first commercially available microfluidic products. In subsequent years, the so far used silicon fabrication techniques, were extended by the utilisation of new materials and micro-fabrication methods to expand the range of applications (Reyes *et al*., 2002). Today research continues to progress and utilises new materials, fabrication approaches, and separation and mixing methods, optimising the performance of biochemical reactors and detection techniques, *etc*.

6.3 Advantages over macrofluidic systems

The advantages of microfluidic devices are the possibility for point of care use, reduced sample and reagent consumption, high versatility and reduced production costs, coupled with shorter reaction times and increased sensitivity, specificity and reproducibility of analyses (Wang, 2002; Vandaveer *et al*., 2004). Furthermore they require fewer, or preferably even no, additional laboratory equipment, reagents, sample preparation and external power sources. This results in increased portability due to reduced size of the devices and less service and maintenance costs leading to less overall costs per test (Weigl *et al*., 2008). Also sample contamination is avoided due to automation of the assay as far as possible (Wang, 2002). This means reduced involvement of humans for sample preparation, and manual reagent or buffer additions during the analysis procedure.

6.4 Micro-fabrication techniques

In the early years silicon or glass substrates dominated microfluidics production due to their excellent surface properties, chemical and physical stability and the already existing micro-fabrication technology from the semiconductor industry. Today the trend is moving towards polymer substrates due to the complicated manufacturing processes (clean room environment, difficult etching procedures) and cost of glass and silicon substrates. Polymers are low cost and available with almost any desired surface properties. Furthermore, they offer an easier fabrication and are, therefore, more efficient and economical (Reyes *et al*., 2002; Fiorini and Chiu, 2005; Baharudin, 2008).

The choice of micro-fabrication method is determined by the number of devices to produce, whether the technique should be suitable for mass production or for prototyping. The fabrication method in turn dictates the possible substrate materials (Fiorini and Chiu, 2005; Baharudin, 2008).

As already mentioned, micro-fabrication techniques are differentiated by silicon or glass, and polymer based methods.

6.4.1 Silicon and glass micro-fabrication

The fabrication technology of silicon based microfluidics is comprised of photolithography, thermal growth of silicon oxide, etching, vapour deposition, epitaxy, and anodic bonding. On glass based substrates, also lithography and etching, are used amongst newer technology such as powder blasting (Fiorini and Chiu, 2005).

6.4.2 Polymer micro-fabrication

On polymer based substrates, fabrication techniques are further differentiated into the following two categories:

Replication methods

In replication methods a metal precision master is fabricated from which many identical polymer copies are produced. This technique is preferable for large scale production, due to high complexity and price. The most used replication

techniques are hot embossing, injection molding and soft lithography (Klank *et al*., 2002; Fiorini and Chiu, 2005).

Direct methods

In direct methods the micro-structures are machined directly without the use of a master. These techniques are suitable for prototype production, as changing the microfluidics layout is relatively inexpensive. The most used direct methods are optical and x-ray lithography and laser photoablation (Fiorini and Chiu, 2005).

The direct method for micro-fabrication, which is used in this project, is further described here. It is possible to use CO_2-laser-cutting and subsequent lamination of polymer layers in order to obtain the desired three dimensional structures (see Figure 10). Unlike ultraviolet (UV) lasers which ablate polymers by a combination of photochemical and photothermal processes, CO_2-lasers work with infrared radiation (at a wavelength of 10.6µm) and break chemical bonds only photothermally. CO_2-laser systems provide a less costly alternative to UV-lasers for rapid prototyping, although the minimal feature size is bigger. Originally, they were used to print logos, signatures and bar codes onto plastic surfaces. The structure of the cut micro-channels is determined by the laser power, the focus point, the scanning speed and the number of repetitions of the laser beam as well as the polymer material used (Klank *et al.*, 2002).

6.5 Microfluidic characteristics

Miniaturisation of analytical devices is not only a matter of downscaling of conventional designs. At the micro-scale, different effects and phenomena, which are negligible in macroscopic devices, become important. These unique effects can be utilised to create new analytical instruments, which do not have a counterpart at the macro-scale (Brody and Yager, 1997).

6.5.1 Laminar flow

There are two basic regimes of fluid flow: laminar and turbulent. Laminar flow implies convective mass transfer only in the flow direction, whereas in turbulent flow convection takes place in all directions. Whether a flow is laminar or

turbulent is characterised by the dimensionless Reynolds number (Re), which is calculated as the ratio of inertial and viscous forces. It is defined as shown in Equation 3.

$$Re = \frac{u D_h}{\nu} \tag{3}$$

Where u is the characteristic flow velocity ($m \cdot s^{-1}$) in the channel, D_h the hydraulic diameter (m) of the channel and v the kinematic viscosity ($m^2 \cdot s^{-1}$) of the fluid. Below a critical value of Re in the range of about 1000 – 2000 the flow is laminar, this means that viscous forces are dominant. Above the critical value the flow is turbulent, which means random eddies and vortices in the fluid are caused by inertial forces. The exact transition Reynolds number is dependent on many factors such as channel shape, aspect ratio and surface properties (Nguyen and Wereley, 2006).

6.5.2 Diffusion

The spreading of particles in a solvent due to the Brownian motion is defined as diffusion. It is caused due to thermal energy and described for spherical molecules in a low Reynolds number fluid by the Einstein-Stokes equation, shown in Equation 4.

$$D_f = \frac{k_B T}{3 \pi \eta d} \tag{4}$$

Where D_f is the molecular diffusion coefficient ($m^2 \cdot s^{-1}$), k_B the Boltzmann's constant ($J \cdot K^{-1}$), T the absolute temperature (K), η the dynamic viscosity (Pa·s) of the fluid and d the diameter (m) of the spherical representation (same volume) of the molecule (Breuer, 2005). D_f is a measure for how far molecules diffuse over time. Broadly speaking, the larger the molecule the smaller the diffusion coefficient, hence the distance travelled in a certain time interval decreases with molecular weight. Equation 6 shows the calculation of the diffusion time for a particle moving in a laminar fluid stream and the relation to the diffusion coefficient. Due to the small size of microfluidic devices, diffusion plays an important role as a means of mass transfer, whereas in macroscopic devices it is negligible (Jönsson, 2004). Two microfluidic devices exploiting

these diffusion effects for diffusion-based separation are, the T-sensor and the H-filter. The principle of the H-filter is further described in the following section, as it is used for the proposed biosensor in the project.

H-filter

One example of a device taking advantage of diffusion in microfluidics is the H-filter, where two parallel laminar streams of fluid flow are brought in direct contact with each other. Due to the laminar nature of the flow they do not mix. The only occurring mass transfer between the fluid streams is due to diffusion. This phenomenon can be used to extract the desired component of a fluid due to the fact that small molecules diffuse faster than large ones without the need for a physical membrane or filter (Weigl *et al*., 2008; Collier and Hart, 2005). Figure 8 shows a scheme and the basic working principle of the intended H-filter in this project.

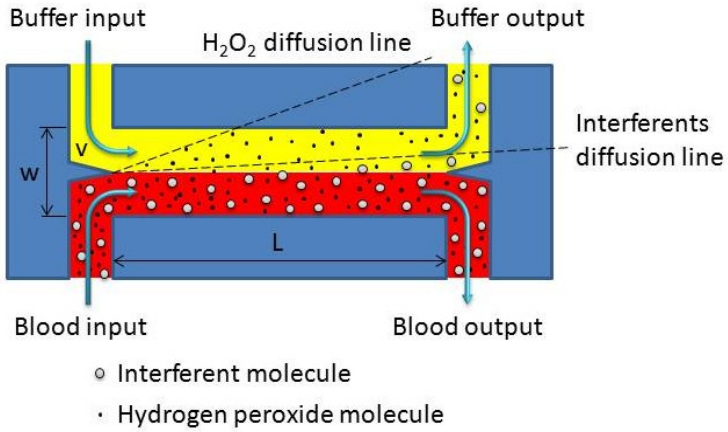

Figure 8: Top view scheme and basic working principle of the H-filter (adapted from Hartmann and Sasso, 2007)

There are two time-scales which characterise the H-filter: the convection time (t_{conv}; see Equation 5) which is the time it takes for the fluid to flow from the inlet to the outlet of the main channel and the diffusion time (t_{diff}; see Equation 6) which refers to the time it takes for a molecule to diffuse across the half width of the main channel.

$$t_{conv} = \frac{L}{v} \tag{5}$$

Where L is the length (m) of the main channel and v the flow speed ($m \cdot s^{-1}$) (see Figure 8).

$$t_{diff} = \frac{(\frac{1}{2}w)^2}{D_f} = \frac{w^2}{4D_f} \quad (6)$$

Where w is the width (m) of the main channel and D_f the diffusion coefficient ($m^2 \cdot s^{-1}$) (see Figure 8).

The H-filter works optimally, if the following specifications are fulfilled: $t_{diff\ H2O2} << t_{conv} << t_{diff\ interferents}$. There are two parameters which can be changed to achieve this situation: either the length or the flow rate of the system (Hartmann and Sasso, 2007).

6.6 Functions of microfluidics

The functions already implemented on microfluidic chips comprise fluid control techniques such as valves, pumps and mixers, analytical separation methods such as chromatography and electrophoresis, and detection techniques such as electrochemical or optical detection (Fiorini and Chiu, 2005).

6.7 Applications of microfluidics

Microfluidics have a broad range of possible applications, particularly in biological, pharmaceutical and medical chemical analysis procedures. The technology is moving forward rapidly towards commercialisation of products in many fields such as drug discovery, tissue engineering, cell culturing, genomics, routine health care, *in vitro* fertilisation (for human and veterinary medicine) and *in situ* environmental monitoring (Fiorini and Chiu, 2005).

6.8 State of the art

Microfluidics are already implemented as lab-on-chip (LOC) or µTAS, which are able to perform sample handling, analysis and detection, all integrated into one hand-held device, easy and robust enough to be used by non-professionals (Fiorini and Chiu, 2005; Baharudin, 2008). The already available advantages over macrofluidic systems, coupled with the currently ongoing research in this field, will make microfluidic devices the tool of choice for many applications in chemistry, physics and biology within the next years.

7 Electrochemical detection

This section describes the electrochemical methods in more detail. Further it explains not only the underlying detection principle, but also the whole measuring setup for this project. The last point states the chemical reaction at the working electrode.

7.1 Detection methods

As already mentioned in Section 3.2, in addition to electrochemical detection, other possible transducers for biosensors include optical, acoustic, calorimetric, micro-mechanical and magnetic ones. The electrochemical detection techniques can be further classified into the following categories.

7.1.1 Potentiometry

Potentiometry is the virtually current-less measurement of the potential difference between two electrodes which are separated by a selectively-permeable membrane. Therefore one electrode is coated with an ion-selective film, resulting in an ion-selective electrode (ISE) combined with a biological recognition element on the surface. The measured potential difference is proportional to the logarithm of the ion activity and therefore to the analyte concentration according to the Nernst equation (Thévenot *et al.*, 1999; Malhotra and Turner, 2003). For room temperature (25°C) and low concentrated solutions (total ionic concentration less than 10mM) the Nernst equation can be simplified to Equation 7.

$$E = E^0 - \frac{0.05916\text{V}}{z} \log \frac{c_{red}}{c_{ox}} \tag{7}$$

Where E is the potential (V) of the electrochemical cell, E^0 is the standard reduction potential (V), z is the number of transferred electrons, and c_{red} and c_{ox} are the concentrations (M) of the reductant and the oxidant, respectively (Lower, 2010).

Another device that operates via potentiometry is the ion-selective field-effect transistor (ISFET). Field-effect transistors are electronic components which can vary the conductivity between two terminals, namely drain and source dependent, on the applied voltage on a third terminal called gate. In the case of

an ISFET, this gate terminal is covered by an ion-selective membrane and a biological recognition element. If this element is of a biocatalytic nature it becomes an enzyme field-effect transistor. In the case of a bioaffinity based biosensor, it is called an immunological field-effect transistor. The operation characteristics are similar to ISE based sensors (Thévenot *et al.*, 1999). The principle was never really caught on because of fabrication problems leading to relatively high production costs.

7.1.2 Amperometry

Amperometry is the measurement of the current produced by the oxidation or reduction of an electro-active compound. This in turn is produced by the biological recognition element, at a defined constant potential of the working electrode (usually platinum, gold or carbon electrode) relative to a reference electrode (mainly silver/silver-chloride electrode) which, in the simplest format serves as the counter electrode at the same time. The detected current is directly proportional to the analyte concentration at the biological recognition element of the biosensor (Thévenot *et al*., 1999). In practical biosensor applications amperometry is more widely used than potentiometry, due to its lower sensitivity to input signal variations and its easier handling due to the linear sensor response (Prudenziati, 1994).

7.1.3 Conductometry

Conductometry is the measurement of change in conductivity and impedance, respectively, due to a change in the ionised compounds in the analyte solution. These ionised species are produced by the biological recognition element and are therefore proportional to the analyte concentration (Malhotra and Turner, 2003).

7.2 Measuring setup for the proposed biosensor

The biosensor built in this project is comprised of three screen-printed electrodes for amperometric measurement (three electrode system). The working and the counter electrode consist of carbon ink. The reference electrode consists of silver/silver-chloride ink, as this is one of the most used in practical measurements, particularly in microsystems, due to its simplicity and

reproducibility (Scholz, 2002). Amperometric measurement is carried out at a constant potential, which detects the reaction discussed in Section 7.3.

7.2.1 Three electrode system

A three electrode system consists of a working electrode (WE), a reference electrode (RE) and a counter electrode (CE) (also referred to as auxiliary electrode). The WE is the electrode at which the reaction to investigate occurs. The current is passed between the WE and the CE. The RE is operated under virtually no current, and provides a stable, drift-free potential which serves as the reference voltage. An electronic instrument called a potentiostat is used to control the mentioned electrode conditions. It maintains the potential of the WE with respect to the RE by adjusting the current at the CE. The electrode arrangement can be either with or without (as in the case of this project) a salt bridge between the measuring and the reference system (Scholz, 2002).

7.2.2 Screen-printing

Screen-printing is a thick film technology, which is probably one of the oldest forms of graphic art reproduction. It was adapted to screen-print electronic circuits in the 1950s and paved the way for many biosensor applications due to its low cost, reproducibility, robustness and its possibility for mass production (Prudenziati, 1994; Newman and Turner, 2005). Figure 9 shows the basic screen-printing process.

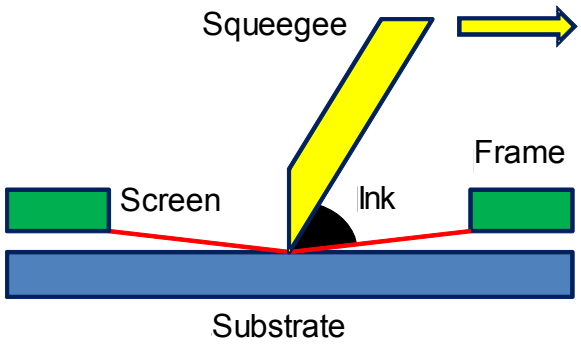

Figure 9: Screen-printing process (adapted from Prudenziati, 1994)

The paste (also called ink, due to its origins in art) is squeezed through a patterned finely woven mesh, the so-called screen, which is mounted on a frame, by a squeegee onto a solid support, the substrate. The deposited ink film

is then cured by heating. One of the early problems was that the available inks had to be cured at high temperatures, hence costly ceramic supports were required. Today there is a wide range of inks for low temperature curing available, which makes the use of inexpensive and easy to manufacture polymer substrates possible (Prudenziati, 1994; Newman and Turner, 2005).

7.3 Reaction at the working electrode

At a certain electrode potential against the silver/silver-chloride reference electrode, the hydrogen peroxide produced by GOx (according to Equation 1 and Figure 7) is further oxidised at the carbon working electrode according to Equation 8.

$$H_2O_2 \rightarrow O_2 + 2\mathrm{H}^+ + 2e^- \quad (8)$$

The produced H_2O_2, hence the produced electrons, are directly proportional to the glucose concentration. The resulting current is quantified by amperometry.

8 Summary of the project

For this project, an enzymatic glucose biosensor with amperometric detection was chosen, as this is one of the best studied biosensors in the literature and most widely applied in practice. The underlying principle of amperometry is described in further detail in Section 7.1.2 and the enzymatic reaction of glucose oxidase can be seen in Section 5.5. Figure 7 shows the basic working principle of such a glucose biosensor.

The biosensor is realised in the form of a microfluidic device, in order to minimise sample size as well as reagent consumption and to make use of the unique fluid characteristics at the micro-scale. Therefore an H-Filter device (see Section 6.5) is built with GOx immobilised on the top layer by physical adsorption and cross-linking with glutaraldehyde in the blood sample channel, near the input. The electrodes for detection are screen-printed in the buffer channel, near the output. The device is assembled by lamination of prior CO_2-laser-cut polymer layers. The layer-by-layer construction can be seen in Figure 10.

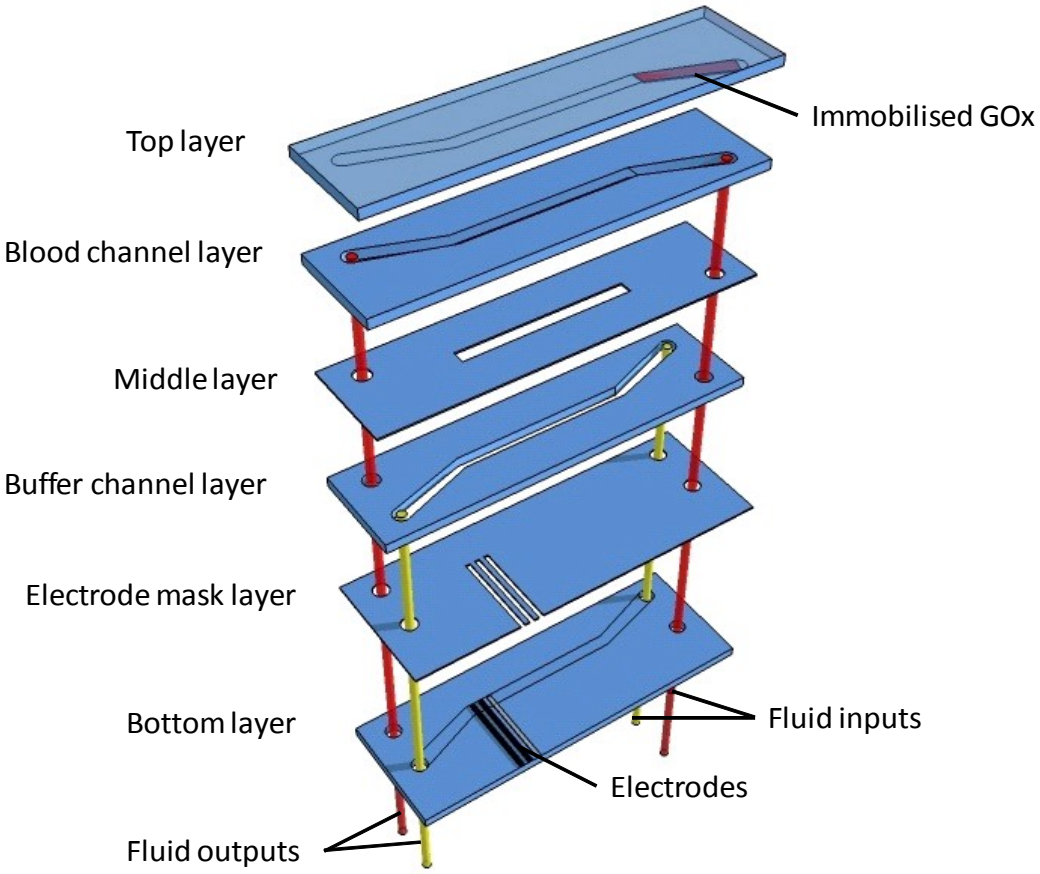

Figure 10: Scheme of layer assembly of the glucose biosensor

Detection is done by amperometry at a constant potential, which detects the electrons produced in the reaction shown in Equation 8. The working and the counter electrode consist of carbon, and the reference electrode of silver/silver-chloride ink.

CHAPTER II: MATERIALS AND METHODS

All procedures were carried out conform to the codes of practice and legal requirements of Cranfield University, School of Health.

1 Used buffer solutions, dilutions and samples

Unless stated differently, for all solutions and dilutions, 0.1M sodium phosphate buffer at pH 7.2, prepared according to Appendix A was used.

1.1 Human blood sample collection

1.1.1 Materials

Butterfly needle
Heparinised blood sample tube 9ml

1.1.2 Methods

The venous blood was taken by venepuncture by a phlebotomist from the Cranfield Medical Centre following safety and hygiene practices. It was collected in heparinised blood sample tubes in order to avoid clotting.

1.2 Viscosity adjustment by carboxymethyl cellulose

1.2.1 Materials

Sodium phosphate buffer 0.1M pH 7.2 (according to Appendix A)

Carboxymethyl cellulose sodium salt, 400 – 800 cps (Sigma-Aldrich, Gillingham, UK)

1.2.2 Methods

In order to avoid clumps, the carboxymethyl cellulose (CMC) powder was added step by step in small amounts to the buffer under constant shaking. For homogeneous distribution it was left on the shaker at 250rpm at room temperature overnight. Furthermore it has been shaken before the experiments at the same parameters for at least 30 minutes.

The methods for preparing the viscous buffer solution are discussed in more detail by Labbé (2010).

1.3 Viscosity adjustment by polyethylene glycol

1.3.1 Materials

Sodium phosphate buffer 0.1M pH 7.2 (according to Appendix A)
Polyethylene glycol av. mol. wt. 600 (Sigma-Aldrich, Gillingham, UK)

1.3.2 Methods

The appropriate volume of polyethylene glycol solution was mixed with the phosphate buffer by shaking briefly.

The methods for preparing the viscous buffer solution are discussed in more detail by Labbé (2010).

1.4 Staining of the used buffers

1.4.1 Materials

Sodium phosphate buffer 0.1M pH 7.2 (according to Appendix A)
Malachite Green (Pro-Lab Diagnostics, Neston, UK)
ZN Carbol Fuchsin (Pro-Lab Diagnostics, Neston, UK)
Eosin Y solution aqueous (Sigma-Aldrich, Gillingham, UK)
Coomassie blue R-250 (LKB-Reactifs IBF, Villeneuve-La-Garenne, France)

1.4.2 Methods

The appropriate stain was mixed, either 1:100, 1:50 or 1:25 depending on the used stain and the intensity wanted (in order to gain a good contrast), with the appropriate phosphate buffer solution by shaking briefly.

The methods for preparing the stained buffer solutions are discussed in more detail by Labbé (2010).

1.5 Hydrogen peroxide dilutions

1.5.1 Materials

Sodium phosphate buffer 0.1M pH 7.2 (according to Appendix A)
Hydrogen peroxide 35wt.% in water (Fisher Scientific, Loughborough, UK)

1.5.2 Methods

A stock hydrogen peroxide solution of about 10mM was prepared, by calculating the appropriate amount of H_2O_2 solution to add, and pipetting it into the

phosphate buffer solution. This solution was titrated according to Appendix B.A to determine the accurate concentration. Afterwards it was diluted to the intended concentrations with phosphate buffer solution.

1.6 Glucose dilutions

1.6.1 Materials

Sodium phosphate buffer 0.1M pH 7.2 (according to Appendix A)
D-(+)-glucose 99.5% (Sigma-Aldrich, Gillingham, UK)

1.6.2 Methods

A stock glucose solution of about 10mM was prepared, by calculating the appropriate amount of glucose to add and dissolving it in the phosphate buffer solution. After calculating the exact concentration based on the exact weight added, the solution was diluted to the intended concentrations with phosphate buffer solution.

1.7 Ascorbic acid dilutions

1.7.1 Materials

Sodium phosphate buffer 0.1M pH 7.2 (according to Appendix A)
L-ascorbic acid 99.7% (Sigma-Aldrich, Gillingham, UK)

1.7.2 Methods

A stock ascorbic acid solution of about 10mM was prepared, by calculating the appropriate amount of ascorbic acid to add and dissolving it in the phosphate buffer solution. After calculating the exact concentration based on the exact weight added, the solution was diluted to the intended concentrations with phosphate buffer solution.

1.8 Acetaminophen dilutions

1.8.1 Materials

Sodium phosphate buffer 0.1M pH 7.2 (according to Appendix A)
Acetaminophen 98% (Sigma-Aldrich, Gillingham, UK)

1.8.2 Methods

A stock acetaminophen solution of about 10mM was prepared, by calculating the appropriate amount of acetaminophen to add and dissolving it in the phosphate buffer solution. After calculating the exact concentration based on the exact weight added, the solution was diluted to the intended concentrations with phosphate buffer solution.

1.9 Uric acid dilutions

1.9.1 Materials

Sodium phosphate buffer 0.1M pH 7.2 (according to Appendix A)
Uric acid 99% (Fisher Scientific, Loughborough, UK)

1.9.2 Methods

A stock uric acid solution of about 2.7mM was prepared, by calculating the appropriate amount of uric acid to add and dissolving it in the phosphate buffer solution. Therefore it was put on a magnetic stirrer at 450rpm for at least 1 hour at 50°C. After calculating the exact concentration based on the exact weight added, the solution was diluted to the intended concentrations with phosphate buffer solution.

2 Device design

2.1 Materials

AutoCAD 2004 (Autodesk, San Rafael, USA)

2.2 Methods

The maximum dimensions of the sensor are given as 41×33mm, due to the maximum possible area the laser marking head is capable of cutting. The final design of the layers is shown in Figure 11. The methods for the design of the microfluidic device are discussed in more detail by Tu (2010).

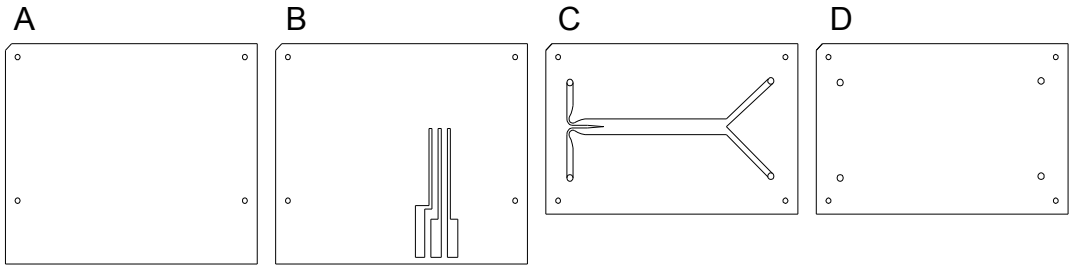

Figure 11: Separate layers of the microfluidic device; A: bottom layer, B: electrode mask layer, C: channel layer, D: top layer

The different layers were saved in separate files in the R12 (.dxf) format, in order to be importable into the laser marking software Synrad WinMark.

3 Laser-cutting

3.1 Materials

Fenix flyer 75W CO_2-laser marker (Synrad, Mukilteo, USA)

Synrad WinMark version 2.1.0.4056 (Synrad, Mukilteo, USA)

Polymer layers:

- Polyester sheet Melinex ST 725 254µm (Tekra, New Berlin, USA)
- PET sheet ARcare 8570 (Adhesives Research, Limerick, Ireland)
- PET sheet ARcare 8565 (Adhesives Research, Limerick, Ireland)
- PET sheet ARcare 90485 (Adhesives Research, Limerick, Ireland)
- PET sheet ARcare 8039 (Adhesives Research, Limerick, Ireland)
- PET tube Nalophan NS (Kalle UK Ltd, Witham, UK)

3.2 Methods

The in AutoCAD designed layers were imported into the WinMark software. During the importing procedure the original dimensions of the AutoCAD design were lost and needed to be adjusted manually. This was done by clicking on the button “Object Transformation”, adjusting the “New Width” to 41mm and clicking “Apply” (not “OK”, as then the aspect ratio was changed). Because the program approximates only to a value near 41mm (presumably due to grid size) at the first time, this step was repeated three times, until the width was truly at 41.0000mm. In order to fit the cutting requirements of the different polymer layers optimally, the most suitable settings were determined empirically by

comparing different configurations of laser velocity, power and mark count (repetitions) on each polymer layer (see Figure 12).

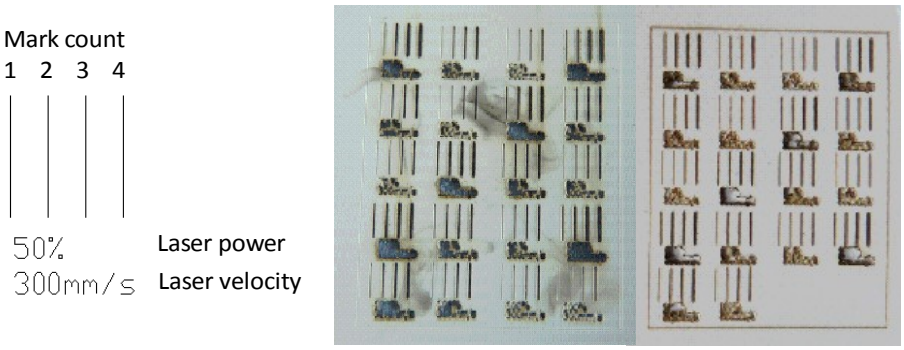

Figure 12: Empirical determination of the optimal laser settings on different polymer materials

Once this procedure was done, the file was saved as a WinMark (.mkh) file, which memorises all the adjusted dimensions and the determined laser settings. Finally, by clicking on the “Mark” button the software controlled the laser beam according to the AutoCAD design and the set parameters.

4 Alignment tool

4.1 Materials

Acrylic glass sheet 41×33×1.85mm (Hobbycraft, Milton Keynes, UK)
Wire wrapping socket 8way 0.3inch (RS-Components, Corby, UK)
Column drill
Drill 0.8mm
Hacksaw
File
Side cutter

4.2 Methods

The acrylic glass sheet was cut by a hacksaw and the sharp edges were filed smooth. Then the holes for the wire wrapping socket pins were drilled by a column drill according to the design of the bottom layer (see Figure 11). Afterwards the wire wrapping socket was cut into single pins and the plastic part was removed with the help of a side cutter. The resulting pins were pressed into the drilled holes.

5 Lamination

5.1 Materials

Laser-cut polymer layers (according to Section 3)
Alignment tool (see Section 4)
Hydraulic press Clark Strong-Arm
Scalpel

5.2 Methods

The bottom layer was placed in the alignment tool, then the protective layer of the polymer layer to stuck was removed with the help of the scalpel and put on top with the help of the alignment tool. The two layers were adhered together, taking care that no air bubbles were produced between them. The best way to prevent air entrapment was to start in the middle of the device pushing the two layers together with the help of the back of the scalpel handle stepwise, first in one direction, then in the other. This procedure was repeated for the residual polymer layers as well, until the complete device was assembled. As the layers were stuck by pressure sensitive adhesives (PSA), subsequently the device was put into a hydraulic press at two tons for at least one minute to establish stable bonding.

6 World-to-chip interface

6.1 Materials

PET sheet 41×25.5×3mm
Column drill
Drill 1mm
Drill 2.75mm
Hacksaw
File
4× Pump tubes red-red 1.14mm PVC (Anachem, Luton, UK)
Silicone rubber compound 555-588 (RS-Components, Corby, UK)
4× O-rings 1/16inch (B&Q, Milton Keynes, UK)
Pipette tip 200µl

6.2 Methods

According to the design of the top layer (see Figure 11) the PET sheet was cut by a hacksaw and the sharp edges were filed smooth. Then the holes for the alignment tool (1mm) and the tubes (2.75mm) were drilled using a column drill. Afterwards the tubes were inserted and fixed to the device by silicone on the top side. On the bottom side the o-rings were attached also by silicone in order to serve as gasket and seal the tube outlets (see Figure 22). The best way to apply the silicone paste was with the help of a pipette tip.

7 Electrode fabrication

7.1 Screen-printing

7.1.1 Materials

Silver/silver-chloride ink Electrodag 6038 SS (Acheson, Plymouth, UK)
Carbon ink Electrodag 423 SS (Acheson, Plymouth, UK)
Fenix flyer 75W CO_2-laser marker (Synrad, Mukilteo, USA)
Hydraulic press Clark Strong-Arm
Scalpel
Polymer layers:

- Polyester sheet Melinex ST725 254µm (Tekra, New Berlin, USA)
- PET sheet ARcare 8570 (Adhesives Research, Limerick, Ireland)
- PET sheet ARcare 8565 (Adhesives Research, Limerick, Ireland)

7.1.2 Methods

The double coated polymer layer ARcare 8570, was adhered to the bottom polyester layer (Melinex ST725), taking care that no air bubbles were produced between them. The best way to prevent air entrapment was to push the two layers together with the help of the back of the scalpel handle stepwise. Then the two layer composite was laser-cut (Melinex St 725 layer on the bottom and Arcare 5870 on the top) according to Figure 13 with the specifications according to Table 1.

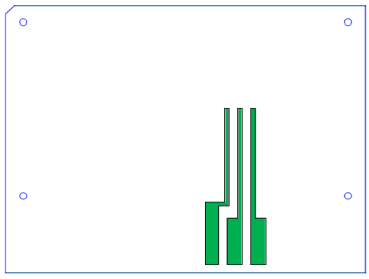

Figure 13: Bottom layer and electrode mask

Table 1: Laser parameters for cutting the two layer composite

	Laser settings		
	Velocity	**Power**	**Mark count**
Edge and holes (blue)	300 mm/s	80 %	7
Electrode mask (black)	380 mm/s	20 %	7

The protective layer was removed from the areas where the electrodes were located afterwards (see Figure 13, green area), forming the electrode channels. Then the carbon ink was deposited onto the two right channels for the working and the counter electrode and flattened by a spatula. After curing the device in the oven at 100°C for at least 30 minutes, the silver/silver-chloride ink for the reference electrode was deposited onto the left channel in the same manner as the carbon ink. It was cured again in the oven at 100°C for at least 30 minutes. These steps were repeated twice, to get a final count of three ink depositions (this value was determined by thickness measurements, see Section 7.2). Subsequently the top protective layer was removed, making the final electrode shape appear. In order to make it non-sticky again, the polymer layer ARcare 5865 was cut (protective layer on the bottom) according to the design of Figure 13, but this time the whole design was cut with the specifications for the edges and holes according to Table 1. The cut layer was adhered to the sticky top surface with the help of the alignment tool. After putting it into the hydraulic press at two tons for at least one minute, the top polymer layer was removed again, leaving behind the protection layer on the device.

7.2 Optimisation of electrode deposition

7.2.1 Materials

Device with electrodes (according to Section 7.1)
Microscope Digital USB 26/130 zoom (Stanley Gibbons, London, UK)
Fenix flyer 75W CO_2-laser marker (Synrad, Mukilteo, USA)
Blu-Tack (B&Q, Milton Keynes, UK)

7.2.2 Methods

The electrodes were produced according to Section 7.1, but three devices with a different number of ink depositions: two, three and four times, were fabricated. In order to produce a cross section of the electrodes, a one mm slice of the device was laser-cut according to Figure 14.

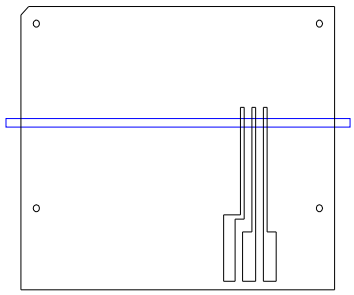

Figure 14: Device cut (blue rectangle) to produce a cross section of the electrodes

The cut slice was put in the microscope in an upright position with the help of Blu-Tack.

8 Microfluidic chip experiments

8.1 Calibration of the syringe pump

8.1.1 Materials

Sodium phosphate buffer 0.1M pH 7.2 (according to Appendix A)
Syringe pump Harvard Compact Infusion Pump Model 975
2× Precision glass syringe 5ml MT5L00 (Hawksley, Lancing, UK)
2× Precision glass syringe 10ml MT10L0 (Hawksley, Lancing, UK)

8.1.2 Methods

The syringe was filled with buffer and bubbles were pressed out. Then it was put into the syringe pump and the time required to collect a reasonable amount of fluid was measured. Subsequently, the volumetric flow rate was calculated.

8.2 Testing assembly

8.2.1 Material

Alignment tool (see Section 4)
World-to-chip interface (see Section 6)
Device with electrodes (according to Section 7)
2× Crocodile clips
2× Permanent magnets

8.2.2 Methods

The connection between the syringes and the microfluidic chip was established by aligning the o-rings of the world-to-chip interface with the holes of the device with the help of the alignment tool. The final testing assembly consisted of the alignment tool at the bottom, the microfluidic device in the middle and the world-to-chip interface on top, pressed together by permanent magnets. Alternatively two crocodile clips, one on the left and one on the right side of the assembly, were also used to press it together for the experiments.

8.3 Fluid conduct experiments

8.3.1 Materials

Syringe pump Harvard Compact Infusion Pump Model 975
2× Precision glass syringe 5ml MT5L00 (Hawksley, Lancing, UK)
2× Precision glass syringe 10ml MT10L0 (Hawksley, Lancing, UK)
Testing assembly (according to Section 8.2)
2× Recipients 10ml
Balance Sartorius BP 110 S
Spectrophotometer Shimadzu UV-1800

Samples:

Sodium phosphate buffer (different viscosities)

Hydrogen peroxide dilutions (different viscosities)

Ascorbic acid dilutions (different viscosities)

8.3.2 Methods

The device to be tested was put in the testing assembly according to Section 8.2. One syringe was filled with buffer, the other one with the appropriate sample and bubbles were pressed out. After connecting the tubes to the world-to-chip interface, the syringe pump was turned on at a flow rate of 860µl·s^{-1} to push the air out of the tubing and the channels. Then the appropriate speed was set at the syringe pump and the fluid was collected in two separate recipients. The amounts and the colour (if the sample was dyed) of the collected fluids were visually compared or in case of doubt with the help of a balance and a spectrophotometer, respectively. In the diffusion experiments (samples not dyed) the concentrations were determined by the appropriate titration.

9 Electrochemical experiments

9.1 Simulation of the channel

9.1.1 Materials

Device with electrodes (according to Section 7)

Insulating ink 242-SB protective polymer (ESL ElectroScience, King of Prussia, USA)

9.1.2 Methods

The prepared electrodes were coated with the insulating ink in order to have the same surface area as in the channel and cured in the oven at 100°C for at least 30 minutes.

9.2 Cyclic voltammetry

9.2.1 Materials

Device with simulated channel (according to Section 9.1)

Autolab module PGSTAT 10 (Eco-Chemie, Utrecht, Netherlands)

Electrochemical analyser software Gpes 4.9

DIP IC test clip
3× crocodile clips
Sodium phosphate buffer (according to Appendix A)
Hydrogen peroxide dilution 10mM
Potassium ferrocyanide 99% (Sigma-Aldrich, Gillingham, UK)

9.2.2 Methods

A 10mM potassium ferrocyanide solution in phosphate buffer was prepared. The device was connected to the Autolab workstation via the IC test clip and the crocodile clips. Subsequently 40µl of buffer, 10mM hydrogen peroxide dilution and potassium ferrocyanide solution, respectively have been applied to the electrodes. The voltammogram has been recorded using the parameters shown in Table 2.

Table 2: Settings used for cyclic voltammetry

Number of cycles	50
Start potential	-0.6V
First vertex potential	+1.0V
Second vertex potential	-0.6V
Step rate	0.02V
Scan rate	$0.2V \cdot s^{-1}$

The electrodes were wiped dry with a tissue after each measurement before applying the next sample.

9.3 Amperometry in beaker

9.3.1 Materials

Device with simulated channel (according to Section 9.1)
Beaker 250ml
Autolab module PGSTAT 10 (Eco-Chemie, Utrecht, Netherlands)
Electrochemical analyser software Gpes 4.9
DIP IC test clip
3× crocodile clips
Magnetic stirrer
Sodium phosphate buffer (according to Appendix A)
Hydrogen peroxide 35wt.% in water (Fisher Scientific, Loughborough, UK)

9.3.2 Methods

The device was cut according to Figure 15.

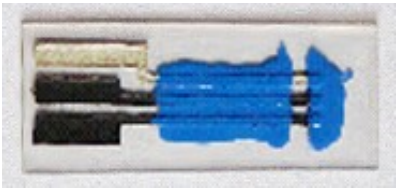

Figure 15: Cut device with simulated channel

The beaker was filled with 250ml phosphate buffer and put on the stirrer at 350rpm at room temperature. The electrical connection of the prepared device to the Autolab workstation was established via the IC test clip and crocodile clips. Then it was dipped into the buffer, so that the electrodes in the simulated channel were in contact with the fluid.

A series of measurements with different voltages (0.6V, 0.7V, 0.725V, 0,75V, 0.775V, 0.8V, 0.825V, 0.85V, 0.9V, 1.0V) was carried out, each with H_2O_2 concentrations increasing from 0 to 9mM. Equation 9 shows the calculation for the amount of H_2O_2 to add to obtain an increase of 1mM.

$$c \cdot FW \cdot V \;=\; m \;=\; 0.001\,mol \cdot l^{-1} \cdot 34\,g \cdot mol^{-1} \cdot 0.25\,l \;=\; 8.5\,mg \tag{9}$$

Where c is the concentration, FW the functional weight, V the volume and m the mass. As a 35wt.% H_2O_2 solution was used and based on the assumption that the density of the solution is equal to water (8.5mg ≙ 8.5µl), Equation 10 calculates the volume of the solution to add.

$$V_1 \;=\; \frac{c_2 \cdot V_2}{c_1} \;=\; \frac{100\,\% \cdot 8.5\,\mu l}{35\,\%} \;=\; 24.3\,\mu l \tag{10}$$

While recording the amperogram every 100 seconds the concentration was increased stepwise by 1mM by adding 24.3µl of hydrogen peroxide solution. The parameters according to Table 3 were used for the amperometry.

Table 3: Settings used for amperometry on cut device in a beaker

Mode	DC amperometry
Pretreatment	none
Interval time	0.2s
Run time	1000s
Potential	0.8V
Standby potential	0.0V

9.4 Amperometry on device with simulated channel

9.4.1 Materials

Device with simulated channel (according to Section 9.1)

Autolab module PGSTAT 10 (Eco-Chemie, Utrecht, Netherlands)

Electrochemical analyser software Gpes 4.9

DIP IC test clip

3× crocodile clips

Samples:

Sodium phosphate buffer (according to Appendix A)

Hydrogen peroxide dilutions (1mM, 2mM, 3mM, 4mM, 5mM)

Ascorbic acid dilutions (1mM, 2mM, 3mM, 4mM, 5mM)

Acetaminophen dilutions (1mM, 2mM, 3mM, 4mM, 5mM)

Uric acid dilutions (0.5mM, 1mM, 1.5mM, 2mM, 2.5mM)

9.4.2 Methods

The electrical connection to the Autolab workstation was established via the IC test clip and crocodile clips. The measurement was started and after 20s, 40µl of the sample was applied to the electrodes. The amperogram was then recorded using the parameters shown in Table 4.

Table 4: Settings used for amperometry on device with simulated channel

Mode	DC amperometry
Pretreatment	none
Interval time	0.4s
Run time	200s
Potential	0.8V
Standby potential	0.0V

The electrodes were wiped dry with a tissue after each measurement before applying the next sample.

9.5 Amperometry on device with channel

9.5.1 Materials

Device with electrodes (according to Section 7)
Testing assembly (according to Section 8.2)
Autolab module PGSTAT 10 (Eco-Chemie, Utrecht, Netherlands)
Electrochemical analyser software Gpes 4.9
DIP IC test clip
3× crocodile clips
2× Precision glass syringe 5ml MT5L00 (Hawksley, Lancing, UK)
Syringe pump HARVARD Compact Infusion Pump Model 975
Samples:

Sodium phosphate buffer (according to Appendix A)
Hydrogen peroxide dilutions (different concentrations)

9.5.2 Methods

The device was put in the testing assembly according to Section 8.2. The syringe was filled with the appropriate sample and bubbles were pressed out. Then it was put into the syringe pump which was set to 860µl·s^{-1} and the tubes were connected to the world-to-chip interface. The electrical connection to the Autolab workstation was established via the IC test clip and crocodile clips. After switching on the syringe pump and waiting until the air inside the connection tubes and the device had been pushed out, the measurement was started with the parameters shown in Table 5 at a flow rate ot 1.5µl·s^{-1}.

Table 5: Settings used for amperometry on device with channel

Mode	DC amperometry
Pretreatment	none
Interval time	0.4s
Run time	3600s / 900s
Potential	0.8V
Standby potential	0.0V

The measurement was carried out for the buffer for 3600s and for the 1mM, 2mM, 3mM, 4mM and 5mM hydrogen peroxide dilutions for 900s each.

9.6 Amperometry with GOx on device with simulated channel

9.6.1 Materials

Device with simulated channel (according to Section 9.1)
Autolab module PGSTAT 10 (Eco-Chemie, Utrecht, Netherlands)
Electrochemical analyser software Gpes 4.9
DIP IC test clip
3× crocodile clips
GOx Type VII Aspergillus Niger (Sigma-Aldrich, Gillingham, UK)
Glucose solutions (3mM, 4mM, 5mM, 6mM, 7mM, 8mM)

9.6.2 Methods

The electrical connection to the Autolab workstation was established via the IC test clip and crocodile clips. The measurement was started and after 20s, 5U of GOx (23µl of GOx solution) had been applied to the electrodes. At 500s, 17µl of the appropriate glucose solution had been added to the glucose oxidase solution. The measurement was done with 3mM, 4mM, 5mM, 6mM, 7mM and 8mM of glucose dilutions. The concentration of the glucose dilutions was calculated, so that it reached the stated concentration in combination with the 23µl of GOx solution. The amperogram was then recorded using the parameters shown in Table 6.

Table 6: Settings used for amperometry on device with simulated channel for measurement with GOx

Mode	DC amperometry
Pretreatment	none
Interval time	0.4s
Run time	2500s
Potential	0.8V
Standby potential	0.0V

The electrodes were wiped dry with a tissue after each measurement and put in the oven at 100°C for 30min before applying the next sample.

CHAPTER III: RESULTS

1 Used buffer solutions and samples

1.1 Viscosity adjustment of the buffer

In order to simulate blood-like behaviour of the buffer solutions in the channel, the buffer viscosity was adjusted according to Chapter II Sections 1.2 and 1.3. Figure 16 shows the influence of the buffer viscosity on the device function with real human blood. For the picture A, the viscosity adjustment was done by carboxymethyl cellulose (CMC). As this is a colloidal solution, it was interfering with the measurements with blood and produced turbulences in the channel (see Figure 16 A).

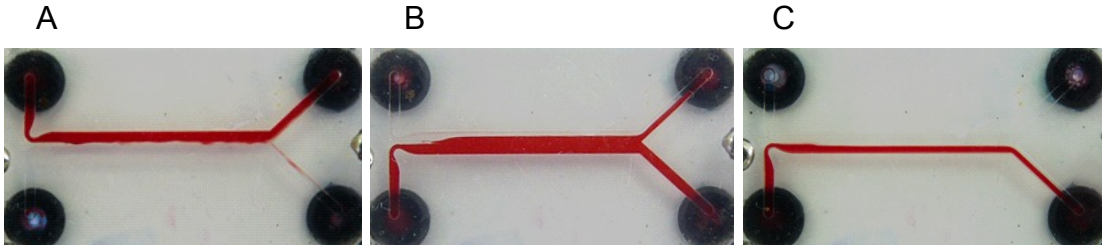

Figure 16: Influence of the buffer viscosity adjustment on the device function with human blood; A: viscosity adjustment with CMC, B: viscosity adjustment with polyethylene glycol less viscous than blood, C: viscosity adjustment with polyethylene glycol higher viscous than blood

To avoid these turbulences and obtain a laminar flow, polyethylene glycol (PEG) was used for further experiments to adjust the viscosity instead of CMC. As can be seen in figures 16 B and C, this method keeps a laminar flow conduct in the micro-channel.

1.2 Selection of stain for fluid distinction in the micro-channel

As the used buffer solutions are transparent, they were stained in order to visualise the flow conduct in the channel, according to Chapter II Section 1.4. This allowed identification of problems such as turbulences and mixing by visual inspection.

Attention has been paid to the fact, that the used dyes do not (or negligibly) change the viscosity and the pH of the original solutions. Furthermore, the

colour and intensity were chosen in order to gain a good contrast between the two fluid streams.

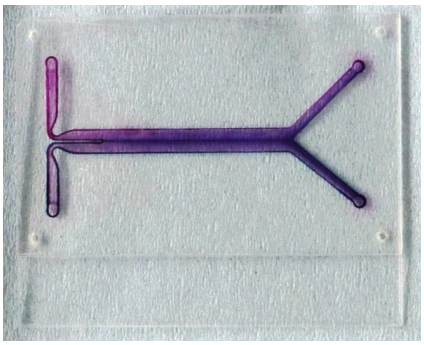

Figure 17: Building up of precipitation where the malachite green and carbol fuchsin solution were in contact with each other (design figure 19 H)

Figure 17 shows a device with 1mm channels used with malachite green and carbol fuchsin stained buffer solutions after an experiment. It was realised that there is a reaction between malachite green and carbol fuchsin. There was precipitation accumulating where the two fluid streams were in contact with each other, building a wall-like structure in the middle along the channel (see figure 17). Furthermore, carbol fuchsin was forming clumps in the viscous buffer solutions prepared with CMC.

For the malachite green it was noticed, that the colour fades over time. After about 12 hours the solution is significantly lighter. This made it harder to compare the fluid conduct experiments.

After some experiments for determining the optimal dye combination, it was discovered that coomassie blue and eosin were working best together. So for further experiments, particularly those with adjusted viscosities, this arrangement was used. Figure 18 shows a device with 2mm channels during an experiment using this dye arrangement.

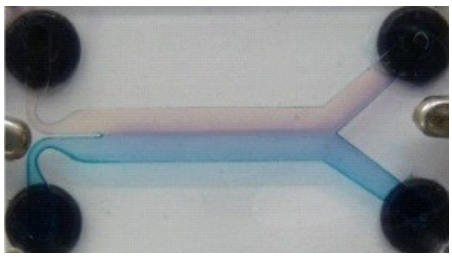

Figure 18: Device testing experiment with coomassie blue and eosin stained buffer solution (design figure 19 H)

2 Device design

The device was designed according to Chapter II Section 2. The individual polymer layers for the devices were designed by the software AutoCAD. The main channel was chosen to be as long as possible, (limited by the maximum area the laser marking head is capable of cutting) in order to have enough time for the hydrogen peroxide diffusion to occur. Furthermore, if the diffusion time is too long (interferents are diffusing as well), it is easy to reduce the channel length by just changing the middle layer of the device, or even just increasing the speed of the syringe pump without changing the device at all. But to increase the length of the channel, the entire design would need to be revised. Because, when testing the initial intended microfluidic chip some problems were encountered (more information in Chapter IV Section 2), Figure 19 shows the evolution of the device's design during the troubleshooting process.

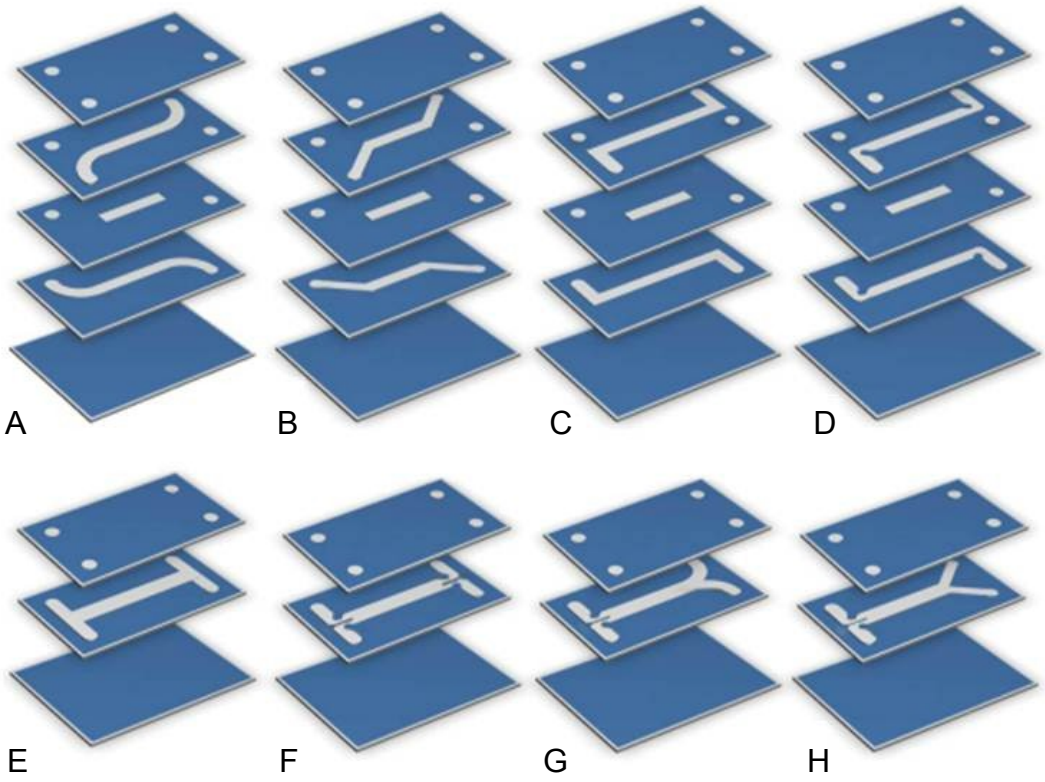

Figure 19: Evolution of the design; A: initial design with curved fluid inlets and outlets, B: Y-filter design with straight fluid inlets and outlets, C: bi-planar H-filter, D: bi-planar H-filter with low dispersion turns, E: mono-planar H-filter, F: mono-planar H-filter with low dispersion turns on fluid inlets and outlets, G: mono-planar H-filter with low dispersion turns on fluid inlets and curved outlets, H: mono-planar H-filter with low dispersion turns on fluid inlets and Y-junction on outlets; the electrodes and the electrode mask layer are not shown in these schematics

The top line (A – D) shows devices with the initially intended design of the channels on top of each other, the bottom line (E – H) shows devices with the channels side by side. The device design shown in figure 19 H was found out to perform best, therefore it was used for all further experiments.

3 Laser-cutting

The polymer layers were cut by a CO_2-laser linked to a computer by the laser marking software Synrad WinMark. Apart from the cumbersome importing procedure of the AutoCAD files (see Chapter II Section 3) this worked well.

In order to fit the cutting requirements of the different polymer layers optimally, the most suitable laser settings for each polymer used were determined. This was done empirically by comparing the different parameter configurations (laser velocity, power and mark count) on each polymer layer and assessing which one was the best (see Figure 12). The optimal configuration cuts the layer through completely without burning or warping the edges, or leaving behind any particles. After comparison and assessment of the best outcome the determined settings can be seen in Table 7. Unless stated differently, these parameters have been used to cut the devices' layers in all the designs.

Table 7: Empirically determined optimal laser-cutting parameters for the different polymer layers

		Laser settings		
Material	**Thickness**	**Velocity**	**Power**	**Mark count**
Melinex ST 725	254.0 µm	300 mm·s^{-1}	55 %	6
Arcare 8565	254.0 µm	320 mm·s^{-1}	70 %	5
Arcare 8890	12.7 µm	400 mm·s^{-1}	40 %	3
Arcare 8039	76.2 µm	320 mm·s^{-1}	60 %	3
Arcare 90485	177.8 µm	400 mm·s^{-1}	40 %	5
Melinex ST 725 + Arcare 8570	266.7 µm	300 mm·s^{-1}	80 %	7
Nalophan NS	25.0 µm	400 mm·s^{-1}	15 %	1

4 Alignment tool

In order to be able to align the separate laser-cut polymer layers accurately for subsequent lamination, an alignment tool was built. It consisted of four pins mounted on a solid support. The used polymer layers were aligned by laser-cut holes in each corner of the design (see Figure 11) which fit the spikes on the alignment tool. Furthermore, this tool was used to align the world-to-chip interface (see Section 6) with the microfluidic device in order to establish the connection to the syringes (see Chapters II and III Section 8.2). The fabricated device is shown in Figure 20.

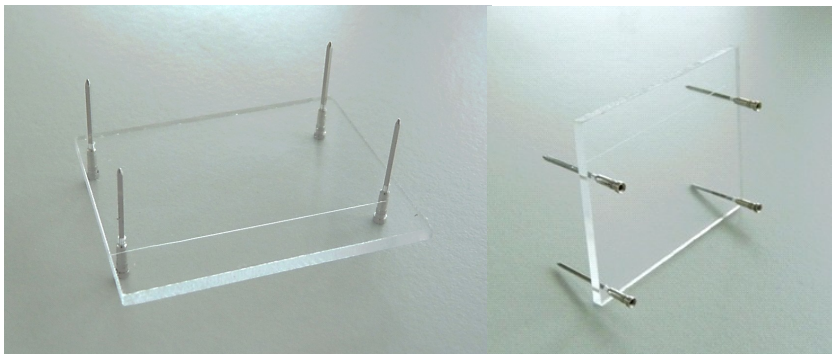

Figure 20: Top (left) and bottom view (right) of the alignment tool

5 Lamination

The microfluidic device was assembled by lamination of the single laser-cut polymer layers according to Chapter II Section 5 and the appropriate design in Figure 19 with the help of the alignment tool. This is the second least accurate step in the device production. The procedure is very prone to air entrapment and can cause warping of the channel in the worst case.

In the project, air bubbles were avoided as much as possible by slowly pushing the layers together with the help of a scalpel handle, starting in the middle and going first in one, then the opposite direction. After repeating this procedure for the residual layers, the device was put in the press to establish bonding distributed over the whole device area and to push out any residual air bubbles.

Figure 21 A shows the hydraulic press used to establish stable bonding between the PSA tapes of the polymer layers. In Figure 21 B a complete microfluidic device with electrodes (design Figure 19 H) after lamination is depicted.

A B

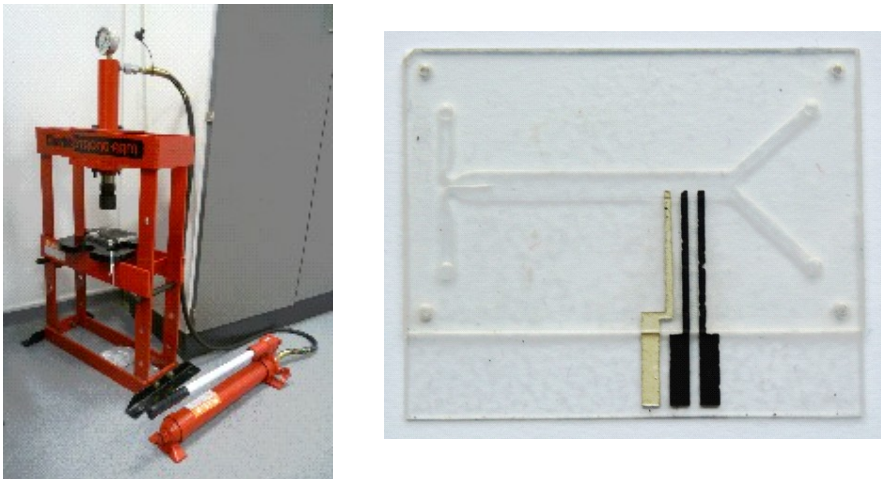

Figure 21: Lamination; A: Hydraulic press used to press the PSA tapes of the device, B: microfluidic device with electrodes (design 19 H) after lamination

6 World-to-chip interface

In order to establish a connection for the introduction of the buffer and sample fluids into the microfluidic device, a world-to-chip interface was built according to Chapter II Section 6. The resulting device can be seen in Figure 22.

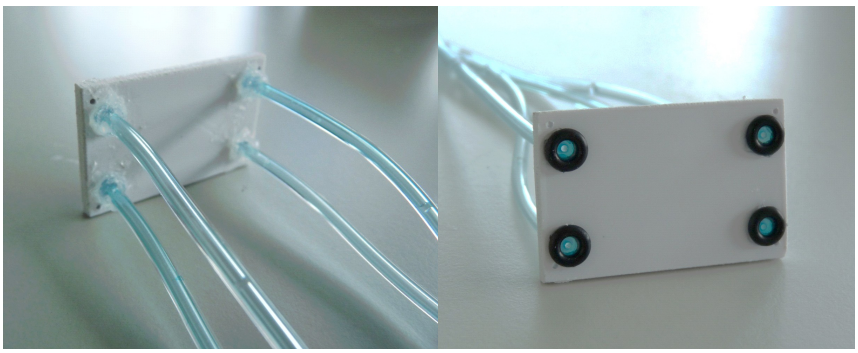

Figure 22: Top (left) and bottom view (right) of the world-to-chip interface

7 Electrode fabrication

7.1 Screen-printing

The electrochemical detection system was realised by an adapted manual screen-printing procedure according to Chapter II Section 7.1. Figure 23 shows the electrode deposition process before and after removing the top protective layer serving as the electrode mask.

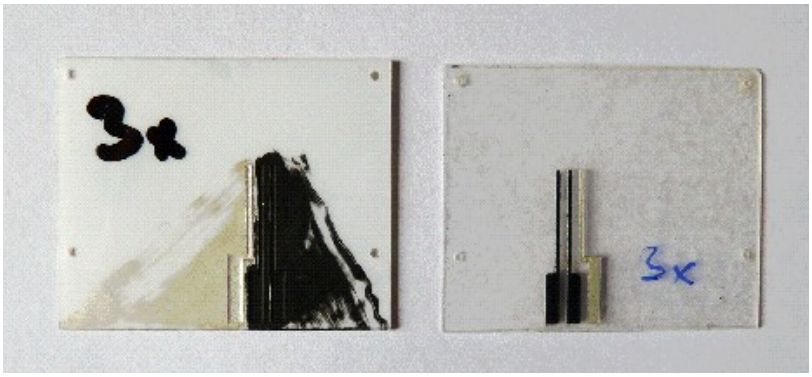

Figure 23: Screen-printed electrodes before (left) and after (right) removing the top protective layer serving as the electrode mask

7.2 Optimisation of electrode deposition

As the electrodes are integrated in the microfluidic channel of the device, they need to be as flat and regular as possible, in order to influence the fluid conduct as little as possible. Therefore thickness measurements of the electrode cross section were carried out. It was found that by depositing the ink twice there was still a cavity in the middle of the electrodes. Whereas after four times of ink deposition the edges of the electrodes were already higher than the electrode mask layer. The most regular and even surface was produced by three times of ink deposition, so this number was used for all the devices produced with electrodes, unless stated differently. Figure 24 shows the pictures taken by the microscope after cutting the device according to Chapter II Section 7.2.

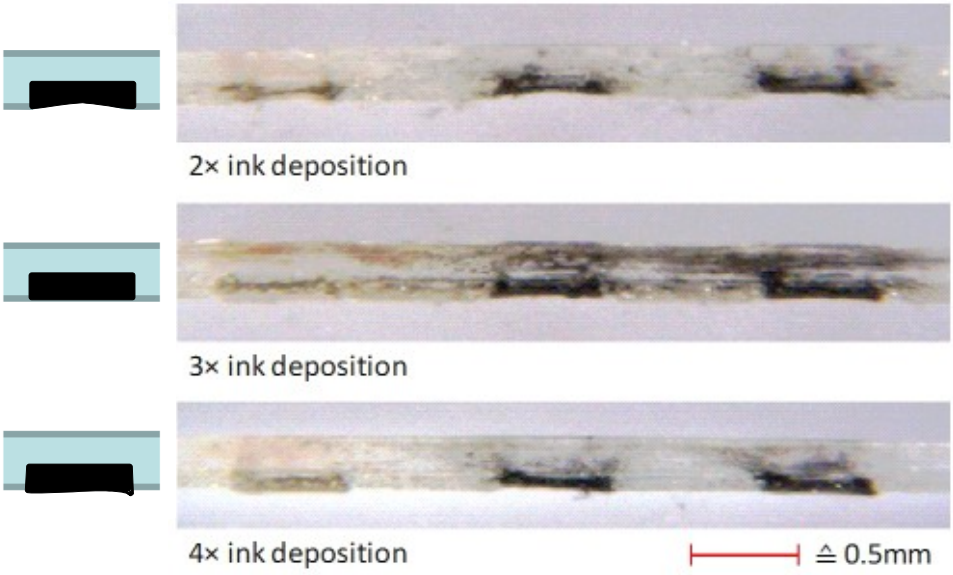

Figure 24: Comparison of electrode thickness after different number of ink depositions

8 Microfluidic chip experiments

8.1 Calibration of the syringe pump

As the syringe pump used was last calibrated in 1999, the flow rates for the different settings of the flow rate selector were determined by experiment. After measuring the time and collected volume of the buffer (according to Chapter II Section 8.1), the volumetric flow rate was calculated for the different speed settings on the syringe pump. The results can be seen in Table 8.

Table 8: Calibration of the syringe pump

Flow rate selector setting	Flow rate 5ml syringe	Flow rate 10ml syringe
1	139.6 µl·s^{-1}	227.6 µl·s^{-1}
2	101.0 µl·s^{-1}	157.6 µl·s^{-1}
3	70.4 µl·s^{-1}	112.9 µl·s^{-1}
4	51.0 µl·s^{-1}	80.0 µl·s^{-1}
6	26.2 µl·s^{-1}	40.5 µl·s^{-1}
8	13.5 µl·s^{-1}	20.6 µl·s^{-1}
10	6.9 µl·s^{-1}	10.6 µl·s^{-1}
12	3.1 µl·s^{-1}	5.4 µl·s^{-1}
14	1.8 µl·s^{-1}	2.8 µl·s^{-1}
16	0.9 µl·s^{-1}	1.5 µl·s^{-1}
18	0.5 µl·s^{-1}	1.4 µl·s^{-1}

8.2 Testing assembly

Figure 25 shows the testing assembly, consisting of the alignment tool, device to be tested and world-to-chip interface, that was used to establish the connections for the buffer and sample solutions for the fluid conduct experiments.

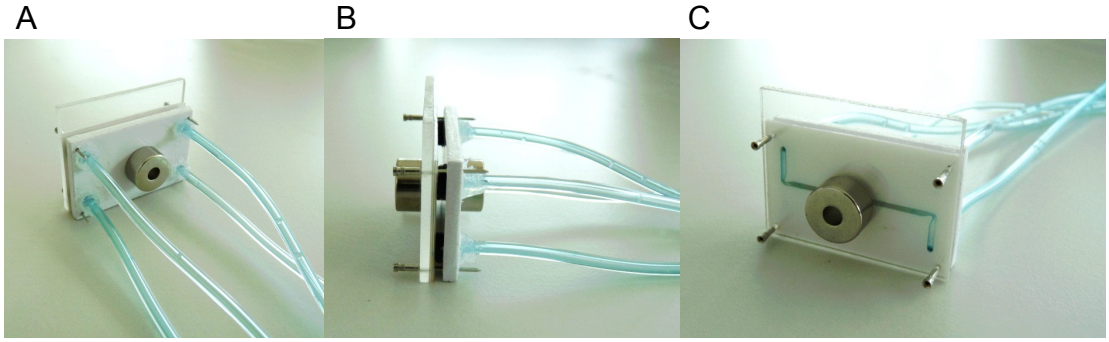

Figure 25: Alignment tool with microfluidic device and world-to-chip interface assembled and pressed together by magnets; A: top view, B: side view, C: bottom view (microfluidic channel, configuration Figure 19 D)

8.3 Fluid conduct experiments

Figure 26 shows an example of the results of the fluid conduct experiments for two designs with different flow rates. Furthermore they were tested with different dyes, coomassie blue and eosin for design Figure 19 F (left), and malachite green and carbol fuchsin for design Figure 19 H (right).

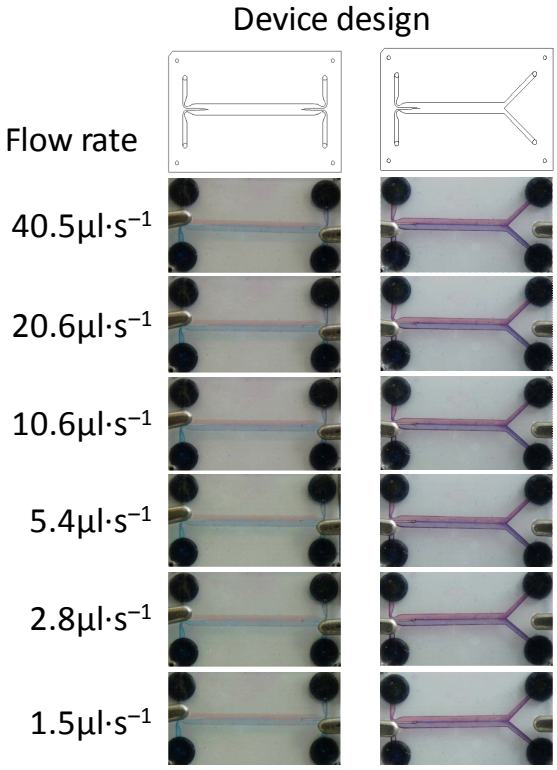

Figure 26: Device testing experiment for design Figure 19 F with eosin and coomassie blue (left) and Figure 19 H with malachite green and carbol fuchsin (right) with different flow rates (adapted from Labbé, 2010)

The Figure exemplifies how the results of the different designs and flow rates were compared.

Figure 19 shows the evolution of the device design. The following paragraphs explain the problems encountered with each design when testing it and the ideas for changing it to the next one. Unless stated differently, all designs had a channel width of 1mm, a channel length of 24mm and were tested with dyed phosphate buffers of different viscosities, or with spiked buffer solutions (either with H_2O_2 or ascorbic acid) for the titration experiments. Furthermore, the devices were tested with two different configurations of polymer layers as shown in Figure 27.

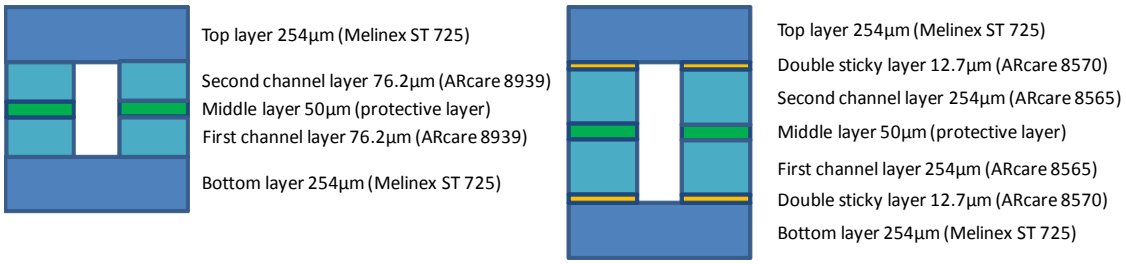

Figure 27: Cross section scheme of the polymer layer configurations tested

In the second configuration, the double sticky layers are used to make the channel layers sticky on both sides, as the 254µm polymer layers are only available as single coated PSA tapes.

On testing the initial design (Figure 19 A) with the curved fluid inlets and outlets, different amounts of fluid were collected at the outputs for both configurations at all reasonable speeds.

To rule out the influence of gravity, the device was operated upside down and still more fluid was collected from the same channel as in the previous experiment. Also the influence of the dye, which could probably change the viscosity of the buffer, was tested by swapping the input tubes. Still more fluid was collected from the same channel as in the previous tests.

As another possible problem, the alignment of the layers was identified. If the holes are not aligned perfectly, the different resistances of the fluid outlets lead to different amounts of fluid being collected. The solution was to use bigger holes for all the layers lying above the channels. Figure 28 illustrates the problem and the solution.

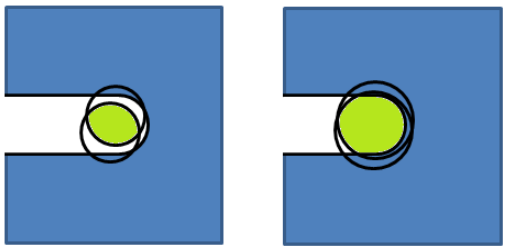

Figure 28: Imperfect alignment of the holes and the channel; holes with the same diameter as the channel (left), holes bigger than the channel diameter (right), the green area illustrates the effective area for fluid transport

All devices from now on were designed with bigger holes for the layers above the channels. But it turned out that this was not the only problem, as the device was still not working.

The next possible problem identified were the curves at the fluid inlets and outlets. These might cause different resistances on the inner and outer walls of the channel due to friction and wall adherence of the fluids. So the next step was a design with straight fluid inlets and outlets (Figure 19 B), referred to as the Y-filter.

The Y-filter worked better, but there was still a difference in the amounts of fluid collected at the outputs for both tested configurations. As long as the collected fluids were not the same amount it made no sense to compare the colours to assess if there was mixing. Hence, the primary problem to solve was to collect the same amount of fluid at both outputs.

As in the literature the mono-planar H-filter was working (Brody *et al.*, 1996; Holl *et al.*, 1996; Verpoorte, 2002; Collier and Hart, 2005), the equivalent in two layers, referred to as the bi-planar H-filter, was built (Figure 19 C) and tested (no literature about this configuration was located). But also in this device the amounts of fluid collected at the outputs were different for both configurations.

The possible problem in this device could be the corners, which affect the flow profile. So the corners of the bi-planar H-filter were modified to low dispersion turns, according to Griffiths and Nilson (2001), to keep the initial flow profile. Figure 29 shows the shape of the turns and the flow profiles before and after the modified corner.

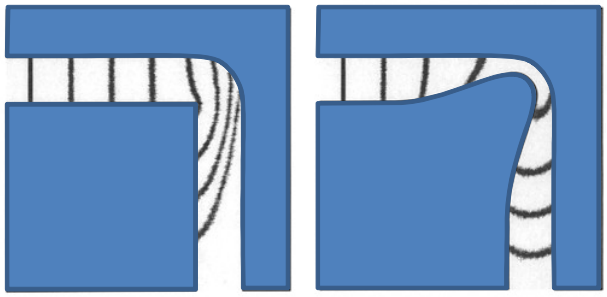

Figure 29: Conventional and modified 90° turns and the flow profile (adapted from Griffiths and Nilson, 2001)

This device was working better than all the previous ones, but still the collected amounts of fluid were not exactly the same. However, an H_2O_2 diffusion experiment of this device was performed, revealing a diffusion of 21.8% with the thin channel layer, and 10.9% with the thick channel layer configuration at 520µl·min^{-1}. But, since exactly the same volume of fluid was not collected, the calculated values were not only due to diffusion but also to convection.

In searching for the problem it was realised that the protective layer, which had been used for the middle layer in all the devices up to now, had different surface properties, in terms of hydrophobicity, on each side. Figure 30 shows a drop of water on the two surfaces of the protective layer.

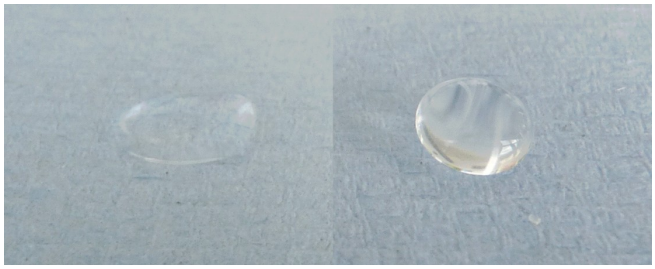

Figure 30: Drop of water on the two surfaces of the protective layer used as the middle layer

It can be clearly seen, that the hydrophobicity is not the same. This is a big problem in microfluidic devices, as it influences the fluid conduct in the channel. The surface to volume ratio in micro-channels is very high, hence effects like wall adsorption and friction (which are, amongst other factors, dependent on the hydrophobicity) play an important role, whereas on a macro-scale these phenomena are negligible (Teo and Khoo, 2009).

Figure 31 shows two extreme examples, but even if the walls are not perfectly hydrophobic or hydrophilic, this effect influences the fluid conduct in the channel.

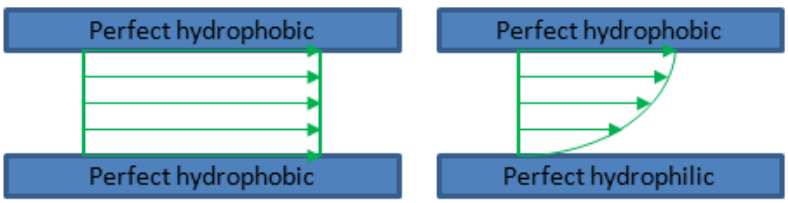

Figure 31: Comparison of fluid conduct in a channel with perfect hydrophobic and hydrophilic walls, respectively (adapted from Teo and Khoo, 2009)

Hence, for all the designs up to now the middle layer was changed, and they were tested again with the polymer layer configurations shown in Figure 32.

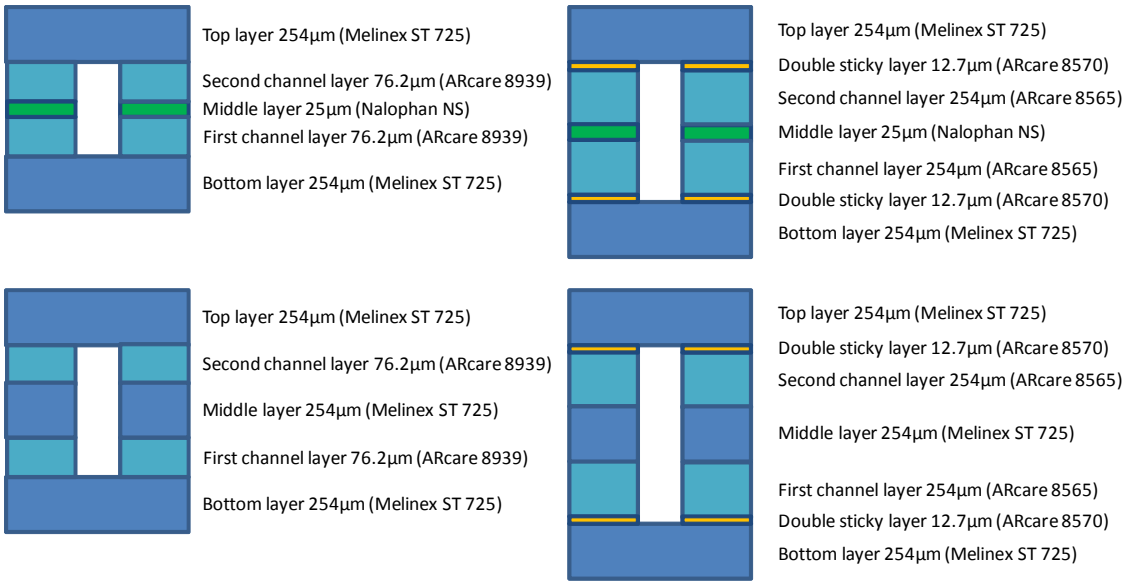

Figure 32: Cross section scheme of the polymer layer configurations tested with new middle layers (same surface properties on both sides)

The devices with the new middle layers did not work any better than the previous ones. In the recipients at the outputs of all the devices, different amounts of fluid were collected. Although they were not performing better, the diffusion experiments were carried out again with the bi-planar H-filter, in order to compare it with the device with the old middle layer. The H_2O_2 diffusion for the device with the thin channel layers and the 254µm middle layer was 18.5%, the ascorbic acid diffusion 5.7% at 520µl·min^{-1}. But as already mentioned, since not exactly the same amount of fluid was collected, the calculated values were not only due to diffusion but also to convection.

As it was still not working, the mono-planar H-filter as it is found in the literature was built (see Figure 19 E) (Brody *et al.*, 1996; Holl *et al.*, 1996; Verpoorte, 2002; Collier and Hart, 2005). Unless stated differently, all the new designs had a main channel width of 2mm and polymer layer configurations according to Figure 33.

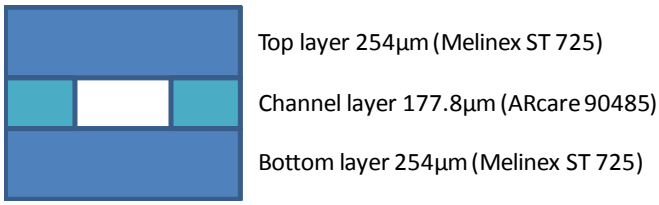

Figure 33: Cross section scheme of the polymer layer configurations of the mono-planar designs

Also, with this device, different amounts of fluid were collected at the outputs. So the low dispersion turns, according to Griffiths and Nilson (2001), were integrated into the mono-planar device leading to the design in Figure 19 F.

It was noticed that it was not the input into the main channel that was the problem, but more the separation at the end of the channel. So the outlets were changed to the designs in Figure 19 G and H. The best results were obtained with 19 H, but there was still a difference in the amounts of collected fluid at the outputs.

As even the designs which worked in literature (Brody *et al.*, 1996; Holl *et al.*, 1996; Verpoorte, 2002; Collier and Hart, 2005) were not working as expected in the experiments, the problem was no longer searched for in the design. The next step in the troubleshooting was to exchange the normal medical plastic syringes (BD-Plastipak 20ml) that had been used up to now for precision glass syringes and test the designs in Figure 19 E, F, G and H again. But this did not result in exactly the same amount of fluid collected at the outputs either. However, the repeatability was improved, as it was always the same difference in the amounts collected.

It was realised at the very end of the project, that each droplet falling from the free outlet tubes influences the separation of the fluids at the Y-junction. A portion of fluid from one stream is contaminating the other outlet, and at the moment a droplet is falling from the outlet tube, the contamination is swapping to the other outlet, and so on. This effect is without doubt due to pressure differences and should be solved if the ends of the outlet tubes are immersed in buffer solution, so that there are no free falling droplets.

As putting the free outlet tubes into buffer solution did not fix this problem, the cause of the phenomenon is almost certainly to be found at the syringe pump. Due to the high price and the time constraints, the only instrument that remained unchanged during the entire project was the syringe pump. Hence, this might be the solution and should be altered for future experiments.

Despite the problems with the device itself, the fluid behaviour with integrated electrodes was tested with the most promising device (design Figure 19 H). The results can be seen in Figure 34.

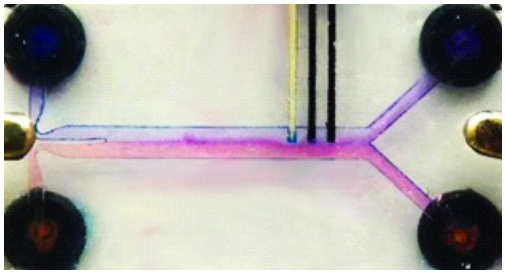

Figure 34: Fluid conduct experiment in device with integrated electrodes

As can be seen, the fluid is circumventing the electrodes. This phenomenon is without doubt due to two reasons: the difference in the surface properties of the polymer layer and the electrodes, and/or the irregularities in the surface of the micro-channel. As already mentioned in Section 7, these problems might be overcome either by using commercial screen-printing or another deposition method such as vacuum evaporation (Hintsche *et al.*, 1991; Shul´ga *et al.*, 1994).

9 Electrochemical experiments

9.1 Simulation of the channel

For the electrochemical measurements on the electrodes (without channel), the channel of the final device was simulated with the help of insulating ink in order to have the same electrode surface area for the reaction, according to Chapter II Section 9.1. Figure 35 shows the resulting device.

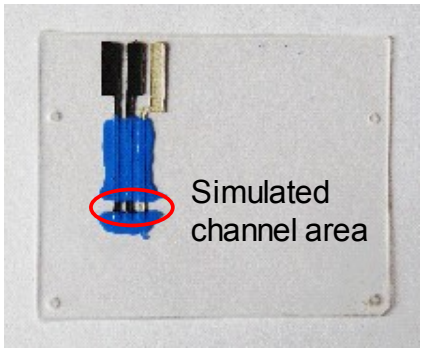

Figure 35: Device with electrodes and simulated channel

9.2 Characterisation of the electrodes

To determine the characteristics of the produced electrodes, a cyclic voltammogram of neat phosphate buffer, 10mM H_2O_2 in phosphate buffer and ferrocyanide ($Fe(CN)_6^{4-}$) as a benchmark was recorded (see Figure 36). It was carried out according to Chapter II Section 9.2. The phosphate buffer was used as kind of a negative control and the hydrogen peroxide dilution shows the analyte signal. The resulting voltammograms can be seen in Figure 36.

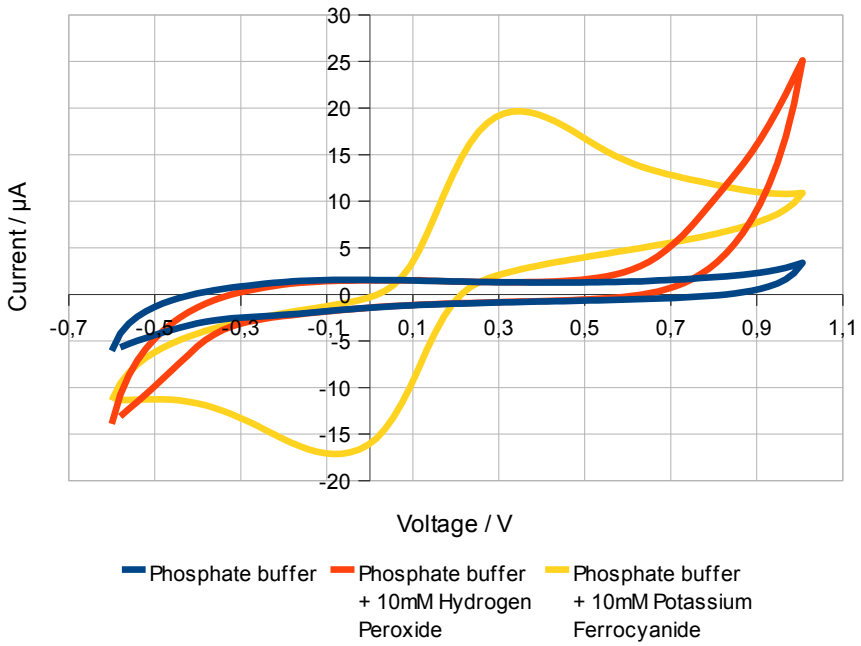

Figure 36: Electrode characterisation: cyclic voltammogram of the electrodes

Due to the much higher peak-to-peak separation than 57mV, and the smaller reduction peak than the oxidation peak, the reaction occurring at the electrodes in the project can be considered as quasi-reversible.

9.3 Determination of the optimal potential for amperometry

An amperometry experiment of increasing H_2O_2 concentrations with different potentials in a beaker under stirring conditions (steady state conditions) was carried out in order to determine the optimal potential for further amperometry measurements, according to Chapter II Section 9.3. Figure 37 shows the recorded amperograms for different potentials. As expected, the measured current is directly proportional to the H_2O_2 concentration and the slope is increasing the higher the voltage used.

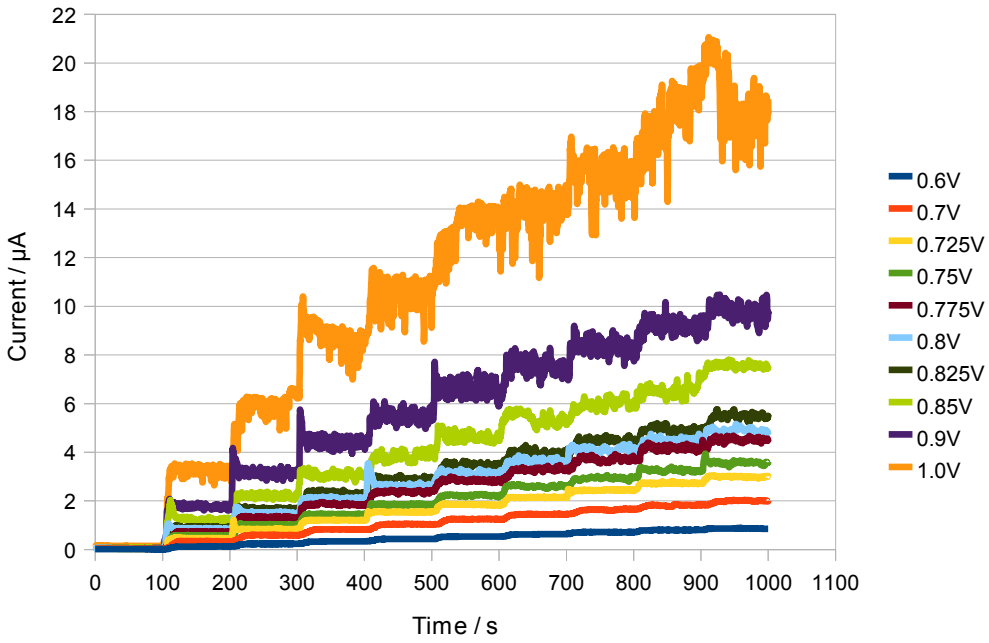

Figure 37: Optimal potential determination: amperometry of stepwise increasing hydrogen peroxide concentrations (every 100 seconds by 1mM) in a beaker under stirring conditions

As can be seen, the curve for 1.0V is quite noisy (in particular for the higher concentrations above 4mM) and not useful for any measurements. Furthermore, the signal is much higher than for the other ones. In order to see the other curves properly, the 1.0V signal is not displayed in the following figures any more, although it was still taken into account for the calculations of the slope in Figure 39.

Figure 38 shows the averaged values of the current for each H_2O_2 concentration based on Figure 37. The first 30s, after changing the concentration (every

100s), have not been taken into account for calculating the average as it takes about this time to obtain a stable signal. Before it is not reproducible, due to the injection procedure with the pipette. Furthermore, it reveals the non linearity for higher concentrations. Therefore, the linear regression lines are based on the measurement of the first four points only.

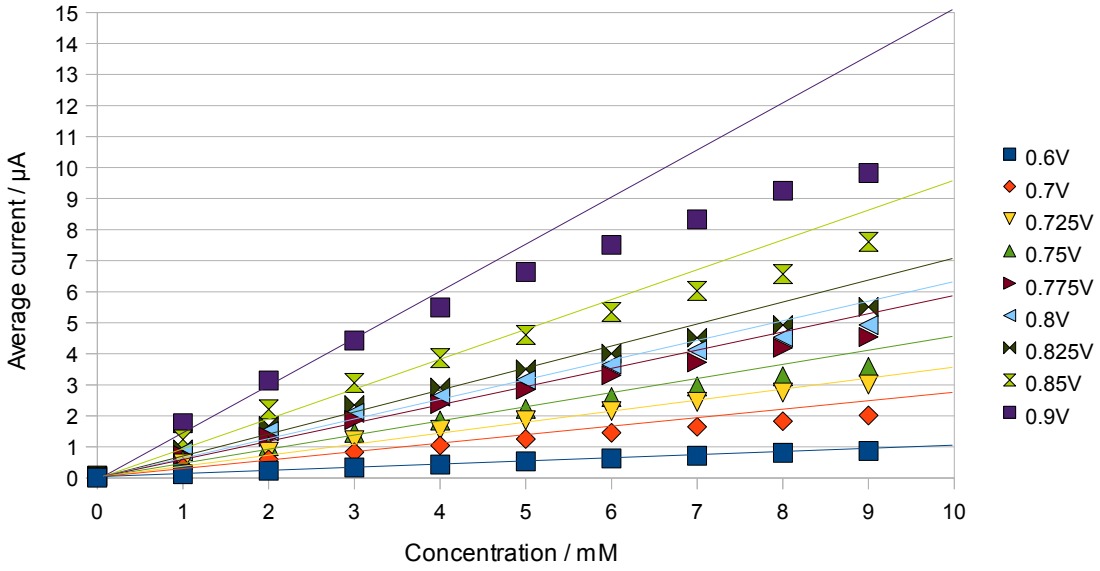

Figure 38: Optimal potential determination: average current vs. concentration of hydrogen peroxide based on the values of figure 37; linear regression line through the first four points

The slope of the linear regression lines in Figure 38 was calculated and printed against the voltage. The resulting curve can be seen in Figure 39. It shows an almost linear increase of the slope at the beginning, reveals a plateau at around 0.8V and a sharp increasing slope afterwards.

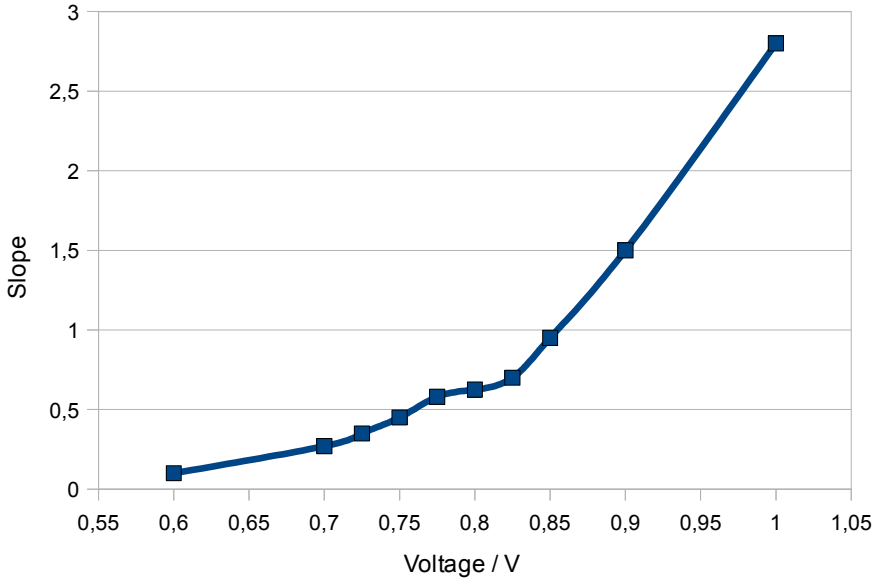

Figure 39: Optimal potential determination: slope vs. voltage; the slope is calculated from the linear regression lines in Figure 38

This potential plateau at 0.8V was taken for all further amperometric measurements as it provides some kind of buffer for potential fluctuations in both directions. Furthermore, good sensitivity and linearity were given at the same time.

9.4 Measurement of interfering species

To determine the influence of interferences, amperometry experiments with interferents were carried out according to Chapter II Section 9.4. Three of the most common interfering species, ascorbic acid, acetaminophen and uric acid, were measured in order to compare them to the hydrogen peroxide signal (Ernst *et al.*, 2002). All recorded signals were measured up to 5mM with 1mM increases in concentration each 200s, apart from uric acid, which was increased in 0.5mM steps up to 2.5mM. As can be seen in Figure 40, the interference signals are less stable and higher than the H_2O_2 signal. The uric acid signal seems to be lower, but the highest concentration measured is 2.5mM, not like the other ones at 5mM (see Figure 41). This was due to the solubility of uric acid. According to the Merck Index (O'Neil *et al.*, 2001) uric acid can be dissolved at a maximum of 1g in 2000l of boiling water and 1g in 15000l of cold water. Furthermore, it is more soluble in alkaline than in acidic environments.

Hence, the highest concentration that can be reached in boiling water is 2.97mM.

For the interference experiment a 2.7mM uric acid stock solution was prepared. Subsequently dilutions of the stock solution in 0.5mM steps up to 2.5mM were done, whereas ascorbic acid and acetaminophen were tested up to 5mM in 1mM steps.

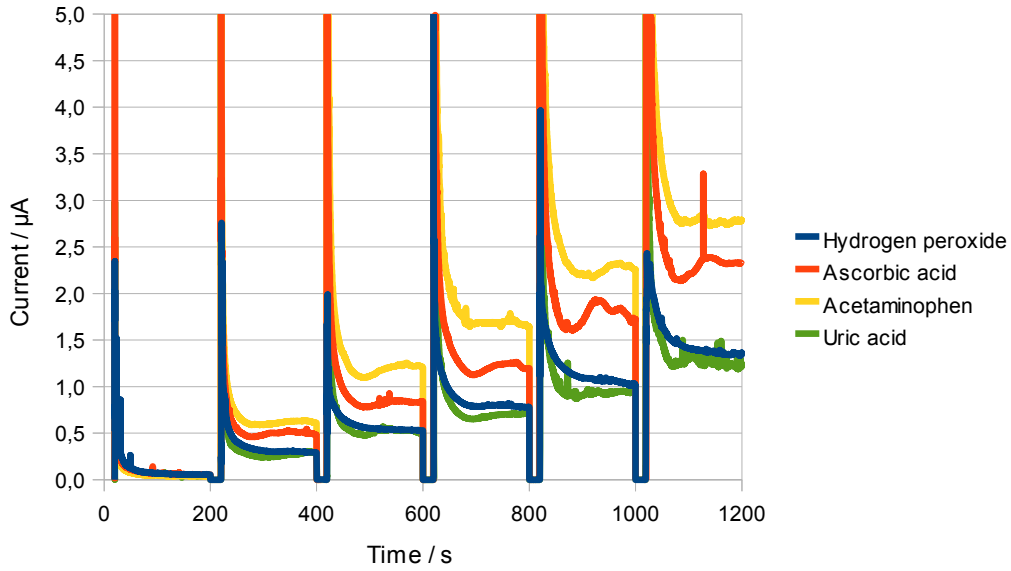

Figure 40: Interference experiment: amperometry of interfering species ascorbic acid, acetaminophen and uric acid in comparison with hydrogen peroxide; stepwise increasing concentrations (every 200s)

Note that each concentration has been measured separately and put together in the figure, this is why every 200s the first 20s show a zero-line. Furthermore, the uric acid signal is not directly comparable, as it is measured with different concentrations (due to solubility reasons).

Figure 41 shows the averaged values of the current for each interferent versus the concentration, based on Figure 40. This shows more clearly that all interferents produce a higher signal than the analyte hydrogen peroxide.

The first 30s, after changing the concentration (every 200s), have not been taken into account for the average as it takes about this time to obtain a stable signal. Before it is not reproducible due to the application procedure with the pipette.

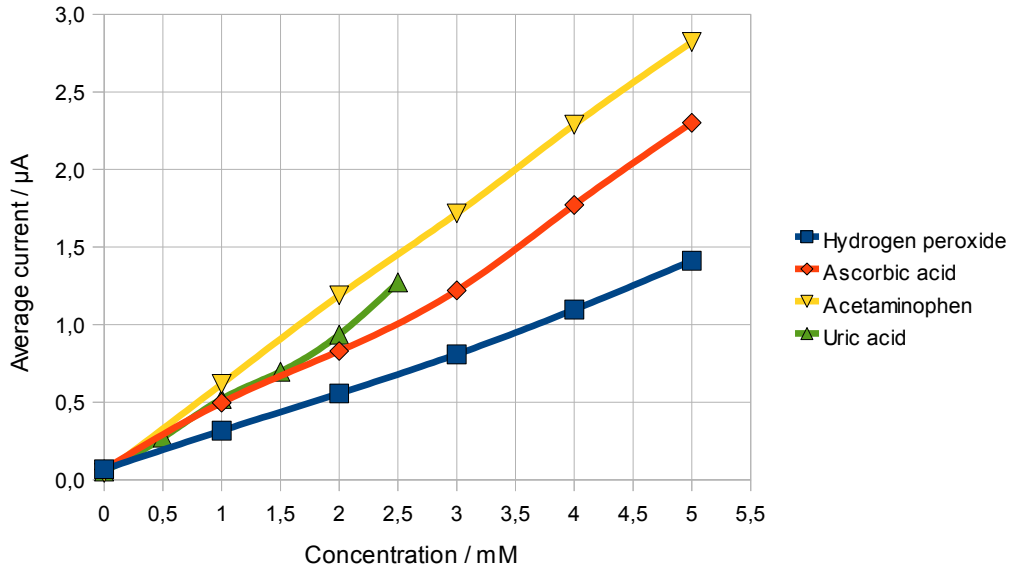

Figure 41: Interference experiment: average current vs. concentration of interferents based on the values of Figure 40

9.5 Measurement variability

To assess the variability of the measurements, ten equal amperometry measurements of phosphate buffer with the same electrodes were carried out according to Chapter II Section 9.4. Figure 42 shows the recorded signals.

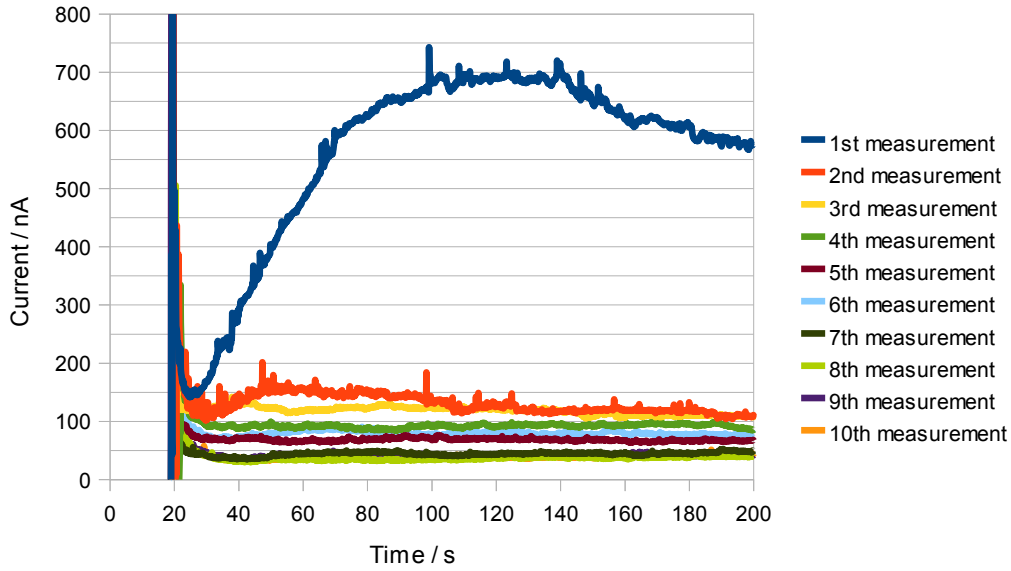

Figure 42: Measurement variability experiment: amperometry of phosphate buffer; ten equal measurements with the same electrode

Figure 43 shows the lower area in more detail by not displaying the first measurement.

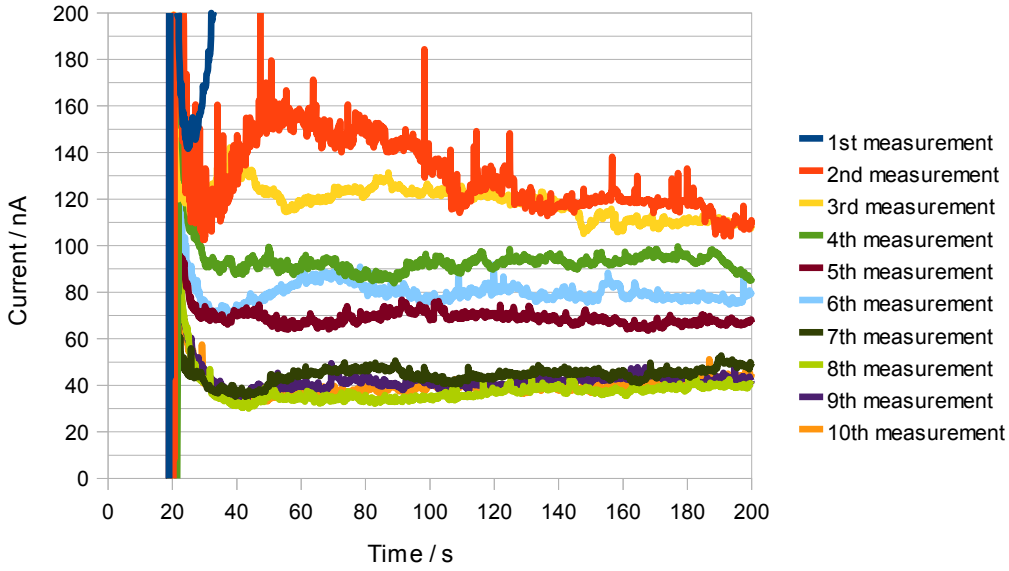

Figure 43: Measurement variability experiment: (detail of Figure 42) amperometry of phosphate buffer; ten equal measurements with the same electrode

In Figures 42 and 43 can be seen that the potential is decreasing during the first six measurements. Afterwards it is quite stable at about 40nA. The only logical explanation is a decrease of the electrochemically active electrode surface area, as all the other parameters remain the same for each measurement.

Subsequently triplicate series of measurements with increasing H_2O_2 concentrations using the same electrodes were carried out according to Chapter II Section 9.4. Figure 44 shows the recorded signals.

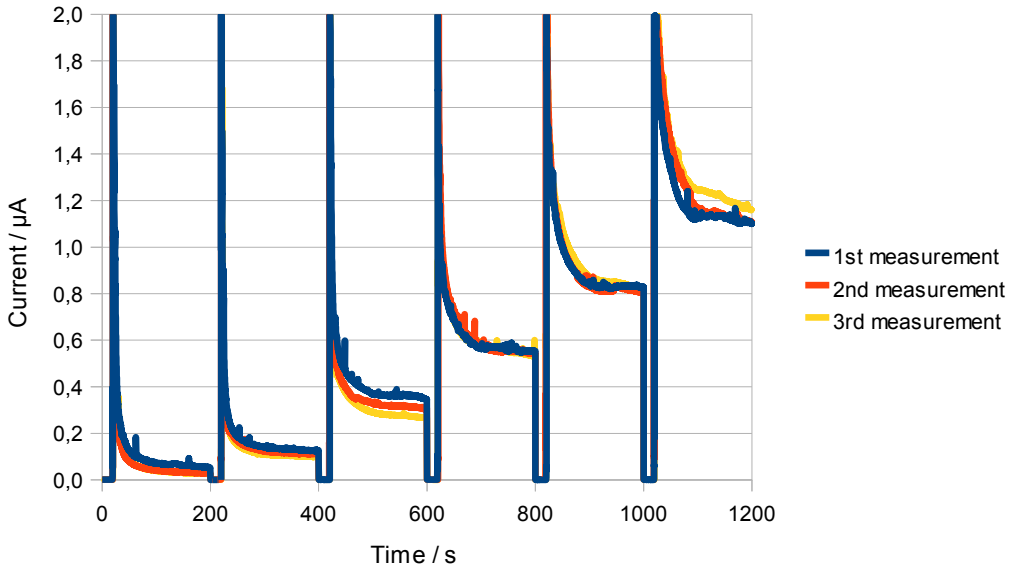

Figure 44: R Measurement variability experiment: amperometry of hydrogen peroxide in phosphate buffer; stepwise increasing concentration (every 200s by 1mM)

Note that each concentration has been measured separately and put together in the figure, this is why every 200s the first 20s show a zero-line.

The current values for each concentration were averaged, where the first 30s after changing the concentration (every 200s) have not been taken into account, as it takes about this time to obtain a stable signal. Before it is not reproducible due to the application procedure with the pipette. Subsequently the average of the three measurements was calculated and is shown in Figure 45.

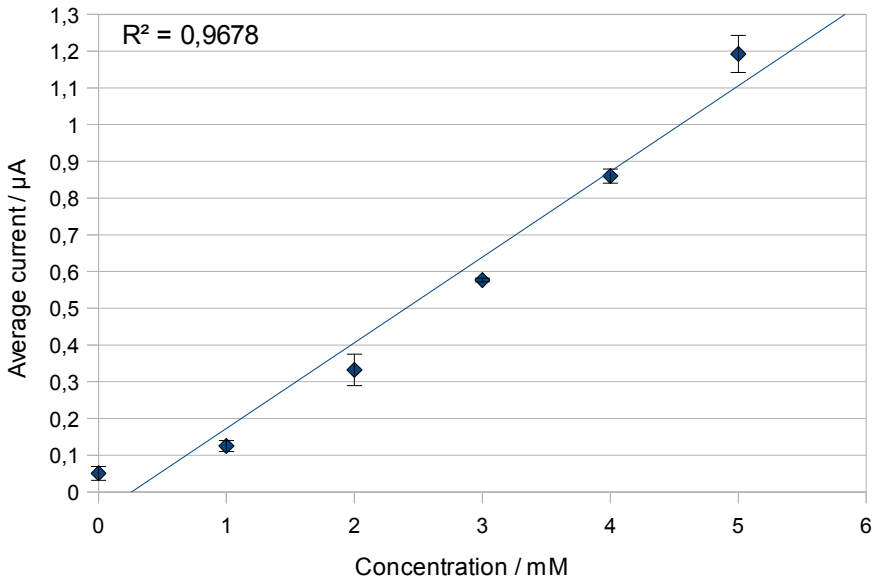

Figure 45: Measurement variability experiment: average current vs. concentration with error bars indicating one standard deviation and linear regression line

The error bars indicate one standard deviation. The linear regression line reveals good linearity with a coefficient of determination (R^2) of 0.9678.

9.6 Determination of fabrication reproducibility

To determine the reproducibility of the screen-printed electrodes, three equal amperometry measurements of H_2O_2 with increasing concentrations were carried out with different devices according to Chapter II Section 9.5. Figure 46 shows the recorded signals, which reveal a good correlation of the responses.

The signals look almost congruent apart from an offset. However, the signal should be stable for each concentration, as it is measured in the flowing buffer, but it looks as if there is hydrogen peroxide depletion anyway.

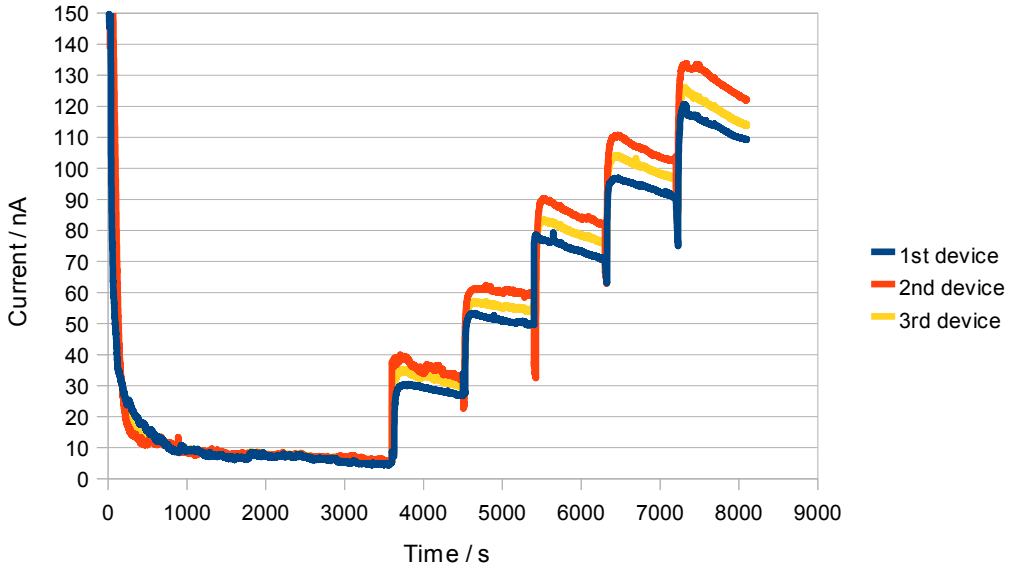

Figure 46: Fabrication reproducibility experiment: amperometry of hydrogen peroxide in phosphate buffer recorded on device with channel; stepwise increasing concentration (every 900s by 1mM)

The current values for each concentration were averaged, where the first 30s after changing the concentration (every 900s) have not been taken into account. Subsequently the average of the three measurements was calculated and is shown in Figure 47.

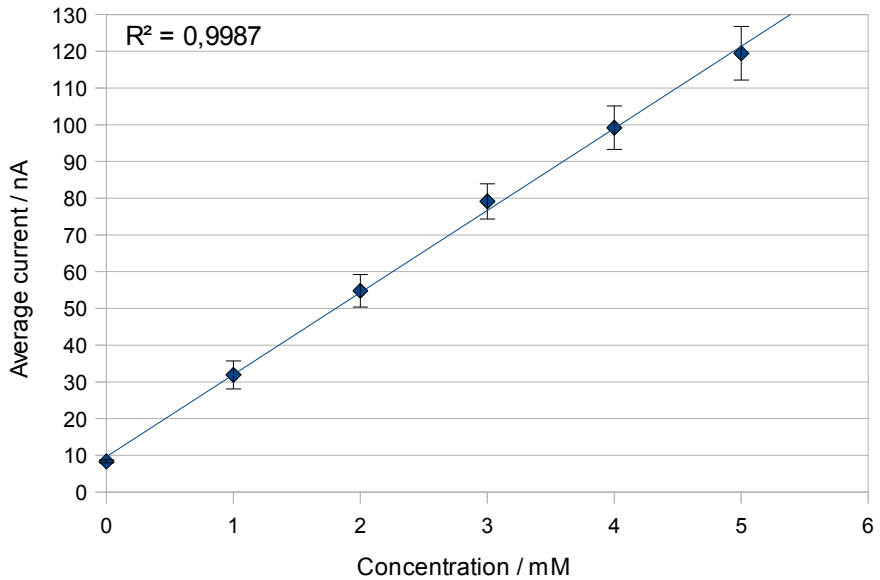

Figure 47: Fabrication reproducibility experiment: average current vs. concentration with error bars indicating one standard deviation and linear regression line

The error bars indicate one standard deviation, showing that the divergence is becoming bigger, the higher the concentration (see Figure 47). The linearity is, with an R^2 of 0.9987, almost perfect. The limit of detection was calculated to be 0.05mM based on the S/N = 3 criterion.

9.7 Linearity determination of device with channel

Figure 48 shows the amperometry measurement of H_2O_2 with increasing concentrations up to 10mM, in order to assess the linearity of the device, according to Chapter II Section 9.5.

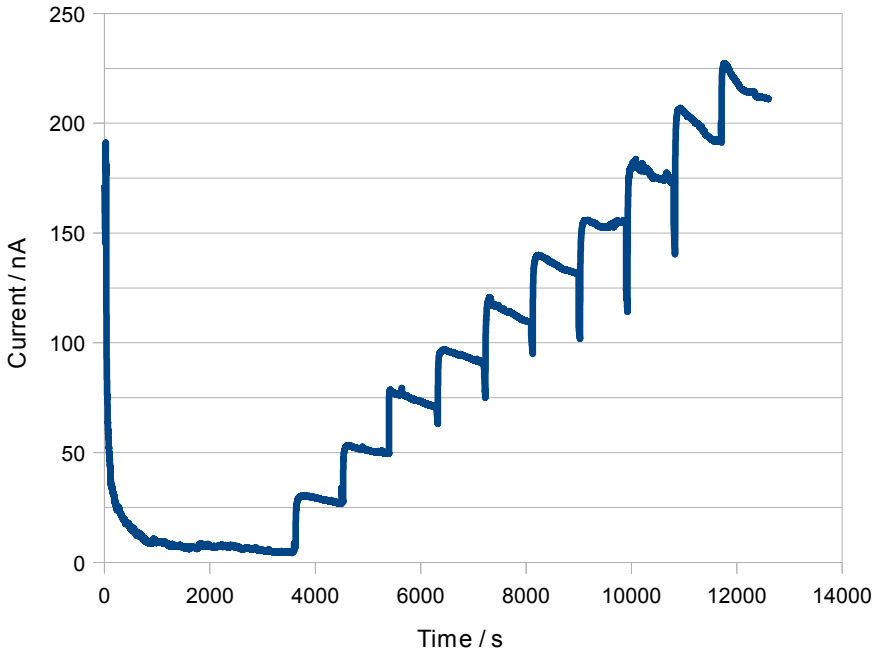

Figure 48: Linearity experiment: amperometry of hydrogen peroxide in phosphate buffer recorded on device with channel; stepwise increasing concentration (every 900s by 1mM)

The current values for each concentration were averaged, where the first 30s after changing the concentration (every 900s) have not been taken into account. Subsequently the average of the three measurements was calculated and is shown in Figure 49. The error bars indicate one standard deviation. The linear regression line reveals an R^2 of 0.9995.

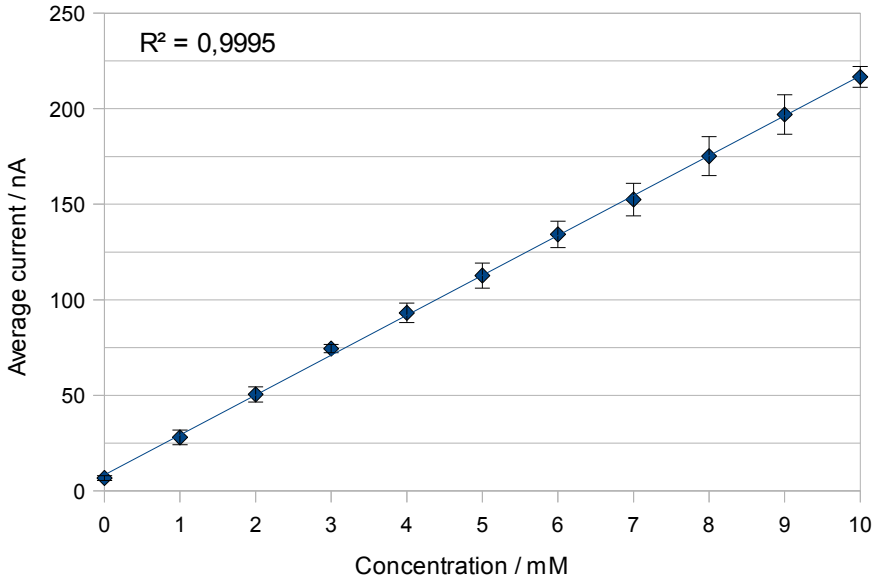

Figure 49: Average current vs. concentration with error bars indicating one standard deviation and linear regression line

10 Measurement of glucose solutions with GOx

In order to determine the response of the electrodes to different concentrations of glucose after adding the enzyme GOx (after 500s), an amperometry experiment, according to Chapter II Section 9.6, was carried out. Figure 50 shows the recorded amperogram.

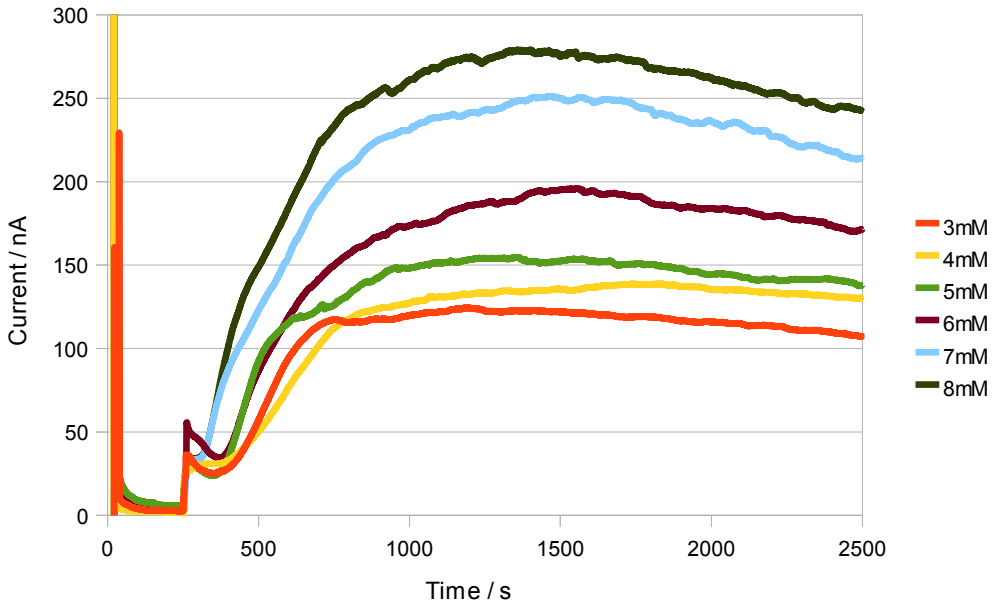

Figure 50: Glucose measurement: amperometry of glucose solutions of different concentrations after adding the enzyme GOx

The current values for each concentration were averaged, where the first 750s after adding the GOx enzyme have not been taken into account, as it takes about this time to obtain a stable signal. Before the enzyme kinetics can be seen. The result is depicted in Figure 51.

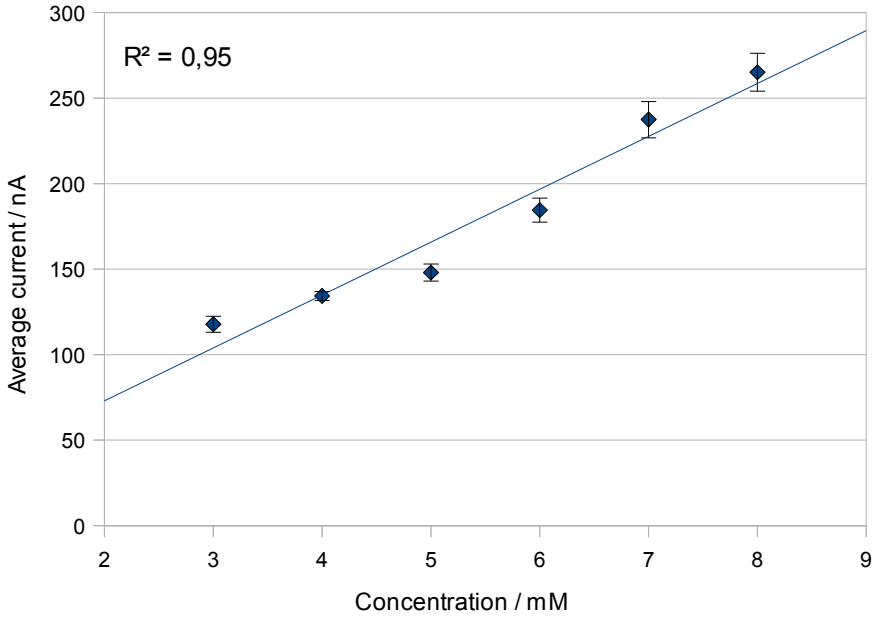

Figure 51: Average current vs. concentration with error bars indicating one standard deviation and linear regression line

The error bars indicate one standard deviation. The linear regression line reveals good linearity with an R^2 of 0.95.

CHAPTER IV: DISCUSSION

1 Used buffer solutions and samples

1.1 Blood sample collection

Some experiments (explicitly stated) were carried out with human blood, therefore the ethical agreement (Project Reference No 06/10) is attached in Appendix D. The blood was donated by healthy adult volunteers, not affected by any clotting problems or diabetes at the time of blood collection. Furthermore, they had not taken any paracetamol or vitamin C supplements during at least ten hours prior blood donation.

1.2 Viscosity adjustment of the buffer

To adjust the viscosity of the buffer to reach blood-like behaviour, carboxymethyl cellulose (CMC) was used. Amongst other compounds, this is used for the production of artificial blood (Liu *et al.*, 2004). As described by Dambrine *et al.* (2009), Figure 52 shows that the higher viscosity fluid occupies more than half the channel.

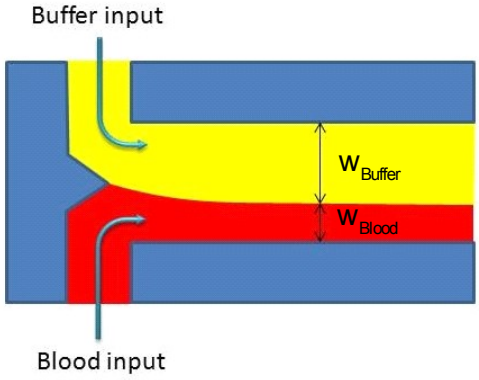

Figure 52: Influence of viscosity on the fluid conduct in the microfluidic channel (adapted from Dambrine et al., 2009)

Labbé (2010) explains all the viscosity phenomena and effects on the microfluidic channels in more detail.

For the H-filter to work perfectly the fluids need to have exactly the same viscosity. As blood viscosity changes over time and is different from individual to individual anyway, this condition cannot be premised in the real sensor application. The best solution for this problem would be to adjust the flow rates

of the buffer and the blood channel individually, so that the contact line is maintained exactly in the middle of the channel. Therefore a feedback loop between an optical detection system and the syringe pumps controlling the flow rates would provide an easy and inexpensive solution. Furthermore, with this system the blood viscosity could be determined at the same time, which may allow conclusions about the blood haematocrit value to be drawn.

2 Device design

Unlike in most publications (Brody *et al.*, 1996; Holl et. al., 1996; Brody and Yager, 1997; Verpoorte, 2002; Collier and Hart, 2005; Fiorini and Chiu, 2005; Hartmann and Sasso, 2007), the initial design was a configuration where the two fluids are flowing on top of each other (instead of side by side), which maximises the area available for diffusion. In fact, no publication was located in scientific literature about lamination of layers in order to achieve this channel arrangement. Figure 53 shows the two configurations.

Figure 53: Cross section of the two possible channel configurations; channels on top of each other (left), channels side by side (right), the green line indicates the area available for diffusion

Figure 19 shows a schematic of all the designs used for fluid conduct experiments. Further details about the evolution of the design and the problems associated with each device is given in Section 8. Detailed dimensions of each design are given by Tu (2010).

3 Laser-cutting

It was noticed that the laser beam is less focused in the margin regions of the marking area than in the centre. Sometimes the edges of the devices had to be cut manually using a scalpel (in particular the corners), whereas the channels in the middle area were cut perfectly. Due to the fact that high precision cutting is needed only in the channels (which are located in the middle of the devices) this did not cause any problems.

4 Alignment tool

The first alignment tool was built according to Chapter II Section 4, but with a 1.2mm aluminium sheet instead of the acrylic glass sheet. The pins were fixed with the help of a two-component adhesive (Araldite Rapid), as shown in Figure 54.

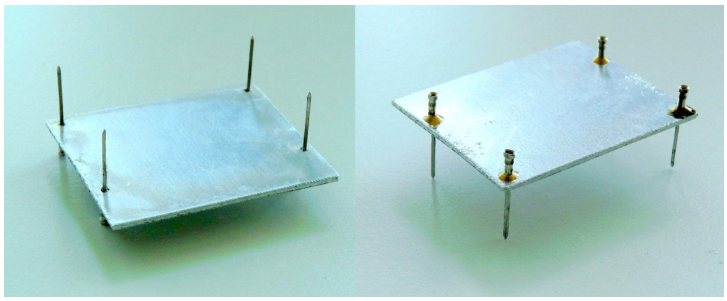

Figure 54: Top (left) and bottom view (right) of the first alignment tool built with aluminium sheet support

The problem was that it was not possible to see what happened in the channels during the experiments, for example if there were any bubbles or turbulences. So the alignment tool with the acrylic glass support, which is described in Chapter II Section 4, was produced.

The alignment of the polymer layers is the least accurate step in the device manufacturing process (compared to the AutoCAD design and the laser-cutting). However, it was the best possible solution in the short time constraints of this project.

5 Lamination

As the microfluidic device assembly is prone to human error, such as air bubbles and contamination of the sticky surfaces (by hair and dust entrapment for example), for mass production, lamination by robots under clean room conditions would provide a solution.

6 World-to-chip interface

In order to be able to connect syringes to the microfluidic chip, a world-to-chip interface device was built. The first world-to-chip interface was produced

according to Chapter II Section 6, but with a 1.2mm aluminium sheet instead of the 3mm PET sheet (see Figure 55).

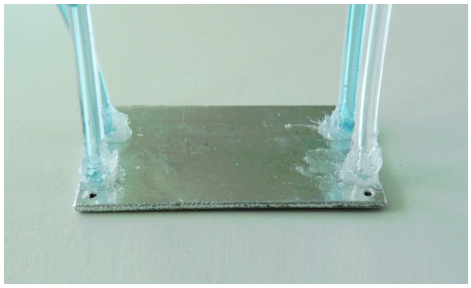

Figure 55: First world-to-chip interface with aluminium sheet support

As a consequence of the thinner support, the connection tubes were not attached very well, so they often fell off during the experiments. Therefore, the world-to-chip interface with the thicker 3mm PET sheet which is described in Chapter II Section 6 was built.

As an alternative, another world-to-chip interface, working by magnetic connectors, was tested, but it did not work. The working principle and approach is attached in Appendix C.

7 Electrode fabrication

7.1 Screen-printing

Due to the time constraints of this project and the cost of designing and producing a new screen for a commercial screen-printer coupled with availability restrictions (as a screen-printer is not available in-house), an adapted methodology for electrode deposition similar to screen-printing was invented for the project. A laser-cut polymer layer was used as the electrode mask analogous to the screen in the screen-printing process. It was found that the ink spreads under this layer if it is not adhered to the support layer.

Hence, for the project, the electrode mask layer was stuck to the bottom layer before the ink was spread into the cut channels in accordance with Chapter II Section 7.1. After deposition and curing of the inks, the protective layer serving as the electrode mask (see Figure 23) needed to be removed very carefully, otherwise the formed electrode would have peeled off as well (see Figure 56).

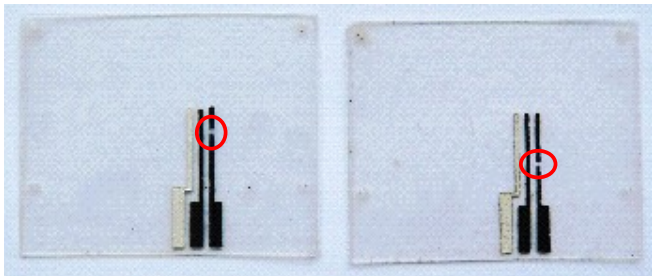

Figure 56: Devices with disrupted electrodes due to the electrode mask removal

Using a commercial screen-printer for producing the electrodes would provide better reproducibility and mass production capacity.

7.2 Optimisation of electrode deposition

The thickness of the electrodes was measured in order to make the surface in the microfluidic channel as least irregular as possible.

The problem of an uneven and irregular surface in the micro-channel due to the electrodes could be reduced by using a conventional screen-printer. Also using another technique such as vacuum deposition might lead to better results (Hintsche *et al.*, 1991; Shul´ga *et al.*, 1994).

8 Microfluidic chip experiments

Based on the encountered problems in the flow conduct experiments, as general rules for all tested microfluidic chips, it can be said that:

- the smaller the flow rate, the more important small inaccuracies in the channel wall and in the alignment of the layers become.
- the smaller the flow rate, the more important differences in the surface properties of the two channels become.
- the smaller the flow rate, the more the flow conduct in the channels is influenced by pressure differences at the outlet tubes.
- the higher the viscosity, the better the performance of the devices remains for smaller flow rates.

9 Electrochemical experiments

9.1 Simulation of the channel

Due to the problems encountered with the flow behaviour in the devices (see Chapter II Section 8) the electrodes were tested separately. In order to obtain comparable results (in terms of electrode surface area), the channel was simulated by covering the rest of the electrodes with insulating ink. The resulting device can be seen in Figure 35.

9.2 Characterisation of the electrodes

Ferrocyanide was available in the form of potassium ferrocyanide ($K_4Fe(CN)_6$), and was chosen as a standard, because the reaction of ferrocyanide to ferricyanide ($Fe(CN)_6^{3-}$) at the electrodes is well known in literature (Scholz, 2002). Equation 11 shows the redox reaction occurring at the working electrode (Scholz, 2002; Wang, 2006).

$$Fe(CN)_6^{4-} \rightleftharpoons Fe(CN)_6^{3-} + e^- \qquad (11)$$

The results of the cyclic voltammetry experiment can be compared with other electrodes, or the same electrodes in other buffers in order to assess their performance (Brett and Brett, 1998; Scholz, 2002).

9.3 Determination of the optimal potential for amperometry

It was found that on (unintentionally) moving the beaker during an experiment (so that the device touched the beaker wall) the measured current dropped significantly. This was without doubt due to the interrupted flow around the device and the disturbed stirring condition, so the device was cut (according to Section 9.2) and put in the middle of the beaker. Figure 57 shows the measurement arrangement before and after noticing this effect.

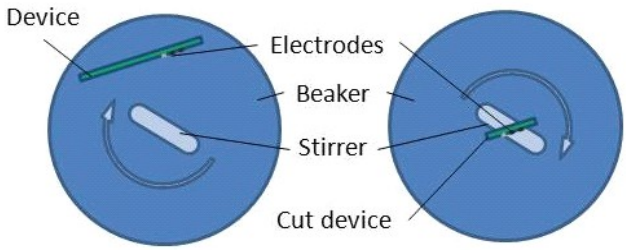

Figure 57: Experimental setup for measurement in a beaker before (left) and after (right) cutting the device

9.4 Measurement of interfering species

Figure 41 shows clearly that all interferents produce a higher signal than the analyte hydrogen peroxide. This is the reason why it is so important to reduce the influence of these interferences in glucose biosensors as far as possible. The maximum physiological concentration for ascorbic acid is 85µM and for uric acid 620µM (Ernst *et al.*, 2002). The highest therapeutic concentration for acetaminophen is 260µM (Ernst *et al.*, 2002). To calculate the maximum relative error, the lowest physiological glucose concentration of 3mM is compared to the maximum concentrations of the interferents. The results are errors of 4% for ascorbic acid, 38% for uric acid and 20% for acetaminophen. This is not surprising, as even commercial home glucose meters, which are comprising measures for interference protection, cannot fulfil the maximum error recommendation of less than 5% of the Diabetes Association (Ernst *et al.*, 2002).

9.5 Measurements variability

The decrease in electro-active surface area of the electrodes may be caused due to two effects: dissolving of ink particles into the sample solution and/or the polishing effect of the electrode surface.

The screen-printed electrodes show a porous fractal surface structure after the curing process. The roughness of this microstucture is highly dependent on the curing temperature (Grennan *et al.*, 2001). It is possible that some of the particles of the ink are just loosely attached to the substrate and therefore become soluble on sample application. This effect has been demonstrated for the silver reference electrodes by Dudeney (2008) and Kadara (2004).

Mechanical polishing is the most used pretreatment method for electrodes, in order to gain reproducible electron transfer kinetics. The procedure removes adhered species from the electrode surface which are blocking the electron transfer. Furthermore, it gives the surface a uniform micro-structure and roughness, hence a defined surface area (Bioanalytical Systems Inc., 2009). The electrode was patted dry with a tissue between the single measurements. This procedure is in fact comparable to a polishing process.

Figure 58 shows a schematic of a screen-printed electrode before and after sample application, as well as after polishing. The circles represent the graphite particles and the grey area represents the binder. As the scheme shows the screen-printed electrodes after curing, the third basic component of carbon ink, the solvent, is not illustrated (it evaporated during the curing process) (Krejčí *et al.*, 2004; Grennan *et al.*, 2001).

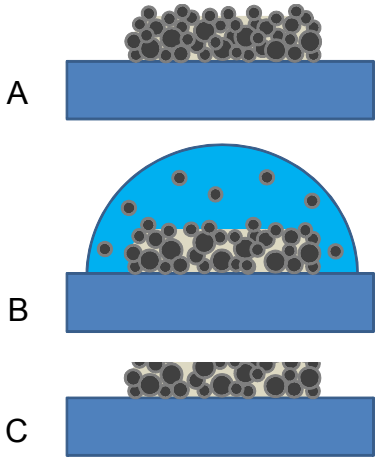

Figure 58: Schematics of screen-printed electrodes; A: before sample application, B: after sample application (some ink particles dissolved), C: after polishing (adapted from Krejčí et al., 2004)

Figures 44 and 45, confirm that after a couple of measurements, which could be simulated by slightly polishing the electrodes before use the repeatability of measurements, is given. Furthermore, commercially screen-printed electrodes provide better repeatability anyway, due to the automated manufacturing process.

9.6 Determination of fabrication reproducibility

All in all it can be said, that the reproducibility of the electrodes, in consideration of the fact that they are manually screen-printed, exceeded expectations. Furthermore, commercially screen-printed electrodes provide better reproducibility anyway, due to the automated manufacturing process.

9.7 Linearity determination of device with channel

This experiment was carried out initially in order to see the extension of the linear range by the introduction of a diffusion limiting membrane such as cellulose acetate on the working electrode. Furthermore the properties of the cellulose acetate membrane and the liquid membrane of the H-filter should have been compared.

However, the tested device already showed a linear response (R^2 = 0.9996) up to 10mM without any membrane, as can be seen in Figure 49, hence the experiment was not conducted any further.

10 Measurement of glucose solutions with GOx

In order to determine the relation between the glucose concentration and the hydrogen peroxide detected at the electrodes, a measurement with GOx was carried out. The result, which can be seen in Figure 50, shows the kinetics of the enzymatic reaction and the stable end point produced by glucose solutions of different concentrations. For the glucose samples, the physiological range from 3 to 8mM was chosen (Ernst *et al.*, 2002).

After averaging the end point values, Figure 51 shows the linear response (R^2 of 0.95) and small fluctuations in the current indicated by the error bars.

CHAPTER V: CONCLUSION

A concept and design for the device meeting the aims of the project which are: building of a low cost electrochemical microfluidic continuous glucose biosensor incorporating a continually renewable liquid membrane in order to avoid electrode fouling and interferences, was successfully developed.

1 Main findings of the project

It was realised, that the influence of channel design and the channel surface properties, as well as other components such as the syringes used, the inlet and outlet tubes and the syringe pump play more important roles in microfluidic devices than initially expected.

For reasons not yet known, the microfluidic chip did not work as expected in the experiments. Neither the bi-planar, nor the mono-planar designs, which should work according to the literature (Brody *et al.*, 1996; Holl *et al.*, 1996; Verpoorte, 2002; Collier and Hart, 2005), provided the anticipated results. The device performance was improved during the troubleshooting procedure, but further research is necessary.

The electrochemical detection system was tested separately due to the difficulties encountered with the microfluidic chip. The performance, variability, and reproducibility of the electrodes was characterised by measurement in simulated channels. The linearity and GOx experiments were carried out by using modified devices with only one micro-channel instead of two. The amperometric measurements revealed, considering the adapted manual screen-printing procedure, good repeatability, reproducibility and linearity, and the linear operating range exceeded the physiological glucose concentrations. The lower limit of detection was calculated to be 0.05mM based on the S/N = 3 criterion.

Due to the time-consuming troubleshooting process for the microfluidic chip, no enzyme immobilisation experiments were carried out. The enzyme was tested in solution by electrochemical detection and showed good response to different glucose concentrations. Immobilisation of GOx should not be a problem, though, as there are many standard procedures available in literature.

2 Future work and recommendations

In order to prove the syringe pump as the source of error for the not working microfluidic chips, it should be changed for a more precise (appropriate for microfluidics) one. If this still does not lead to the expected results, the device should be produced by another manufacturing method, which worked in the literature (Fiorini and Chiu, 2005; Klank *et al.*, 2002; Yamaguchi *et al.*, 2002). The most suitable technique would be optical lithography, due to the rapidness, ease and low cost of device production (Collier and Hart, 2005). Unfortunately, the bi-planar devices cannot be manufactured by this method.

Commercial screen-printing or another suitable electrode deposition technique, such as vacuum evaporation, could be used, in order to gain a more even and regular surface, for optimal integration into the microfluidic channel (Hintsche *et al.*, 1991; Shul´ga *et al.*, 1994).

Enzyme immobilisation was intended to be done by physical adsorption and cross-linking with glutaraldehyde, due to the simplicity, low cost and availability of this method, in this project. Other immobilisation methods, such as covalent bonding or entrapment, could be investigated, as they may provide better activity, stability and bonding to the substrate (Turner *et al.*, 1978; Price and Stevenson, 1999; Gizeli and Lowe, 2003; Malhotra and Turner, 2003; Wu *et al.*, 2004).

After succeeding in designing a working microfluidic device, the flow velocity and channel length are determined in order to allow H_2O_2 diffusion, but prevent diffusion of interferents. A convenient way to investigate and visualise these diffusion effects would be by using Raman spectroscopy (Dambrine *et al.*, 2009).

After optimisation of the designed prototype, a clinical trial should be carried out, in order to prove the laboratory based findings and identify possible limitations of the technique. If the clinical study is successful, mass production for commercialisation could be started.

References

Amiel, S. A., Dixon, T., Mann R. and Jameson K. (2008), “Hypoglycaemia in Type 2 diabetes”, *Diabetic Medicine*, vol. 25, pp. 245-254

Atencia, J., Cooksey, G. A., Jahn, A., Zook, J. M., Vreeland, W. N. and Locascio, L. E. (2010), "Magnetic connectors for microfluidic applications", *Lab on a Chip - Miniaturisation for Chemistry and Biology,* vol. 10, no. 2, pp. 246-249.

Baharudin, L. (2008), "Microfluidics: Fabrications and applications", *Instrumentation Science and Technology,* vol. 36, no. 2, pp. 222-230.

Bankar, S. B., Bule, M. V., Singhal, R. S. and Ananthanarayan, L. (2009), "Glucose oxidase - An overview", *Biotechnology Advances,* vol. 27, no. 4, pp. 489-501.

Bioanalytical Systems Inc. (2009)*, Instruction Manual for BASi Epsilon for Electrochemistry*, available at: www.basinc.com/mans/EC_epsilon/index.html (accessed 08/2010).

Brett, C. M. A. and Brett, A. M. O. (1998), *Electroanalysis,* Oxford University Press Inc., Bath (UK).

Breuer, K. S. (ed.) (2005), *Microscale Diagnostic Techniques,* Springer-Verlag Berlin Heidelberg, Germany.

Brody, J. P., Yager, P., Goldstein, R. E. and Austin, R. H. (1996), "Biotechnology at low Reynolds numbers", *Biophysical journal,* vol. 71, no. 6, pp. 3430-3441.

Brody, J. P. and Yager, P. (1997), "Diffusion-based extraction in a microfabricated device", *Sensors and Actuators, A: Physical,* vol. 58, no. 1, pp. 13-18.

Cass, A. E. G., Davis, G., Francis, G. D., Hill, H. A. O., Aston, W. J., Higgins, I. J., Plotkin, E. V., Scott, L. D. L. and Turner, A. P. F. (1984), "Ferrocene-mediated enzyme electrode for amperometric determination of glucose", *Analytical Chemistry,* vol. 56, no. 4, pp. 667-671.

Collier, W. A. and Hart, A. L. (2005), "Electrochemical Detection in Microfluidic Devices", *1st International Conference on Sensing Technology,* Vol. 1, 21-23/11/2005, New Zealand, Dairy Science & Technology, New Zealand, pp. 589 - 593.

Dambrine, J., Géraud, B. and Salmon, J. -. (2009), "Interdiffusion of liquids of different viscosities in a microchannel", *New Journal of Physics,* vol. 11.

Dudeney, R. (2008), *Electrochemical Method for the Determination of Arsenic in the field using Screen-printed Gold Electrodes* (PhD thesis), Cranfield University, Cranfield (UK).

Ernst, H., Roß, B. and Knoll, M. (2002), "Reliable glucose monitoring through the use of microsystem technology", *Analytical and Bioanalytical Chemistry,* vol. 373, no. 8, pp. 758-761.

Ferrante do Amaral, C. E. and Wolf, B. (2008), "Current development in non-invasive glucose monitoring", *Medical Engineering and Physics,* vol. 30, no. 5, pp. 541-549.

Fiorini, G. S. and Chiu, D. T. (2005), "Disposable microfluidic devices: Fabrication, function, and application", *BioTechniques,* vol. 38, no. 3, pp. 429-446.

Gizeli, E. and Lowe, C. R. (eds.) (2002), *Biomolecular Sensors*, TJ International Ltd., Padstow, Great Britain.

Grennan, K., Killard, A. J. and Smyth, M. R. (2001), "Physical characterizations of a screen-printed electrode for use in an amperometric biosensor system", *Electroanalysis,* vol. 13, no. 8-9, pp. 745-750.

Griffiths, S. K. and Nilson, R. H. (2001), "Low-dispersion turns and junctions for microchannel systems", *Analytical Chemistry,* vol. 73, no. 2, pp. 272-278.

Hartmann, C. and Sasso, L. (06/2007)*, Convection-Diffusion in Microchannels*, available at: www2.mic.dtu.dk/research/MIFTS/publications/3week/Jun2007_ConvectionDiffusion.pdf (accessed 08/2010).

Hintsche, R., Möller, B., Dransfeld, I., Wollenberger, U., Scheller, F. and Hoffmann, B. (1991), "Chip biosensors on thin-film metal electrodes", *Sensors and Actuators: B.Chemical,* vol. 4, no. 3-4, pp. 287-291.

Hirsch, I. B., Bode, B. W. and Verderese, C. A. (01/2010)*, Accuracy of Point-of-Care Blood Glucose Monitoring in the Presence of Interfering Substances: Chronicle of a Medical Alert and Implications for Patient Safety in Different Clinical Settings*, available at: cme.medscape.com/viewarticle/714742 (accessed 06/2010).

Holl, M. R., Galambos, P., Forster, F. K., Brody, J. P. and Yager, P. (1996), "Optimal design of a microfabricated diffusion-based extraction device", *American Society of Mechanical Engineers, Dynamic Systems and Control Division (Publication) DSC,* vol. 59, pp. 189-195.

Holt, T. and Kumar, S. (2010), *ABC of Diabetes,* 6th ed, John Wiley & Sons Ltd., Malaysia.

Jia, W.-Z., Wang, K. and Xia, X.-H. (2010), "Elimination of electrochemical interferences in glucose biosensors", *TrAC - Trends in Analytical Chemistry,* vol. 29, no. 4, pp. 306-318.

Jönsson, H. (2004), *Microfluidics for lab-on-a-chip applications* (MSc thesis), Lund Graduate School of Biomedical Research, Lund (Sweden).

Jungheim, K. and Koschinsky, T. (2002), "Glucose monitoring at the arm: Risky delays of hypoglycemia and hyperglycemia detection", *Diabetes Care,* vol. 25, no. 6, pp. 956-960.

Kadara, R. (2004), *Development of electrochemical sensors for heavy metal ions detection in environmental samples* (PhD thesis), Cranfield University, Cranfield (UK).

Klank, H., Kutter, J. P. and Geschke, O. (2002), "CO_2-laser micromachining and back-end processing for rapid production of PMMA-based microfluidic systems", *Lab on a Chip - Miniaturisation for Chemistry and Biology,* vol. 2, no. 4, pp. 242-246.

Krejčí, J., Prášek, J., Fujcik, L., Khatib, S., Hejátková, E., Jakubka, L. and Giannoudi, L. (2004), "Screen-printed sensors with graphite electrodes - Comparison of properties and physical method of sensitivity enhancement", *Microelectronics International,* vol. 21, no. 3, pp. 20-24.

Labbé, M. Q. D. (2010), F*abrication and optimisation of an analytical microfluidic device for blood glucose analysis and assessment of fluids viscosity effect on its performance* (unpublished MSc thesis), Cranfield University, Cranfield (UK).

Liu, Y., Xie, J.-J., Zhu, M.-F. and Zhang, X.-Y. (2004), "A study of the synthesis and properties of AM/AMPS copolymer as superabsorbent", *Macromolecular Materials and Engineering,* vol. 289, no. 12, pp. 1074-1078.

Lower, S. (2010)*, All about Electrochemistry: The Nernst Equation*, available at: www.chem1.com/acad/webtext/elchem/ec4.html (accessed 07/2010).

Malhotra, B. C. and Turner, A. P. F. (eds.) (2003), *Advances in Biosensors - Perspectives in Biosensors,* Elsevier Science B.V., Hungary.

Mendosa, D. (11/1999), Blood Glucose Meters, available at: www.mendosa.com/bgmeters.htm (accessed 06/2010).

Newman, J. D. and Turner, A. P. F. (2005), "Home blood glucose biosensors: A commercial perspective", *Biosensors and Bioelectronics,* vol. 20, no. 12, pp. 2435-2453.

Newman, J. D. and Setford, S. J. (2006), "Enzymatic biosensors", *Molecular biotechnology,* vol. 32, no. 3, pp. 249-268.

Newman, J. D. (2010), "Biosensors - A One-Trick Pony", presentation at: *Biosensors 2010*, 26-28/05/2010, Glasgow (UK).

Nguyen, N. T. and Wereley, S. T. (2006), *Fundamentals and applications of microfluidics,* 2nd ed, Atech House Inc., USA.

O'Neil, M. J., Smith, A., Heckelman, P. E. and Budavari, S. (eds.) (2001), *The Merck Index: An Encyclopedia of Chemicals, Drugs and Biologicals,* 13th ed, John Wiley & Sons Ltd., USA.

Piechotta, G., Albers, J. and Hintsche, R. (2005), "Novel micromachined silicon sensor for continuous glucose monitoring", *Biosensors and Bioelectronics,* vol. 21, no. 5, pp. 802-808.

Price, N. C. and Stevenson, L. (1999), *Fundamentals of Enzymology - The Cell and Molecular Biology of Catalytic Proteins,* 3rd ed, Oxford University Press Inc., New York.

Prudenziati, M. (ed.) (1994), *Handbook of Sensors and Actuators 1 - Thick Film Sensors*, Elsevier Science B.V., Netherlands.

Reach, G. and Wilson, G. S. (1992), "Can continuous glucose monitoring be used for the treatment of diabetes", *Analytical Chemistry,* vol. 64, no. 6, pp. 381 A-386 A.

Reyes, D. R., Iossifidis, D., Auroux, P. -. and Manz, A. (2002), "Micro total analysis systems. 1. Introduction, theory, and technology", *Analytical Chemistry,* vol. 74, no. 12, pp. 2623-2636.

Ricci, F., Moscone, D., Tuta, C. S., Palleschi, G., Amine, A., Poscia, A., Valgimigli, F. and Messeri, D. (2005), "Novel planar glucose biosensors for continuous monitoring use", *Biosensors and Bioelectronics,* vol. 20, no. 10 Spec. Iss., pp. 1993-2000.

Rose, A. H. (ed.) (1980), *Economic Microbiology - Microbial Enzymes and Bioconversions*, Academic Press Inc. (London) Ltd., Great Britain.

Scholz, F. (ed.) (2002), *Electroanalytical Methods: Guide to Experiments and Applications*, Springer-Verlag Berlin Heidelberg, Berlin.

Schultz, D. G. (08/2009), FDA Public Health Notification: Potentially Fatal Errors with GDH-PQQ Glucose Monitoring Technology, available at: www.fda.gov/medicaldevices /safety/alertsandnotices/publichealthnotifications/ucm176992 (accessed 06/2010).

Shul'ga, A. A., Soldatkin, A. P., El'skaya, A. V., Dzyadevich, S. V., Patskovsky, S. V. and Strikha, V. I. (1994), "Thin-film conductometric biosensors far glucose and urea determination", *Biosensors and Bioelectronics,* vol. 9, no. 3, pp. 217-223.

Steil, G. M. and Rebrin, K. (2005), "Closed-loop insulin delivery - What lies between where we are and where we are going?", *Expert Opinion on Drug Delivery,* vol. 2, no. 2, pp. 353-362.

Teo, C. J. and Khoo, B. C. (2009), "Analysis of Stokes flow in microchannels with superhydrophobic surfaces containing a periodic array of micro-grooves", *Microfluidics and Nanofluidics,* vol. 7, no. 3, pp. 353-382.

Thévenot, D. R., Toth, K., Durst, R. A. and Wilson, G. S. (1999), "Electrochemical biosensors: Recommended definitions and classification (Technical Report)", *Pure and Applied Chemistry,* vol. 71, no. 12, pp. 2332-2348.

Trevan, M. D. (1980), *Immobilized Enzymes - An Introduction and Applications in Biotechnology,* John Wiley & Sons Ltd., USA.

Tu, M-A. M. (2010), *Channel design and optimization for the development of a 2D microfluidic device on chip* (unpublished MSc thesis), Cranfield University, Cranfield (UK).

Turner, A. P. F., Karube, I. and Wilson, G. S. (eds.) (1987), *Biosensors - Fundamentals and Applications,* Oxford University Press Inc., Great Britain.

Turner, A. P. F. (ed.) (1992), *Advances in Biosensors - A Research Annual,* JAI Press Ltd., USA.

Turner, H. E. and Wass, J. A. H. (2002), *Oxford Handbook of Endocrinology and Diabetes,* 1st ed, Oxford University Press Inc., China.

Vandaveer IV, W. R., Pasas-Farmer, S. A., Fischer, D. J., Frankenfeld, C. N. and Lunte, S. M. (2004), "Recent developments in electrochemical detection for microchip capillary electrophoresis", *Electrophoresis,* vol. 25, no. 21-22, pp. 3528-3549.

Verpoorte, E. (2002), "Microfluidic chips for clinical and forensic analysis", *Electrophoresis,* vol. 23, no. 5, pp. 677-712.

Wang, J. (2001), "Glucose biosensors: 40 Years of advances and challenges", *Electroanalysis,* vol. 13, no. 12, pp. 983-988.

Wang, J. (2002), "On-chip enzymatic assays", *Electrophoresis,* vol. 23, no. 5, pp. 713-718.

Wang, J. (2006), *Analytical electrochemistry,* 3rd ed, Wiley, New York (USA).

Wang, J. (2008), "In vivo glucose monitoring: Towards 'Sense and Act' feedback-loop individualized medical systems", *Talanta,* vol. 75, no. 3, pp. 636-641.

Watkins, P. J. (1998), *ABC of diabetes,* 4th ed, BMJ Publishing Group, London.

Weigl, B., Domingo, G., LaBarre, P. and Gerlach, J. (2008), "Towards non- and minimally instrumented, microfluidics-based diagnostic devices", *Lab on a Chip - Miniaturisation for Chemistry and Biology,* vol. 8, no. 12, pp. 1999-2014.

White, S. F., Tothill, I. E., Newman, J. D. and Turner, A. P. F. (1996), "Development of a mass-producible glucose biosensor and flow-injection analysis system suitable for on-line monitoring during fermentations", *Analytica Chimica Acta,* vol. 321, no. 2-3, pp. 165-172.

WHO (2004), *Diabetes Action Now: An Initiative of the World Health Organization and the International Diabetes Federation*, WHO Document Production Services, Geneva (Switzerland).

WHO (2006), *Definition and Diagnosis of Diabetes Mellitus and Intermediate Hyperglycaemia,* WHO Document Production Services, Geneva (Switzerland).

WHO (2009), Diabetes - Fact Sheet No. 312, available at: www.who.int/mediacentre/factsheets/fs312/en/index.html (accessed 05/2010).

Wilkins, E. and Atanasov, P. (1996), "Glucose monitoring: State of the art and future possibilities", *Medical Engineering and Physics,* vol. 18, no. 4, pp. 273-288.

Wu, B., Zhang, G., Shuang, S. and Choi, M. M. F. (2004), "Biosensors for determination of glucose with glucose oxidase immobilized on an eggshell membrane", *Talanta,* vol. 64, no. 2, pp. 546-553.

Yamaguchi, A., Jin, P., Tsuchiyama, H., Masuda, T., Sun, K., Matsuo, S. and Misawa, H. (2002), "Rapid fabrication of electrochemical enzyme sensor chip using polydimethylsiloxane microfluidic channel", *Analytica Chimica Acta,* vol. 468, no. 1, pp. 143-152.

Zhang, S., Wright, G. and Yang, Y. (2000), "Materials and techniques for electrochemical biosensor design and construction", *Biosensors and Bioelectronics,* vol. 15, no. 5-6, pp. 273-282.

Appendices

A Sodium phosphate buffer preparation

Materials

Sodium dihydrogen phosphate 99% (Sigma-Aldrich, Gillingham, UK)
Disodium hydrogen phosphate 98.5% (Sigma-Aldrich, Gillingham, UK)
Potassium chloride 99.74% (Fisher Scientific, Loughborough, UK)
Distilled water Direct-Q3 UV (MilliPore, Billerica, USA)
pH-meter HI 8519N (HANNA Instruments, Woonsocket, USA)

Methods

All experiments were carried out, using a 0.1M sodium phosphate buffer at pH 7.2. Furthermore they contained 0.1M potassium chloride (KCl), which is similar to the physiological concentration of chloride in blood, as supporting electrolyte for electrochemical detection (White *et al.,* 1996; Ernst *et al.*, 2002). It was prepared by combining sodium dihydrogen phosphate (NaH_2PO_4) solution 0.1M in distilled water and disodium hydrogen phosphate (Na_2HPO_4) solution 0.1M in distilled water, each also containing 0.1M KCl. The two solutions were prepared independently and poured together to adjust the final H^+ concentration under constant observation of a pH-meter. To reach pH 7.2, about 2.5 times more Na_2HPO_4 solution than NaH_2PO_4 solution was needed.

B Titrations

B.A Hydrogen peroxide titration

Materials

Potassium permanganate 99.3% (BDH Laboratory Supplies, Poole, UK)
Sulphuric acid solution 1M (Fisher Scientific, Loughborough, UK)

Methods

As hydrogen peroxide is degradable by light and heat, the concentration of the stock solution has to be determined prior to use. Therefore a redox titration with potassium permanganate ($KMnO_4$) was done prior to the experiments.

Furthermore, it was used to determine the H_2O_2 concentrations after the diffusion experiments. The reaction shown in Equation 12 takes place during the titration process.

$$5\,H_2O_2 + 2\mathrm{MnO_4^-} + 6\mathrm{H^+} \longrightarrow 2\mathrm{Mn^{2+}} + 8\mathrm{H_2}O + 5\mathrm{O_2} \qquad (12)$$

As the H^+ source, sufficient sulphuric acid (H_2SO_4) has to be added to the hydrogen peroxide solution prior titration, in order to make the H_2O_2 the limiting compound rather than the H^+. This means, as long as there is H_2O_2 in the solution it reacts with the permanganate and the purple colour disappears. At the endpoint of the titration, when all hydrogen peroxide is consumed, any additional permanganate turns the solution purple. The ratio of hydrogen peroxide to permanganate is 5:2 according to Equation 12. The exact H_2O_2 concentration (M), based on the volume of potassium permanganate solution (l) used to reach the endpoint, is calculated according to Equation 13, where V is the volume of the appropriate solution (l).

$$[H_2O_2] = \frac{5}{2}\frac{V_{KMnO_4}}{V_{H_2O_2}}\,[KMnO_4] \qquad (13)$$

To make sure the solution was acidic enough some more drops of sulphuric acid were added after titration, in order to see if the slightly pink colour faded again.

All hydrogen peroxide titrations were carried out in triplicate and the average was calculated. Erlenmeyer flasks (250ml) containing 10ml of the H_2O_2 solution and 25 drops of sulphuric acid and a 50ml burette (class B) were used. During the titration, the recipient was stirred by a magnetic stirrer at about 500rpm at room temperature.

B.B Ascorbic acid titration

Materials

Ascorbic acid 99.7% (Sigma-Aldrich, Gillingham, UK)
Potassium iodate 99.5% (Sigma-Aldrich, Gillingham, UK)
Potassium iodide 99.5% (Sigma-Aldrich, Gillingham, UK)
Starch solution 1% (Sigma-Aldrich, Gillingham, UK)
Sulphuric acid solution 1M (Fisher Scientific, Loughborough, UK)

Methods

To determine the ascorbic acid concentrations before and after the diffusion experiments a redox titration with iodine was carried out. The iodine solution was prepared with distilled water containing 0.06M potassium iodide (KI), 2.5mM potassium iodate (KIO_3) and 90ml of 1M sulphuric acid. The iodine combines with iodide to form triiodide (I_3^-) according to Equation 14.

$$I_{2(aq)} + I^- \rightleftharpoons I_3^- \tag{14}$$

The reaction shown in Equation 15 takes place during the titration process.

$$I_3^- + C_6H_8O_6 + H_2O \rightleftharpoons C_6H_6O_6 + 3I^- + 2H^+ \tag{15}$$

The triiodide oxidises ascorbic acid ($C_6H_8O_6$) in the presence of water to dehydroascorbic acid ($C_6H_6O_6$). This means, as long as there is ascorbic acid in the solution, the I_3^- is converted to iodide ions (I^-) and the brown colour disappears. Adding starch solution, as an indicator, to the ascorbic acid solution, turns it blue when all the ascorbic acid is consumed, as any additional triiodide reacts with the starch suspension. The endpoint of the titration is reached when the first sign of blue colour still remains after at least 20s of stirring.

To determine the exact concentration of the iodine solution, a standardisation procedure with an ascorbic acid standard solution needs to be done first. Then any unknown ascorbic acid concentration (M) can be calculated, based on the volume of iodine solution (l) used to reach the endpoint, according to Equation 16, where V is the volume of the appropriate solutions (l).

$$[C_6H_8O_6] = \frac{V_{iodine\ solution}}{V_{C_6H_8O_6}} [iodine\ solution] \tag{16}$$

For standardisation, a 5.7mM ascorbic acid standard solution was prepared. All ascorbic acid titrations were carried out in triplicate and the average was calculated. Erlenmeyer flasks (250ml) containing 10ml of the ascorbic acid solution and 25 drops of 1% starch solution and a 50ml burette (class B) were used. During the titration, the recipient was stirred by a magnetic stirrer at about 500rpm at room temperature.

C Magnetic world-to-chip interface

An interface between the microfluidic device and the syringe was tested, which established the connection with the help of magnetic connectors according to Atencia *et al.* (2010). Figure 59 shows a schematic of the interface in cross sectional view.

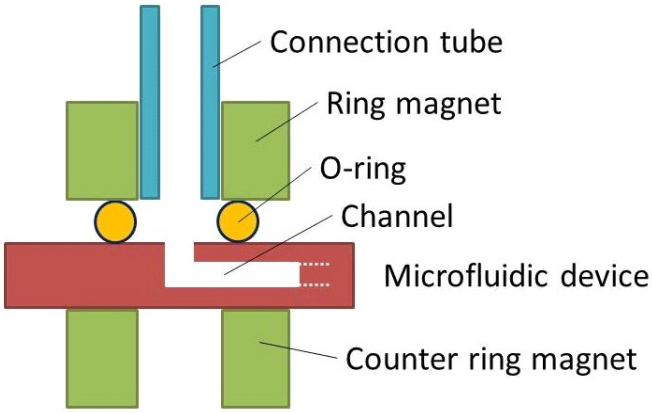

Figure 59: Schematic view (cross section) of the magnetic world-to-chip interface (adapted from Atencia et al., 2010)

The device was simply built by attaching a tube to a ring magnet with silicone on the top side. On the bottom side an o-ring was fixed, also by silicone, which serves as a gasket and seals the connection. The whole assembly is held in place by the counter ring magnet on the other side of the microfluidic device. Figure 60 shows one of the built magnetic connectors.

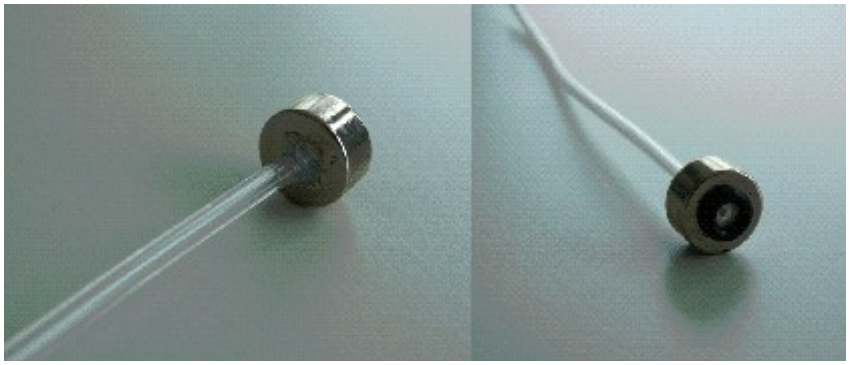

Figure 60: Top (left) and bottom view (right) of the magnetic connector

The problem was that the magnets used (outer Ø 12mm, inner Ø 4mm and height 6mm with a pull force of 3.2 kg) were much too powerful; they were not only attracted by the counter magnet, but also by the other connector's

magnets. So all the connectors stuck together, instead of staying aligned with the inputs and outputs of the microfluidic device. With weaker magnets and/or bigger dimensions of the microfluidic device (more distance between the fluid input and output holes) these magnetic connectors might work properly. But in the present project the size of the microfluidic chip was limited by the laser marking head.

D Ethical approval

Cranfield Health

Cranfield UNIVERSITY

Vincent Building
Cranfield University
Cranfield
Bedfordshire
MK43 0AL
England
T: +44 (0)1234 758300
F: +44 (0)1234 758380
www.cranfield.ac.uk/health

4th August 2010

Dear Maxime

Project Reference No 06/10: Study of the influence of the blood viscosity on the diffusion of H202 through a blood glucose microfluidic device

Thank you for submitting the requested amendments to the above project, I can confirm that I am happy to take Chairman's Action approving the study can go ahead.

Yours sincerely

El Jones

PP

Professor Paul Harrison
Chairman
Cranfield University Health Ethics Committee

Cranfield UNIVERSITY

STUDY INFORMATION SHEET

Assessing the blood sampling for blood glucose microfluidic device optimisation.

The purpose of this document is to provide you (the Volunteer) with enough information to assist you in making a decision to take part in this study. If this document does not answer your questions to your satisfaction, please do not hesitate to contact the Principal Investigator (Jeff Newman) or to ask your questions to the person responsible for taking your consent (Maxime Labbé).

Introduction

Blood glucose quantification is important for diabetes monitoring. Normally, this measurement is achieved with the help of classical biosensors. However, with these kind of sensors can be subject to "fouling" where biological fluids can bind to the surface and give incorrect results. In this study, the blood glucose level will be measured by a microfluidic device in order to avoid these problems by separating the hydrogen peroxide (coming from a glucose enzymatic reaction) from the inferferences (ascorbic acid, paracetamol, uric acid). Furthermore, because of the continuous flow of the microfluidic device, the fouling problems linked with the proteins and cells present in blood will also be avoided. At this moment, the blood samples will only be used for studying the fluid dynamics within the main microchannel and for optimising the diffusion of H202. No precise & quantitative measurements will be achieved on the blood samples.

Recruitment Criteria

You must be a healthy adult (more than 18 years old). People with diabetes or clotting problems are excluded. You must have the ability to give informed consent.

What you will be asked to do

If you decide to take part in the study, you will be asked to do the following:

1. You will be ask to give consent
2. You will be asked to not take any paracetamol or ascorbic acid (Vitamin C) tablets during the ten hours before the blood sampling.
3. A sample of 20 ml of your blood will be collected by trained phlebotomist by following the normal safety & hygiene practices.
4. You will be asked to contact as soon as possible Jeff Newman or Maxime Labbé if you have any problem or discomfort.

The blood sampling will take approximately 10 minutes overall to complete.

What if anything goes wrong ?

Blood collection can sometimes cause discomfort and can lead to some slight bruising after the procedure.

Cranfield UNIVERSITY

If at any time you feel any discomfort, please inform one of the investigators, and the experiment will be terminated. If you have any complications after the blood sampling, please contact Jeff Newman or Maxime Labbé.

You are under no obligation to join the study if you do not wish to do so. You may withdraw your participation in the study at any point without reason. Data collected from this study will be stored on a personal computer on a password protected Cranfield networked server. The data will not contain any personal information about the volunteers but will be stored according to a random volunteer number. The results of this study may be published in a peer-reviewed journal and may form part of Maxime Labbé, Christian Huber and Minh- Anh TU Msc thesis.

There is no payment for taking part in this study.

If you are unhappy with the manner in which you have been treated, or the experiment has been conducted, please do not hesitate to contact the Head of School, Prof Joe Lunec (j.lunec@cranfield.ac.uk, +44 (0)1234 758300).

Volunteers expressing interest will need to sign a Consent Form.

Contact Information

Dr. Jeff.D Newman
Advanced Bioscience
MSc Programme Director
Course Director,
MSc Medical Diagnostics
Cranfield Health
Vincent Building
Cranfield University
Cranfield
Bedfordshire
MK43 0AL
Telephone: +441234 758300
E-mail: j.d.newman@cranfield.ac.uk

Maxime Labbé
Msc Student
Molecular Medicine
Cranfield Health
Vincent Building
Cranfield University
Cranfield
Bedfordshire
MK43 0AL

Telephone : +32498673047
E-mail:
m.labbe@cranfield.ac.uk

This ethical approval has been granted

email: j.d.newman@cranfield.ac.uk
email: m.labbe@cranfield.ac.uk

Centre: Cranfield University, Cranfield campus.
REC Reference Number:
Volunteer Identification Number for this study: .....

CONSENT FORM

Title of Project: ***Study of the influence of the blood viscosity on the diffusion of hydrogen peroxide through a blood glucose microfluidic device***

Name of Researcher: *Jeff Newman*

		(Please tick box)
1.	I confirm that I have read and understood the information sheet that has been provided for the study named above. I can confirm that I have been given opportunity to ask questions regarding the study, and that they have been answered to my satisfaction.	☐
2.	I understand that my participation in this study is entirely voluntary, and I am free to withdraw my consent at any time without giving any reason. My legal or medical rights shall not be affected.	☐
3.	I understand that data (results) acquired during this study may be looked at by authorized individuals (project supervisors) from Cranfield University and may be used in a peer-reviewed article. I give my consent for these individuals to access my data.	☐
4.	I agree to take part in the above-mentioned study.	☐

.....	.....	.....
Name of volunteer	**Date**	**Signature**
.....	.....	.....
Researcher	**Date**	**Signature**

Original (to be filed) ☐ Volunteer Copy ☐ (please tick)
Volunteer consent form (Version 1) Date: 19/07/10